

UNIVERSITY OF OKLAHOMA

GRADUATE COLLEGE

STRATIGRAPHIC ARCHITECTURE OF THE MISSISSIPPIAN LIMESTONE
THROUGH INTEGRATED ELECTROFACIES CLASSIFICATION, HARDTNER
FIELD AREA, KANSAS AND OKLAHOMA

A THESIS

SUBMITTED TO THE GRADUATE FACULTY

in partial fulfillment of the requirements for the

Degree of

MASTER OF SCIENCE

By

NILES WETHINGTON

Norman, Oklahoma

2017

STRATIGRAPHIC ARCHITECTURE OF THE MISSISSIPPIAN LIMESTONE
THROUGH INTERGRATED ELECTROFACIES CLASSIFICATION, HARDTNER
FIELD AREA, KANSAS AND OKLAHOMA

A THESIS APPROVED FOR THE
CONOCOPHILLIPS SCHOOL OF GEOLOGY AND GEOPHYSICS

BY

Dr. Matthew J. Pranter, Chair

Dr. Kurt J. Marfurt

Dr. Roger M. Slatt

© Copyright by NILES WETHINGTON 2017
All Rights Reserved.

ACKNOWLEDGEMENTS

This research was funded through the Reservoir Characterization and Modeling Laboratory and the sponsors of the Mississippi Lime Consortium: Chesapeake Energy, Devon Energy, QEP Resources, and Sinopec (Tiptop Oil and Gas). I would like to recognize and thank Dr. Matthew Pranter for his guidance, patience, and support throughout the course of this project. I would also like to thank Dr. Kurt Marfurt and Dr. Roger Slatt for their input and advice. I would like to thank Dr. Sal Mazzullo, Brian Wilhite, and Woosley Oil and Gas for their technical guidance and permission to use relevant core descriptions. I would also like to thank the Kansas Geological Survey, especially Nikki Potter, for their help getting access to important data and the Integrated Core Characterization Center at OU for their assistance in data measurements. I would like to acknowledge Schlumberger for their donation of Petrel and Techlog, and IHS for their donation of Petra. Lastly, I would like to thank my friends and fellow students for their time and valuable contributions.

TABLE OF CONTENTS

Acknowledgements.....	iv
List of Tables.....	vi
List of Figures.....	vii
Abstract.....	viii
Introduction	1
Geologic Setting	9
Methods	13
Lithofacies Determination.....	13
Electrofacies Classification.....	14
Log Attribute Analysis.....	16
Stratigraphic and Structural Framework.....	19
Lithology and Petrophysical Modeling.....	22
Results	23
Lithologies and Lithofacies.....	23
Electrofacies Classification.....	27
Stratigraphic and Structural Framework.....	33
Spatial Distribution of Lithologies.....	46
Porosity Distribution.....	53
Conclusions.....	58
References	61
Appendix A. Geologic Setting.....	66
Appendix B. Quantitative Mineralogy and Petrophysical Measurements.....	82
Appendix C. Lithology and Electrofacies.....	88
Appendix D. Stratigraphic Framework.....	102

LIST OF TABLES

Table 1: Lithologies and Lithofacies.....	26
---	----

LIST OF FIGURES

Figure 1: Geological Provinces of Oklahoma, Kansas and Texas.....	2
Figure 2: Stratigraphic Column & Type Log	4
Figure 3: Detailed Basemap	7
Figure 4: Paleogeography of North America	10
Figure 5: Summary of DTA	17
Figure 6: Correlations using DTA.....	20
Figure 7: Lithofacies Core Samples.....	24
Figure 8: Lithofacies Thin Sections.....	25
Figure 9: Comparison of Electrofacies Classifications.....	29
Figure 10: Accuracy of ANN.....	31
Figure 11: Stratigraphic Cross Sections.....	34
Figure 12: Mississippian Cycles through DTA.....	38
Figure 13: Mississippian Isopach Map.....	45
Figure 14: 3-D Model Results.....	47
Figure 15: Stratigraphic Framework Through 3-D Models.....	48
Figure 16: Vertical Proportion Curves.....	50
Figure 17: Analysis of Vertical Porosity Trends.....	54
Figure 18: 3-D Models of Lithology and Porosity.....	57

ABSTRACT

The Mississippian Limestone formed through complex structural, stratigraphic, and diagenetic processes involving subsidence, tectonic uplift leading to periodic subaerial exposure, changes in ocean chemistry, variability inherent with carbonate cyclicity, as well as post-depositional alteration. These geologic complexities have led to significant heterogeneity and compartmentalization within Mississippian mid-continent reservoirs. In the Hardtner Field area, the Mississippian Limestone is comprised of five main lithologies including tripolitic chert, green shale spiculite, gray shale spiculite, limestone, and shale. A novel log-based approach, termed derivative trend analysis (DTA), is used to identify and correlate depositional cycles, which can be associated with five major stratigraphic zones. In the absence of abundant and complete core data, DTA serves as a rudimentary, yet informative, tool to effectively develop a sequence-stratigraphic framework.

Generation of accurate electrofacies estimations is in many ways essential for effective reservoir characterization. Classifying electrofacies, especially those constrained to core observations, can elucidate key relationships between depositional environments and reservoir properties, as well as provide an improved understanding of the vertical and lateral heterogeneity of the deposits of interest. For this study, three methods of electrofacies classification (including artificial neural network (ANN), kmeans clustering and KNN clustering) are compared and ultimately used to create predictive lithology logs based only on the combined signatures of open-hole digital well logs in non-cored wells. These lithology logs are subsequently integrated with an interpreted stratigraphic framework to generate 3-D reservoir models, which reveal the

stratigraphic, lithologic, and petrophysical trends of Mississippian carbonates and cherts in the Hardtner Field area.

Stratigraphic models produced from this study reveal a relatively uniform, flat-lying basal Kinderhookian section, overlain by prograding clinoforms with internally shoaling-upward cycles of limestone, shales, and spiculites deposited during Osagean and Meramecian stages. The sequence is capped by a high-porosity unit comprised mostly of brecciated chert associated with subaerially exposed strata underlying the sub-Pennsylvanian unconformity. Hardtner Field is located on the downthrown block of a major north-south trending fault, where relatively thick intervals of Osagean limestones are overlain by spiculitic units. Towards the south and east, Osagean strata thin significantly and are covered by Meramecian spiculites of the Cowley formation. The Mississippian section as a whole thins up-dip toward the north, where most of the upper Mississippian is missing from significant erosion. Spatial porosity distributions reveal high reservoir quality deposits associated with regressive phases of 3rd-order cycles, with highest porosity intervals occurring up-section and toward the northeast of the study area.

INTRODUCTION

Mississippian carbonates and cherts deposited on the Anadarko ramp in the mid-continent region, collectively known as the “Mississippi Lime,” have produced large volumes of hydrocarbons. Many of the most prolific reservoirs in the Mississippian section are composed of highly porous, weathered and chert-replaced intervals associated with the sub-Pennsylvanian unconformity (Watney et al., 2001). These porous chert intervals are informally referred to as the “Mississippi Chat,” and have been the focus of a great deal of research (e.g., Peeler, 1985; Parham and Northcutt, 1993; Montgomery et al., 1998; Rogers, 2001; Watney et al., 2001; Mazzullo et al., 2009; Lindzey, 2015; and Turnini, 2015). A complex structural and stratigraphic history involving subsidence, uplift, sea-level fall leading to periodic subaerial exposure, changes in ocean chemistry and circulation, and variability inherent with carbonate cyclicity has led to significant heterogeneity and compartmentalization within the Mississippian reservoirs. Both localized and widespread diagenetic processes have altered lithofacies and effected reservoir properties, further obscuring the rock record. As a result, establishing unanimously agreed upon stratigraphic sequences and patterns has proved challenging. Adding to this challenge has been an inconsistent and evolving nomenclature associated with Mississippian strata in the mid-continent. These complexities call for a detailed examination of the stratigraphic relationships and reservoir property distribution within the Mississippian interval of the American mid-continent. A regional picture of the Mississippian tectonic provinces is shown in Figure 1.

Many of the concepts developed from previous work on Mississippian

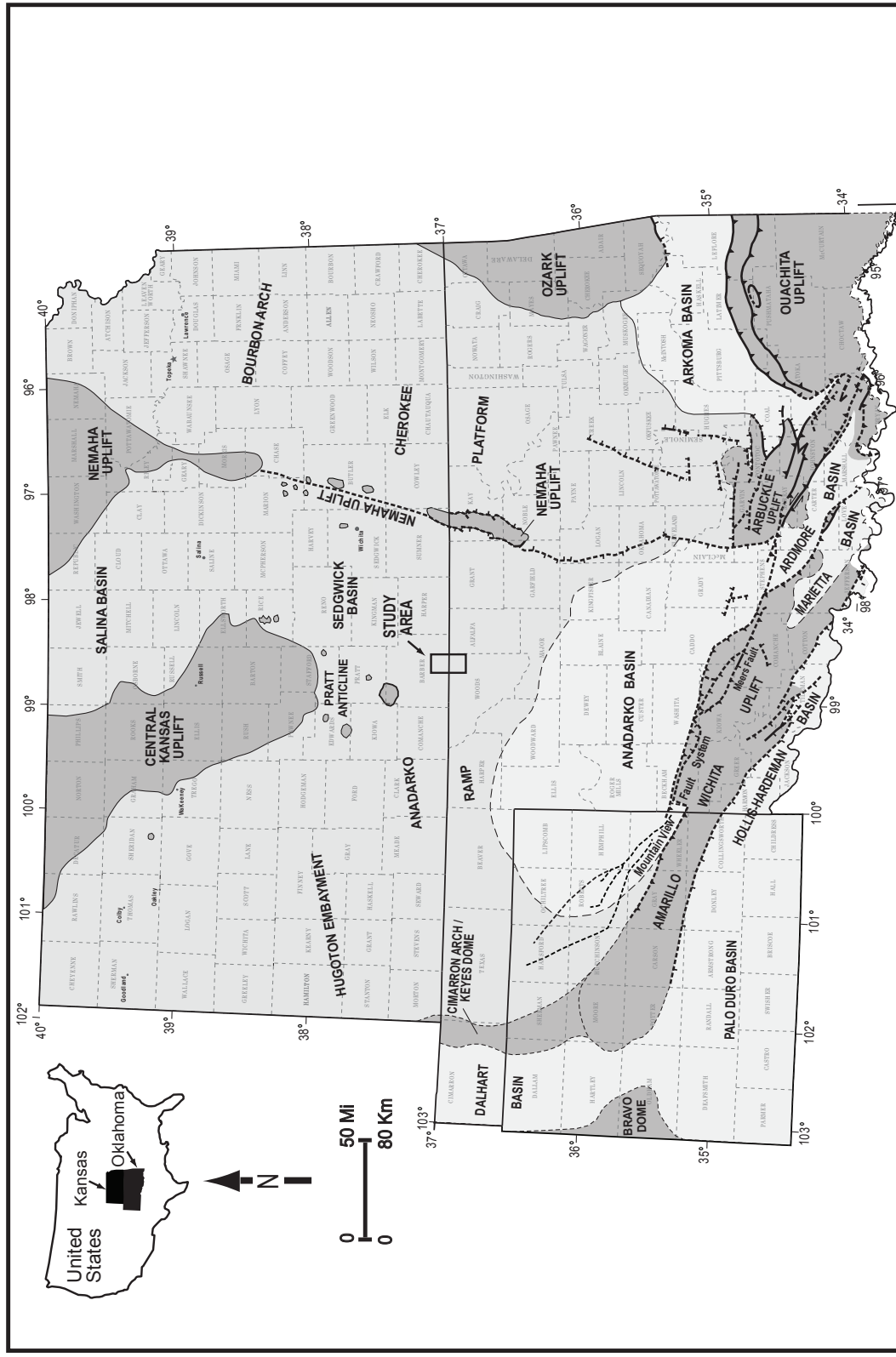


Figure 1. Map of tectonic provinces of the mid-continent region. Study area outlined. (Modified from Dutton, 1984; Campbell, 1988; McConnell, 1989; Northcutt and Campbell, 1995; Johnson and Luza, 2008; LoCriccho, 2012)

carbonates and cherts were applied for the purposes of this study. Watney et al. (2001) identified the dominant lithologies and lithofacies in several south-central Kansas counties by examining core and well-log patterns to identify seven distinct lithofacies. He analyzed the vertical stacking of these lithofacies and proposed 4 separate transgressive-regressive cycles within an overall shallowing upward sequence. Others, such as Doveton (1973), Duren (1960), and Peeler (1985) examined well-log signatures to identify petrophysically distinct units. Their studies revealed characteristically low resistivity and high porosity in reservoir intervals (Figure 2). Low resistivities are attributed to high irreducible saline water saturations as well as an exceptionally abundant silica content. Costello et al. (2014) examined the Mississippian in northeast Woods county using core, log, and 3-D seismic data to assess producible lithofacies. Costello et al. (2014) found that weathered chert, limey-dolomitic chert, and cherty limestone were the most prospective based on favorable petrophysical characteristics.

An understanding of the lithofacies, and consequently the reservoir potential, in this area requires a grasp of the diagenetic processes that have severely altered these deposits. Rogers (2001) examined the depositional and diagenetic origin of the Mississippian “Chat.” Well-log data, thin sections, and cores samples from northern Oklahoma revealed that most of the silica-rich chat zone resulted from replacement of calcite by silica from supersaturated meteoric waters during successive periods of subaerial exposure. This exposure was likely due to a combination of eustatic sea-level fall and local tectonic uplift. A similar study by Mazzullo et al. (2008) concluded there were likely three specific stages of chert generation. Ramaker et al.

(2014) and Montalvo (2015) focused on paragenesis of the Mississippian through core, thin section, and fluid-inclusion analysis. They developed a detailed sequence of diagenetic events highlighted by several stages of silicification and dolomitization during; deposition, meteoric diagenesis, burial diagenesis, and hydrothermal diagenesis.

While the stratigraphy of this area has remained elusive, there have been studies elucidating some of the significant issues. Mazzullo et al. (2009) examined the stratigraphy and reservoir potential of the economically significant Cowley Formation (Figure 2) in south-central Kansas, including the area of interest for this study. He used core samples and log data to distinguish lithologies and infer a broad sequence-stratigraphic framework. From this work, he generated a 2-D depositional model suggesting the Cowley Formation is not a deep-water facies, but instead a distinct progradational spiculite-dominated formation. He concluded that the most productive Cowley reservoirs exist in the bedded and “lenticular-nodular-flaser” spiculite interval near the top of the formation. Mazzullo et al. (2016) later discussed the stratigraphy of the lower Mississippian St. Joe Group. Through outcrop and core examinations he was able to identify a paleo-structure, referred to as the Kanoka ridge, near the southern margin of the Anadarko ramp, where early Osagean shallow-water deposits exist. Lindzey (2015) used 3-D modeling guided by seismic data to examine changes in lithology and petrophysical characteristics for northeast Woods County. Lindzey (2015) divided the Mississippian section into 4 stratigraphic zones based mainly on log characteristics and inferred flooding surfaces. Her results indicated a decrease in siliceous rocks with depth, identifying tripolitic chert and

chert-rich limestones as the most prospective lithologies. Several recent sequence-stratigraphic investigations of the Mississippian interval have worked to establish cycle hierarchies as a means to explain and predict lateral reservoir facies distributions (Price, 2014; LeBlanc, 2014; Childress and Grammer, 2015; Jaeckel, 2016). Jaeckel (2016) used cores and wireline logs from Comanche County, Kansas and Woods County, Oklahoma to interpret a single 2nd-order sequence with a series of prograding 3rd-order cycles controlling facies distribution. Several internally embedded 4th-order cycles were also noted.

This study expands upon relevant previous work and further refines the stratigraphic framework and patterns created by carbonate cyclicity as well as variable depositional and diagenetic conditions. The examination of the stratigraphic controls on reservoir quality distribution is accomplished through several key steps. First, predictive lithology logs are created from integrated electrofacies classifications founded on core descriptions. Next, a stratigraphic framework is developed through the incorporation of novel log analysis as a means of guiding and improving well-log correlations. The lithology logs and stratigraphic framework are then combined to create 3-D lithology models, which are supplemented with certain petrophysical models, allowing for the examination of depositional and diagenetic stratigraphic trends. Vertical and spatial stratal relationships provide insight into the geologic processes responsible for the formation of hydrocarbon reservoirs.

The study area extends from south-central Kansas (Barber County) to north-central Oklahoma (Woods County) (Figure 3). This area represents a spectrum of depositional environments, marking the transition from “main shelf” facies to more

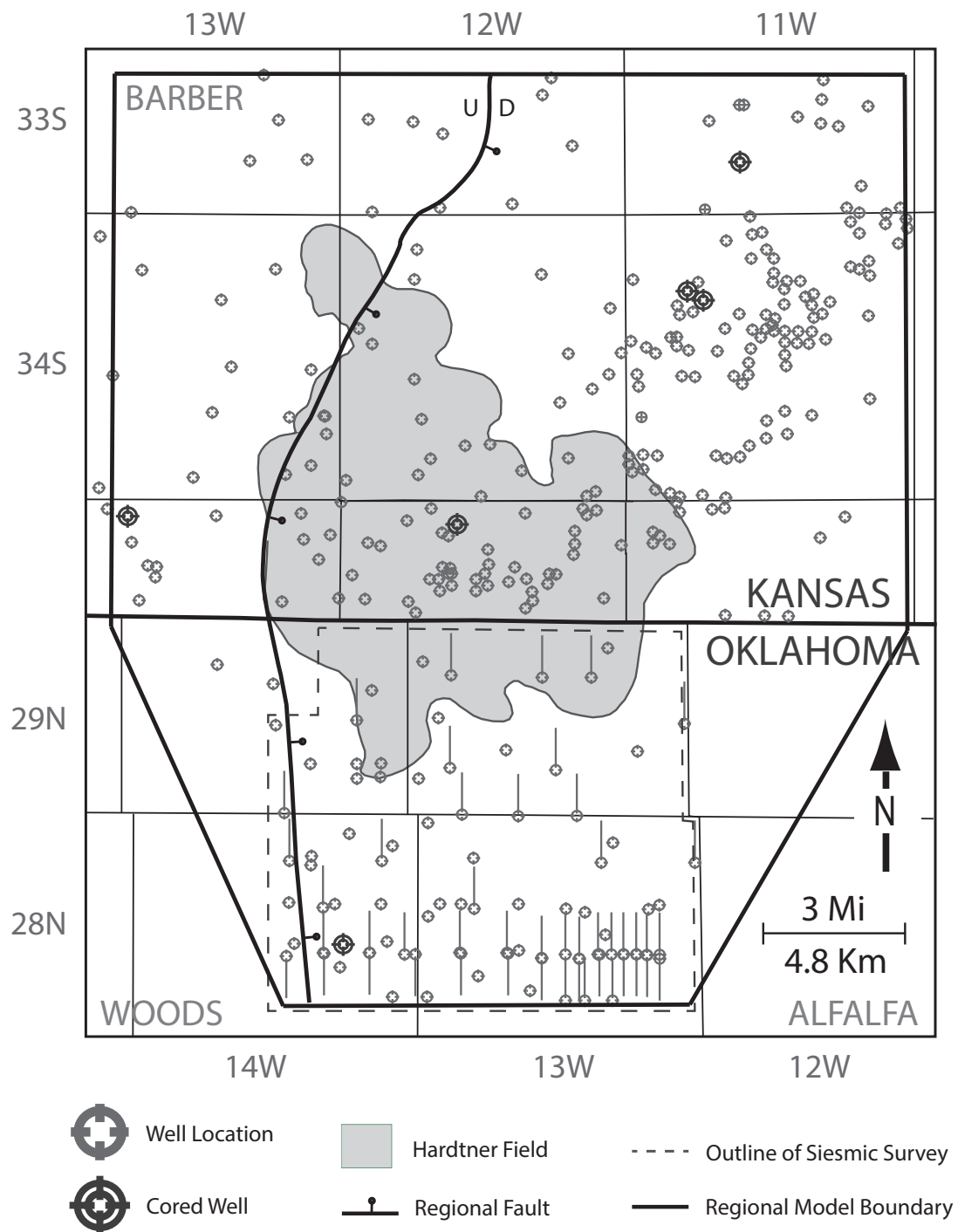


Figure 3. Detailed map of the study area showing location of wells with logs (vertical and horizontal), outline of Hardtner field (modified from Chesapeake Energy), position of an interpreted north-south trending fault, an outline of the 3-D model, as well as an outline of the seismic survey.

distal “shelf margin” facies (Lane and De Keyser, 1980), and defines the up-dip limit of the Cowley Formation (Mazzullo et al., 2009). This transitional area has clouded regional stratigraphic correlations, making local interpretations of stratal architecture difficult, particularly when crossing the Kansas-Oklahoma state border. Many previous studies have focused on either the thicker, distal deposits of Oklahoma (Rogers, 2001; Costello et al., 2014; Lindzey, 2015) or the thin proximal section in Kansas (Rogers et al., 1995, Watney et al., 2001; Mazzullo et al., 2009). Those that have crossed the border have done so as part of regional studies, where data points are separated by a significant distance. This study ties these different depositional environments together on a local field scale using densely spaced log data. The study area includes all of Hardtner Field, which, since its discovery in 1954, has been one of the most prolific gas fields in Kansas producing well over 133 MMcf (3.8 MMm³) of cumulative natural gas (Young, 1968; Watney et al., 2001). Historically, drilling targets for this field have included basal Pennsylvanian conglomerates and porous silica-rich chat intervals. Traps are dominantly stratigraphic as productive zones either pinch out or grade laterally up-dip into impermeable limestone units.

The principal contribution of this project is the clarification of stratigraphic relationships for the area of study through 3-D modeling. In order to accomplish this, a thorough understanding of both the lithofacies and electrofacies as well as their associated reservoir properties was essential. These topics were investigated through core, thin section, and well-log analysis, ultimately revealing a structurally influenced southward progradational architecture of Osagean and Meramecian strata with reservoir quality generally improving up-section and up-dip.

GEOLOGIC SETTING

The paleogeography of North America during the Mississippian was shaped as the result of three major tectonic events; the Acadian, Antler, and Proto-Ouachita Orogenies (Gutschick and Sandberg, 1983; Northcutt et al., 2001). Combined motion of these events formed the Transcontinental Arch, which separated the Madison Carbonate ramp to the west-northwest, and the Burlington ramp to the east-southeast (Figure 4). By the early Mississippian, the expansive shallow marine Burlington shelf and was blanketed by a warm epeiric sea, which gave way to slope and basinal environments down-dip to the south (Elebiju et al., 2011).

Carbonate sedimentation likely took place on a low-gradient ramp environment (Mazzullo et al., 2009; Montalvo, 2015) with scattered calcareous mud mounds, heterozoan assemblages, and abundant sponge bioherms (Rogers et al., 1995). Intermittent stages dominated by siliceous monaxon spicule demosponges are thought to have periodically suppressed carbonate deposition (Watney et al., 2001; Mazzullo et al., 2009). Thus, siliceous spiculite-dominated rocks are very common in Mississippian carbonates (Rogers et al., 1995). Spiculite is a term used to describe deposits of cemented sponge spicules which form following the disaggregation and lithification of siliceous sponge skeletons. In the context of this study, these skeletons likely belonged to demosponges with needle-like monaxon megascleres (Mazzullo et al., 2009). Abundant spiculite deposition was encouraged by elevated dissolved silica concentrations in nutrient-rich marine waters. Such conditions, possibly originating from suppressed ocean mixing, were likely maintained for significant periods of time in order to account for the vastly abundant spiculite deposits observed in the Cowley

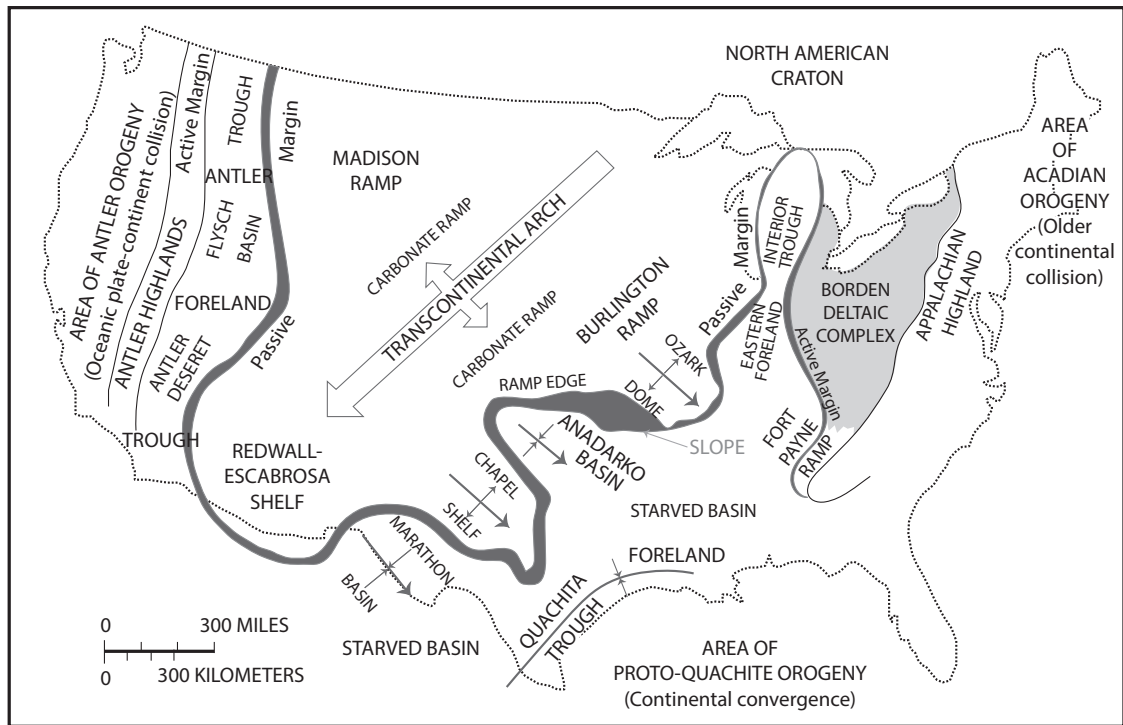


Figure 4. Paleogeography of the North American continent during the Mississippian, showing the position of the Burlington Ramp and Anadarko Basin (modified from Gutschick, 1993).

Formation (Mazzullo 2009). Several possible sources of this elevated silica include volcanic emissions (Watney et al., 2001), weathering of silica-rich rocks, hydrothermal emanations (Rogers, 2001), upwelling (Ramaker et al., 2014), and blooms of pelagic siliceous radiolarian (Gutschick and Sandberg, 1983). Spiculites were likely deposited below fair-weather wave base in nutrient-rich, moderately oxygenated, calm waters based on the presence of bioturbation and interbedded shale layers (Mazzullo 2009). However, shallow-water bedded spiculites with minimal shale content are also observed in the area of study.

Rising eustatic sea level throughout most of the Mississippian facilitated progradational wedges of carbonate and spiculite sedimentation towards the south-southeast (Watney et al., 2001). The direction of progradation was likely influenced by locally significant structural features including the Central Kansas uplift and Pratt anticline (Figure 1) (Gutschick and Sandberg, 1983). These tectonic uplifts, coupled with eustatic sea-level fall in the late Mississippian accompanying the onset of global icehouse conditions (Appendix A-1), led to significant post-Mississippian subaerial exposure and resultant erosion (Rogers, 2001). This erosion is responsible for substantial localized missing sections, and resulted in the major, regionally extensive Mississippian-Pennsylvanian unconformity (Watney et al., 2001). The Mississippian interval is characterized by four distinct stages of deposition. From oldest to youngest these stages include; Kinderhookian, Osagean, Meramecian, and Chesterian (Appendix A-2) (Watney et al., 2001). In the area of interest, only Kinderhookian through Meramecian stages are observed (Figure 2). The “Mississippi Lime” is a broad informal term that refers to dominantly carbonate deposits of the mid-continent of Kinderhookian, Osagean, and Meramecian stages (Parham and Northcutt, 1993).

Three main depositional environments are recognized within the Mississippi Lime including inner ramp, main ramp, and outer ramp settings (Parham and Northcutt, 1993), representing a basin-ward trend from north to south. These environments produced a set of commonly acknowledged facies within Mississippian carbonates, ranging from basal argillaceous mudstones, to spiculitic packstones with nodular or bedded chert, to autoclastic chert, to bioclastic grainstones (Watney et al., 2001; Mazzullo et al., 2009).

The Mississippian section as whole represents a single 2nd-order transgressive-regressive cycle (Sloss, 1963), bounded by a minor basal disconformity (Comer, 1991) and a major overlying unconformity associated with the top of the Kaskasia sequence (Sloss, 1963). Within this section there are several higher order shallowing-upward transgressive-regressive sub-cycles, each bounded by unconformities (Watney et al., 2001). In the study area, the entire Mississippian, as well as each sub-cycle, contains increasing spiculite content upwards, which is an indication of a progradational, shallowing-upward sequence (Mazzullo et al., 2009). Cycles tend to display basal shale-rich units overlain by successively more spiculitic and cherty packstones. These higher order cycles are controlled primarily by eustatic sea-level fluctuations associated with Milankovitch cycles, however several factors including sedimentation rate, subsidence, climate, and tectonics could also have had an impact (Leblanc, 2014; Birch, 2015).

As a result of their depositional and structural history, mid-continent Mississippian deposits were heavily influenced by diagenesis, especially in regards to petrophysical characteristics. A summary of key diagenetic features and events is provided in Appendix A-2.

METHODS

Lithofacies Determination

Key lithologies in the Mississippian section were identified through detailed core descriptions of six wells within the study area. These include the Gulf 4-4 School Trust, the Nichols 1-8 George Michel, the Continental 1 Harbaugh, the Chesapeake 1-14 Bann, the Woosley A-5 Oakes, and the Woosley B-1 Wiley (Figure 3). Core descriptions include observations of primary lithology, grain type, porosity, sedimentary structures, and diagenetic textures. Seven core plugs from the Gulf 4-4 School Trust were analyzed for porosity and permeability using Mercury Injection Capillary Pressure (MCIP) and Nuclear Magnetic Resonance (NMR) measurements. Mineralogy of the core plugs were analyzed using both X-ray diffraction (XRD) and Fourier transform infrared spectroscopy (FTIR).

Eighteen unpolished thin sections from the Gulf 4-4 School Trust, Nichols 1-8 George Michel, and Continental 1 Harbaugh cores were acquired through Spectrum Petrographics Inc. Samples were injected with blue epoxy to emphasize porosity, and stained with alizarin red S to identify calcite. Standard transmitted light, plane polarized light, and cross polarized light microscopy was conducted on a Zeiss Axio Imager.Z1m microscope. Mineralogic and diagenetic petrographic observations were used to bolster depositional and post-depositional interpretations. Scanning Electron Microscopy (SEM) was also used for supplementary mineral identification and textural analysis of thin sections. An acceleration voltage of 20 kV was used to acquire images for concentric back-scattered (CBS) as well as secondary Everhart Thornley detectors (ETD).

Electrofacies Classification

Effective and innovative electrofacies classification was among the principal goals of this study. Electrofacies represent “the set of log responses which characterizes a sediment and permits this to be distinguished from others” (Serra and Abbot, 1982). In essence, the physical characteristics of specific rock types that make them unique can be indirectly estimated by log measurements. Therefore, specific sets of log values, known as electrofacies, correspond to distinguishable sedimentary facies. Electrofacies classification is the process of categorizing depth intervals into distinct rock types, based solely on wireline-log properties; thus providing a valuable predictive capability in non-cored wells. Two classification approaches were utilized. These approaches, explained below, include a supervised method (artificial neural network), and two unsupervised methods (Kmeans and KNN clustering).

Artificial Neural Network

Artificial Neural Networks (ANNs) are an increasingly popular method of pattern recognition with broad applications that can be applied in nearly every modern industry. In the geosciences, they have become an effective instrument for electrofacies classification. ANNs are useful classification tools that work by minimizing the error between a given output and an estimated or calculated output, a process known as backpropagation (Kumar and Kishore, 2006). This is accomplished through combining and weighting several input variables. ANN's are able to effectively construct complex decision boundaries for multiple classes, separating data into similar groups. In the context of this study, an ANN is used to relate electrofacies to lithologies. Core

descriptions identifying lithofacies are used as the target output, and different combinations of well-log curves are used as inputs. The neural network combines and weights the inputs in an iterative process to recreate the core descriptions as closely as possible. Once a satisfactory match is achieved, the ANN is applied to non-cored wells using the same well-log curves as inputs in order to “predict” the lithofacies for each depth.

PCA K-means/KNN Clustering

A combination of principal component analysis (PCA) and clustering is another proven system of pattern detection. The purpose of PCA is to find linear combinations of input variables (in this case well-log values) that best account for the variability in the data set. This is accomplished by finding the covariance matrix of the mean subtracted data points for each variable, then computing the eigenvectors and eigenvalues of that covariance matrix (Smith, 2002). Those eigenvectors represent principle components, where each successive principle component describes a direction of decreased anisotropy. PCA is an important first step in the clustering process, as it effectively reduces the number of dimensions considered by rotating the data cloud onto perpendicular axes of central variability. Cluster analysis is a means of grouping multivariate data into internally similar categories or classes. In most cases, including this study, clustering is an unsupervised classification technique, meaning no target output is provided prior to clustering. Instead, the desired number of clusters or classes is user defined.

K means is a commonly used method of clustering. This algorithm minimizes the sum of squared distances from each point to the centroid within each cluster

(Hartigan, 1975). First K (a user defined number) centroids are randomly placed among the data. Then points are assigned to a class based on the closest centroid. The position of each centroid is then recalculated to reflect the mean position of its assigned data points. Points are reassigned and centroids recalculated in an iterative process until each point is as close as possible to a representative centroid (Hartigan, 1975). Deciding what value to use for K is of vital importance in K means clustering. The optimal value should follow the number of classes observed in hard data, in this case the number of lithologies observed in core samples. However, if core data do not include all of the lithologies or not all lithologies can be resolved by logs, a statistical approach can be used to determine an optimal K value through the creation of sum of squares within and sum of squares between plots (Appendix C-7).

K nearest neighbor (KNN) is another method of clustering that classifies an unknown data point based on the most frequently occurring class of its nearest previously defined data points (Allen and Pranter, 2016). The number of neighboring points considered (K) is user defined and should be adjusted to find an optimum value for each data set. For this study, K was set at 10. The number of log curves used as inputs defines the dimensionality of the data set around the sampling point that is searched to find the surrounding points with the smallest euclidan distance.

Log-Attribute Analysis

Attribute analysis has become a common practice when processing and interpreting seismic data; however, it has not effectively transitioned to well-log data. This study examines log attributes through a novel approach to well-log analysis referred to as Derivative Trend Analysis (DTA) (Figure 5).

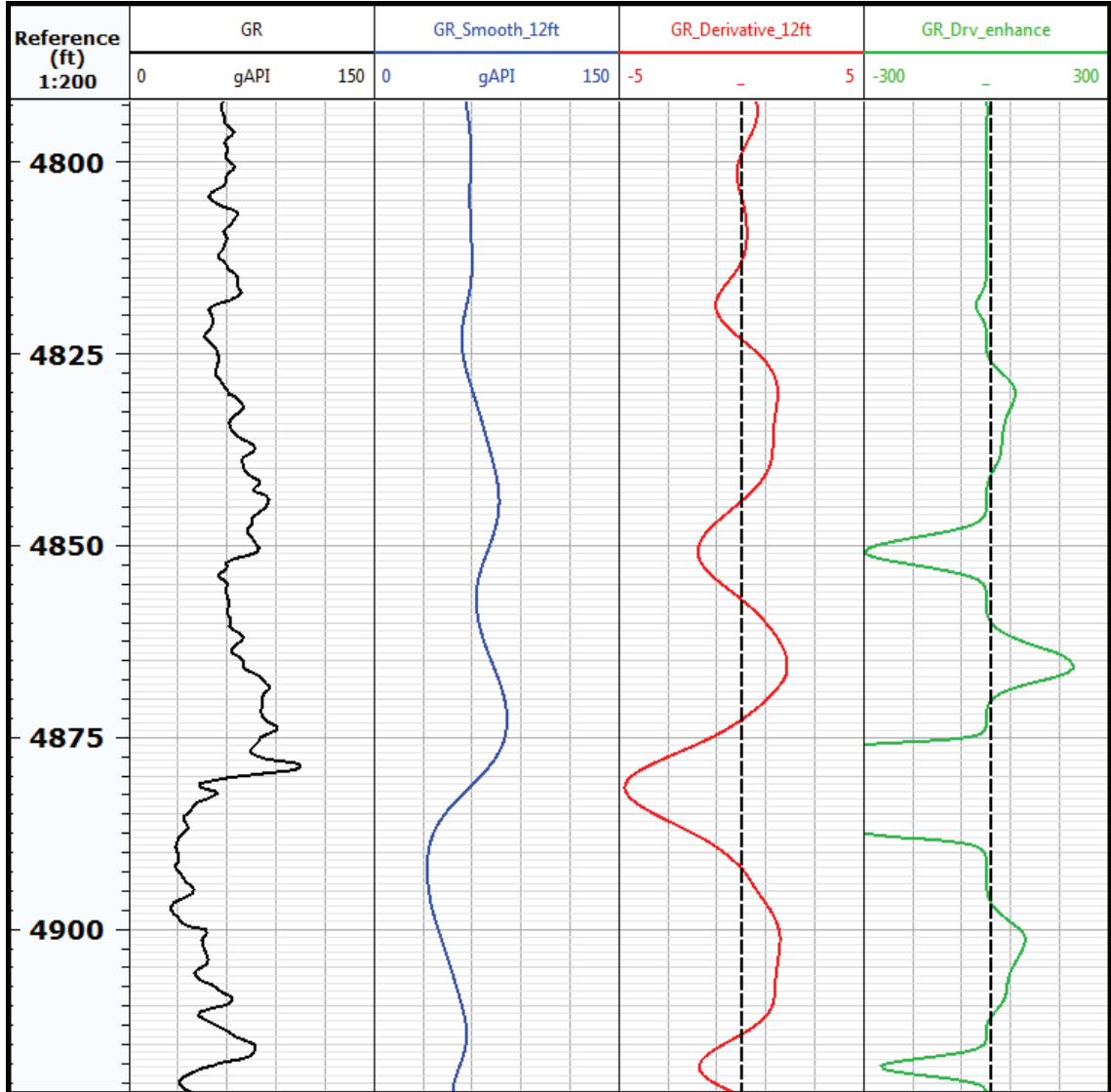


Figure 5. Example of Derivative Trend Analysis (DTA) for the Woosley 1 Cundiff well. The first track represents the unaltered Gamma Ray curve. The second track shows the GR curve after application of a Gaussian smoothing filter using a 12 ft (3.6 m) window. Track 3 shows the derivative curve for the smoothed GR. The last step (track 4) emphasizes important signals and suppresses probably “noise.”

The motivating principal behind this analysis is to identify and emphasize the log signals that are geologically significant in an automated fashion. When interpreting well logs, it is often insufficient to solely observe the measured value associated with a given log. Instead, characteristic motifs over a range of depths can provide more meaningful information that can be tied to geologic processes. For example, a single gamma-ray value may not be totally informative, however a generally decreasing-upward curve may indicate a coarsening trend associated with a sea-level regression. For this study, well-log interpretation and correlation were guided by not only measured values, but also calculated trends and quantified shapes.

Mathematical log analysis was conducted using *Techlog* petrophysical software. The first step of the DTA process is to filter the log data to the appropriate frequency for the investigation at hand. This is accomplished through the application of a Gaussian smoothing function, in which values within a user-defined smoothing window are assigned weights based on distance from the original point of interest (Shapiro and Stockman, 2000). Each data point is then recalculated as a weighted average of its neighboring points. The filter attenuates high-frequency “noise” while preserving lower frequency trends, resulting in smoothed log curves. Smoothed curves are then differentiated using the central-difference method.

$$Derivative(i) = (Value(i+1) - Value(i-1)) / (Depth(i+1) - Depth(i-1))$$

This method essentially calculates the slope between neighboring points on a curve to estimate the derivative of the point of interest. Once the derivative at each point is calculated, the resulting curve shows positive values when the original curve is decreasing upward and negative values when the original curve is increasing upward.

The magnitude of the derivative curve indicates how quickly the original curve is changing. For example, large positive values on a gamma-ray derivative curve would indicate that gamma ray is rapidly decreasing (becoming cleaner) upward, which might be expected when a limestone is overlying a shale. The final step in DTA is applied only in certain scenarios. It involves intensifying important signals and suppressing minor “noise.” This is accomplished by first multiplying or dividing the derivative data so that the majority of “important” signals are values greater than 1 or less than -1, then raising the data to an odd power (generally 3 or 5). This ensures that relatively small peaks become suppressed, while larger peaks are enhanced. In other words, this step isolates major changes in log character that mark significant changes in lithology, depositional process, and diagenetic events. An example of correlations guided by DTA is provided in Figure 6.

Log-attribute analysis for this study is restricted to single wells. This is akin to single-trace attribute analysis in seismic interpretation. Progressing this methodology to include not only the well at hand, but also its neighboring wells would allow for multi-trace operations that could greatly aid in the correlation of geologically significant features.

Stratigraphic and Structural Framework

A stratigraphic and structural framework was developed to gain an understanding of the lithologic variability present. The Mississippian section was divided into 5 major lithologically distinct intervals which were then subdivided according to potential cyclicity. Multiple scales of correlation were conducted in order to observe both the general patterns associated with Kinderhookian, Osagean, and

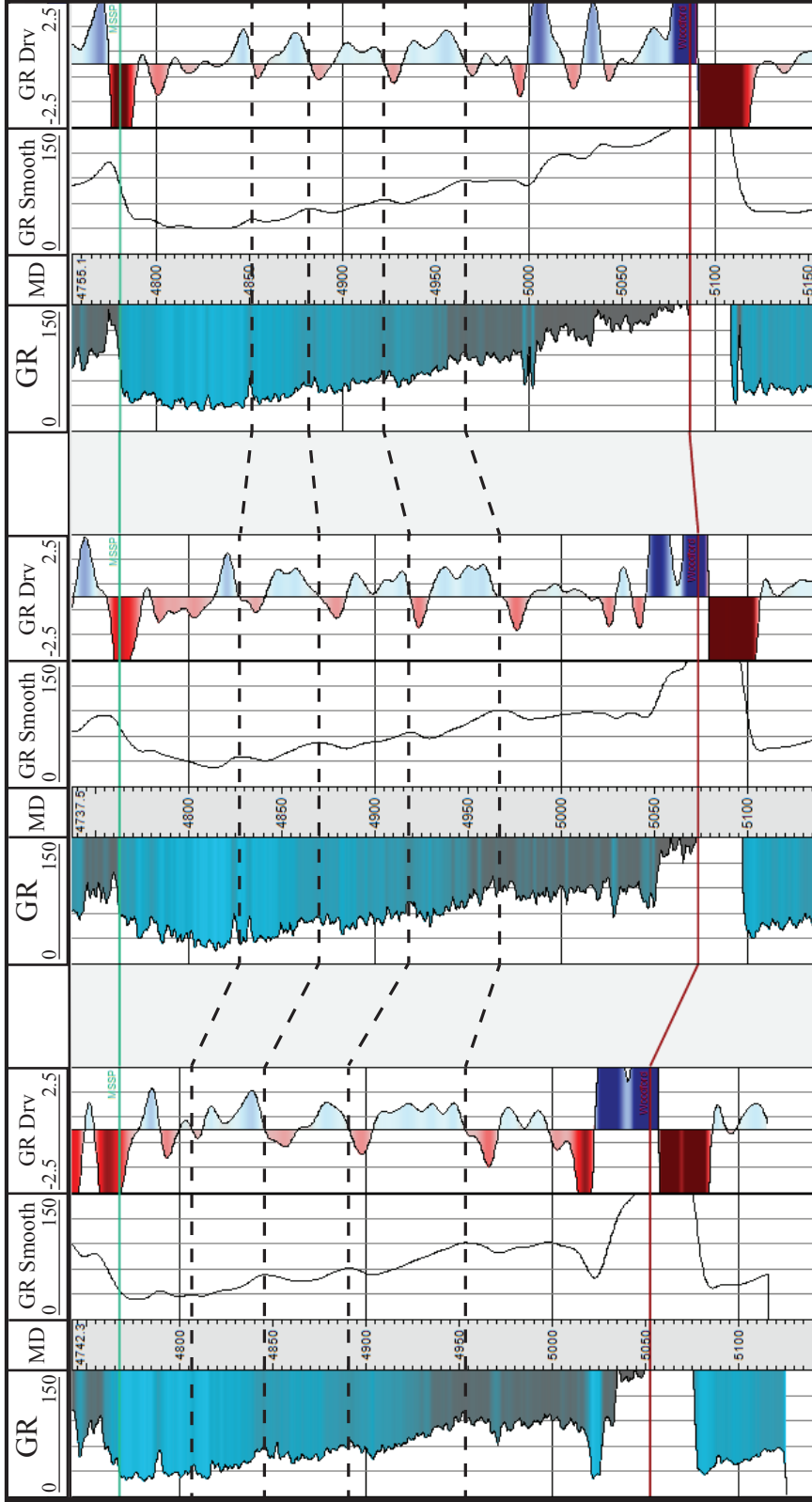


Figure 6. Example of well-log correlations guided by GR derivative curves. In this case, tops are picked at the top of inferred Regressive-Transgressive cycles (based on cleaning upward and fining upward GR responses). The track on the left is a regular GR curve with an interpretive color fill to represent lithology. The next track is the GR after a Gaussian smoothing filter with a 12 ft (3.6 m) window applied. The third track is the GR derivative with a blue fill for positive values (times when GR is decreasing or cleaning upward) and a red fill for negative values (times when GR is increasing or fining upward). The darkness of the color fill represents the degree of GR change.

Meremecian series, as well as internal variability.

Well-log interpretation and correlation of 342 wells (Figure 3) provided reasonable control on spatial structural relief of interpreted surfaces. Of these wells, 89 come from Woods County, while the remaining 253 were drilled in Barber County. Raster logs for 61 wells were digitized using IHS Petra software. Wells offered a wide variety of log suites, with each having one or more of the following logs; gamma ray (GR), density porosity (DPHI), neutron porosity (NPHI), deep resistivity (RESD), and photoelectric factor (PE). Formation tops were initially identified from interpreted logs in previous nearby studies (Young, 1968; Montgomery et al., 1998; Mazzullo et al., 2009; Wilhite and Mazzullo, 2013; Montalvo, 2015; Watney, 2015; Lindzey, 2015; Mazzullo et al., 2016). These tops were then adjusted and correlated by means of a grid of north-south and east-west oriented cross sections spanning the study area.

Formation tops and sequence-stratigraphic cycles were identified and correlated using DTA. The Mississippian interval, especially the Cowley Formation, is characterized by a somewhat repetitive series of stacked lithofacies that correspond to changes in base level during deposition. The cyclic lithofacies are manifested in log signatures by consistent increasing or decreasing motifs. In particular, the GR log shows increasing trends representing coarsening or shoaling-upward sequences and decreasing trends representing fining-upward sequences. Analyzing and quantifying these trends using DTA allows for the successful isolation of individual cycles to use for developing a sequence-stratigraphic interpretation (Figure 6). In the absence of adequate core coverage and length to reveal lithofacies stacking patterns, DTA provides a serviceable estimation of cyclic trends.

Lithology and Petrophysical Modeling

In order to better understand the 3-D architecture of the reservoirs of interest, a detailed static model was generated using *Petrel*. Cell-based geostatistical modeling techniques were employed to estimate the distribution of specific lithofacies (defined from core and well logs), and petrophysical properties. First, a 3-D structural and stratigraphic framework (3-D grid) was created using structure maps from well tops and fault surfaces. The framework covers approximately 326 mi² (844 km²) with an aerial grid cell size of 150 ft x 150 ft (46 m x 46 m). Vertical cell thickness is an average of 3.5 ft (1.1 m), and varies depending on total unit thickness. Total model dimensions are 593 x 681 x 100 cells which equates to roughly 40 million cells. These cells were then populated with upscaled lithology estimations (from electrofacies classifications) using a Sequential-Indicator Simulation (SIS). Reservoir property models, including; gamma ray, porosity, resistivity, photoelectric and various derivative curves, were created using Sequential-Gaussian Simulation (SGS) (Figure 15). Estimates of vertical variability for each lithology and zone were attained through vertical variography. Horizontal ranges produced from 2-D variogram maps (polar plots) were adjusted in accordance with previous, seismically constrained studies of Lindzey (2015) (Appendix C-8). Variogram ranges for petrophysical models were decreased to account for heterogeneity internal to each lithology.

RESULTS

Mississippian Lithologies and Lithofacies

The Mississippian section in south-central Kansas consists of several dominant lithofacies that were identified through an examination of available core samples. This relatively sparse data was supplemented by core descriptions (Sal Mazzullo, 2016, personal communication) for two key wells (Woosley A-5 Oakes and Woosley B-1 Wiley). In addition, comparisons of well-log signatures with key lithologies identified in relevant previous studies (Watney et al., 2001; Mazzullo et al., 2009; Montalvo, 2015, Lindzey, 2015) helped capture lithologic variations for the entire Mississippian section.

Key lithofacies defined from firsthand core observations include 1) chert breccia, 2) bedded spiculite, 3) clast/bedded cherty spiculite, 4) interbedded lenticular spiculite, and 5) argillaceous dolomitized cherty spiculite (Figure 7, Figure 8). Inferred lithofacies from donated and published core descriptions include 6) lenticular gray shale spiculite, 7) gray bioturbated cherty limestone, 8) shaly limestone and 9) dark spiculitic shale. Table 1 provides a summary of each lithofacies, including identifying characteristics and interpreted depositional setting. Detailed descriptions and interpretations of lithofacies are offered in Appendix A-4.

Each lithofacies can display significant variability. While distinct lithofacies are distinguishable in core samples, they tend to exist on a spectrum with end members that gradually transition into one another. This is particularly true for spiculite-rich intervals, where chert replaced spiculitic lithofacies are differentiated by their shale content and

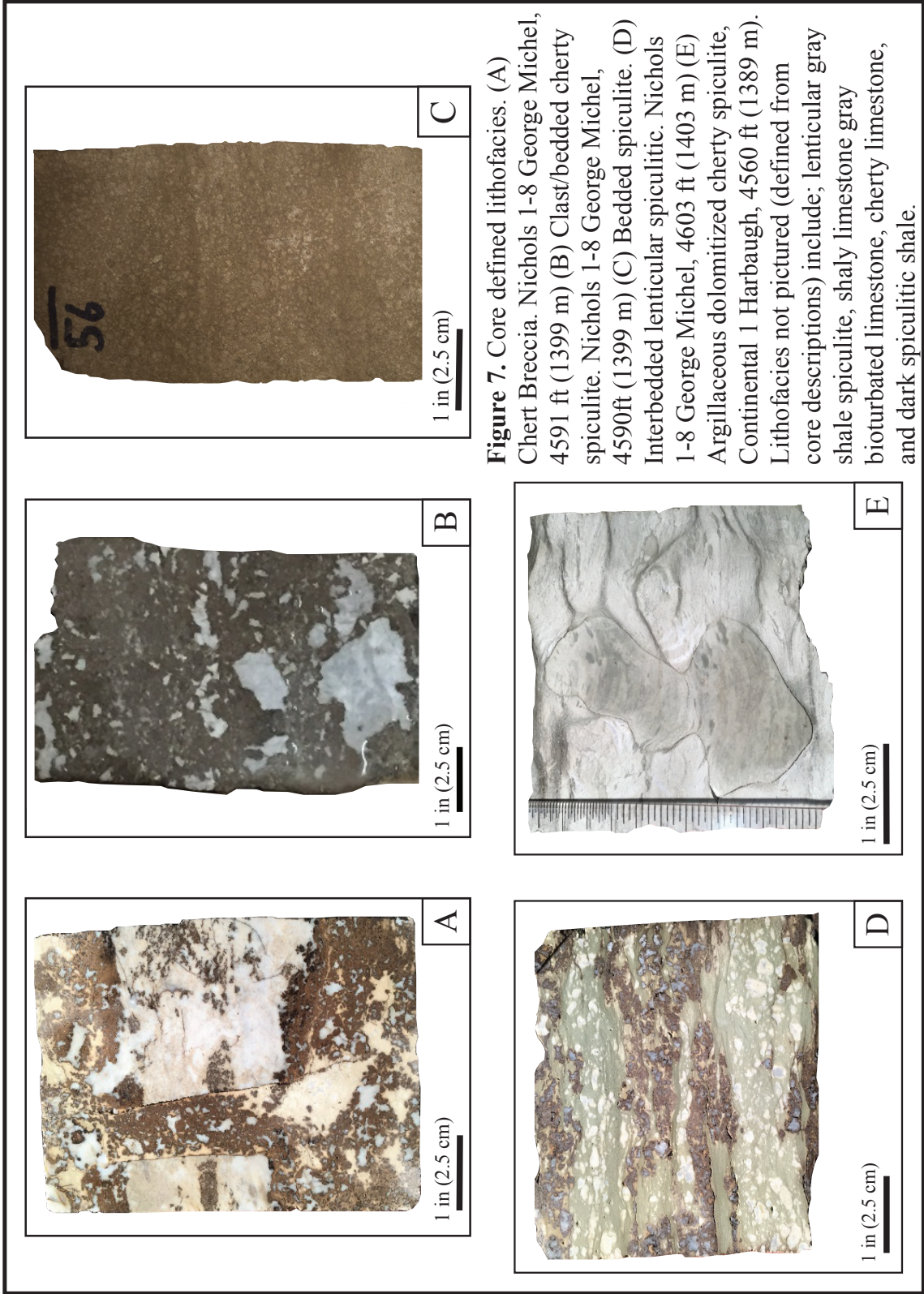


Figure 7. Core defined lithofacies. (A) Chert Breccia. Nichols 1-8 George Michel, 4591 ft (1399 m) (B) Clast/bedded cherty spiculite. Nichols 1-8 George Michel, 4590ft (1399 m) (C) Bedded spiculite. (D) Interbedded lenticular spiculitic. Nichols 1-8 George Michel, 4603 ft (1403 m) (E) Argillaceous dolomitized cherty spiculite, Continental 1 Harbaugh, 4560 ft (1389 m). Lithofacies not pictured (defined from core descriptions) include; lenticular gray shale spiculite, shaly limestone gray bioturbated limestone, cherty limestone, and dark spiculitic shale.

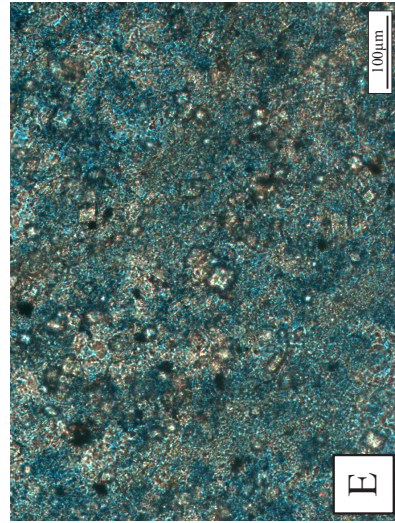
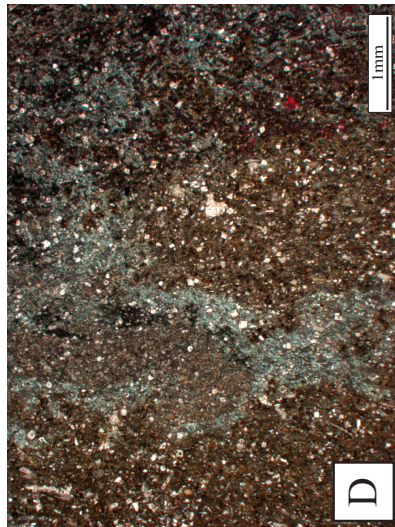
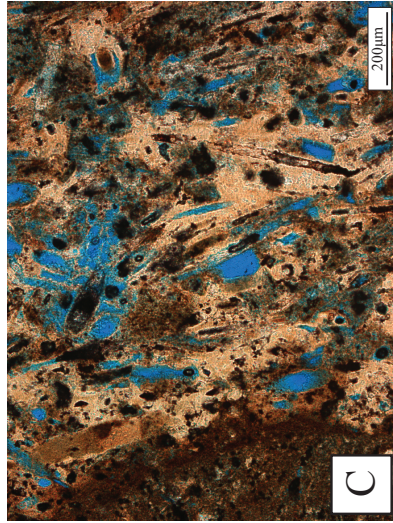
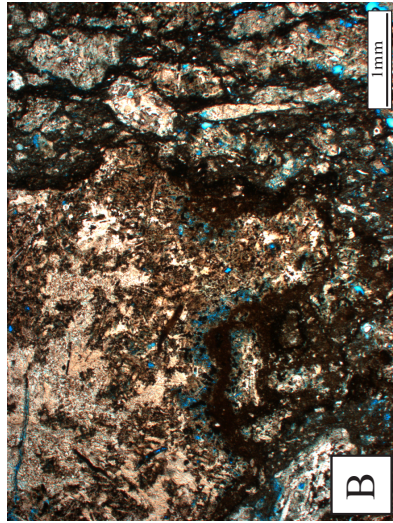
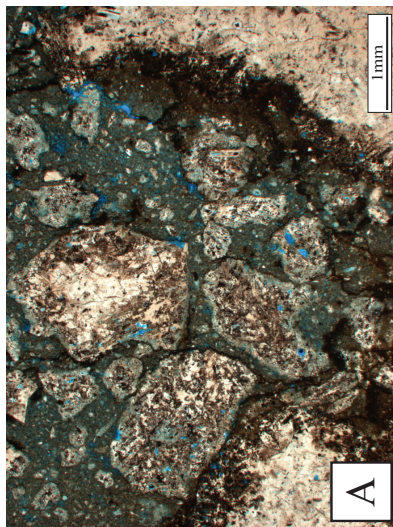


Figure 8. Representative thin-section photomicrographs of each core defined lithofacies. (A) Chert Breccia showing small angular chert clasts within a green shale matrix. (B) Clast/bedded chert spiculite. (C) Bedded spiculite showing vuggy and modic porosity from spicule dissolution. (D) Interbedded lenticular spiculite showing silicified green shale matrix and remnant calcite grains. (E) Argillaceous dolomitized cherty spiculite.

Lithology	Lithofacies	Description	Relative Log Response	Depositional Setting
Tripartite Chert	Chert Breccia	Angular grain supported chert clasts in a silicified shale matrix. Chert clasts are composed of amalgamated silicified spicules. Three generations of chertification are apparent.	Low GR, Low RESD, Low PE, DPPI > NPHI	Diagenetically formed through autobrecciation, karstification, and/or solution collapse related to subaerial exposure
	Clas/Bedded Chert Spiculite	Irrregular opaque chert clasts occasionally forming continuous beds within dark brown spiculite and clay rich layers. Pervasive microcrystalline quartz replacement.	Low GR, Low RESD, Moderate Porosity	Inner-ramp, shallow water deposits. Post positionally altered
Green Shale Spiculite	Bedded Spiculite	Disarticulated silicified spicules with little to no shale content. Occasional inclined laminations.	Low GR, Low RESD, Moderate Porosity	Inner to mid-ramp, moderate energy deposit with consistent wave agitation, common sponge bioherms.
	Interbedded Lenticular Spiculite	Wavy laminations of continuous and discontinuous green shale heterolithically interbedded with lenses of spiculite rich wackestone to packstone.	Low to Moderate GR, Low RESD, Moderate to low porosity	Mid-ramp, moderate to shallow water environment with periodic wave agitation. Suboxic conditions, common sponge bioherms.
Gray Shale Spiculite	Argillaceous Dolomitized Cherty Spiculite	Deformed layers of light gray chert replaced spiculite within a dark gray argillaceous dolomitic matrix. Commonly bioturbated.	Moderate GR, Moderate RESD, Moderate to low porosity	Mid to outer ramp facies deposited under relatively quiescent conditions
	Lenticular Gray Shale Spiculite	Dark gray shaly lime mudstone interbedded with lenses of fine grained spiculite.	High GR, Moderate RESD, NPHI > DPPI	Mid to outer ramp facies. Anoxic conditions
Limestone	Gray Bioturbated Cherty Limestone	Medium to light gray wackestone to packstone with variably sized horizontal and subvertical burrows. Common small opaque chert nodules observed.	Low GR, High RESD, Low Porosity	Inner-ramp, shallow water deposit with rare instances of subaerial exposure.
	Shaly Limestone	Green to gray shaly lime mudstone to wackestone. Commonly bioturbated.	Low to Moderate GR, High RESD, Low Porosity	Inner ramp, moderate to shallow water deposit. Slow sedimentation.
Shale	Dark Spiculitic Shale	Medium to dark gray shale with occasional faint laminations. Scattered spicules are	High GR, Moderate to Low RESD, NPHI >> DPPI	Deep water, outer ramp deposit dominated by pelagic sedimentation.

Table 1. Summary of dominant lithofacies present in the Mississippian section within the area of study. There are a total of 9 lithofacies, which are grouped into 5 lithologies. Groupings are based on common responses in order to obtain differentiable classes necessary for electrofacies classification. Lithofacies described from firsthand cored descriptions include; chert breccia, clast/bedded chert spiculite, bedded spiculite, interbedded lenticular spiculite, and argillaceous dolomitized cherty spiculite. Remaining lithofacies are inferred from core descriptions for two logged wells within the study area (Woosley B-1 Wiley and Woosley A-5 Oakes).

degree of silicification or dolomitization. A mineralogic analysis of lithofacies shows striking compositional similarities. Despite a limited sample size, XRD, FTIR, and SEM all show very high abundances of microcrystalline quartz with only minor components of calcite, dolomite, ankerite, and clay minerals for all core defined lithofacies (lithofacies 1-5 listed above) (Appendix B). In light of these similarities, lithofacies have been grouped into broader, categorical lithologies. These lithologies include 1) tripolitic chert, 2) green shale spiculite, 3) gray shale spiculite, 4) limestone and 5) shale. Grouping of lithofacies into parent lithologies is summarized in Table 1.

Electrofacies Estimation

In the area of study, lithofacies of similar lithologies are not discernable by their log signatures, as they are often based on fine-scale properties including bedding type, grain texture, sedimentary structures and minor ancillary components. Because lithofacies share gradational boundaries, different lithofacies can be very similar to one another. Only after being grouped into parent lithologies do individual classes become resolvable by log response (Appendix C-13). Therefore, the specific focus of this study is on the prediction of lithologies, as opposed to lithofacies.

Electrofacies classifications are used to estimate lithology in non-cored wells in order to aid in correlation and construct 3-D models that show spatial changes in lithology throughout the study area. The accuracy of electrofacies classifications are measured by comparing estimated lithologies to core-defined lithologies for control wells. These comparisons are carried out through confusion matrices. A visual comparison of accuracies for key wells are presented in Appendices C-1 through C-3. A confusion matrix is a tool used to evaluate the effectiveness of various forms of

artificial intelligence (Ting, 2011; Allen and Pranter, 2016). By charting predicted classes in columns and measured, or actual classes in rows, confusion matrices are able to quickly identify and quantify instances of successful and unsuccessful classification. Overall accuracy values are obtained by dividing the number of correctly predicted classes by the total number of predicted classes. Similarly, the prediction accuracy of individual classes can be calculated by dividing the number of correctly predicted instances for a particular class by the actual number of instances of that class. This is known as user's accuracy (Janssen and van der Wel, 1994).

This study compares the ability of three trained classifiers to correctly predict lithology (electrofacies class) in control wells. Both overall accuracy and user's accuracy are used to compare predictive capabilities of ANN's, kmeans clustering, and KNN clustering for various combinations of inputs. The effectiveness of four different well-log assemblages are compared, as summarized in Figure 9. These assemblages were chosen based on their availability in wells across the study area and their distinctive ties to specific lithologies. As with most data sets, wells used for this study do not all have identical log suites. This means each specific combination of logs will necessarily apply to a different number of wells. If too few wells are used, the resulting lithology model is negatively influenced by lengthy interpolation distances associated with data sparsity. A careful balance must be achieved between using the most descriptive inputs and ensuring representative data coverage. Therefore, the numbers of wells available for modeling are included in Figure 9, and are used as a factor in determining which well-log assemblage is ultimately best able to represent the subsurface.

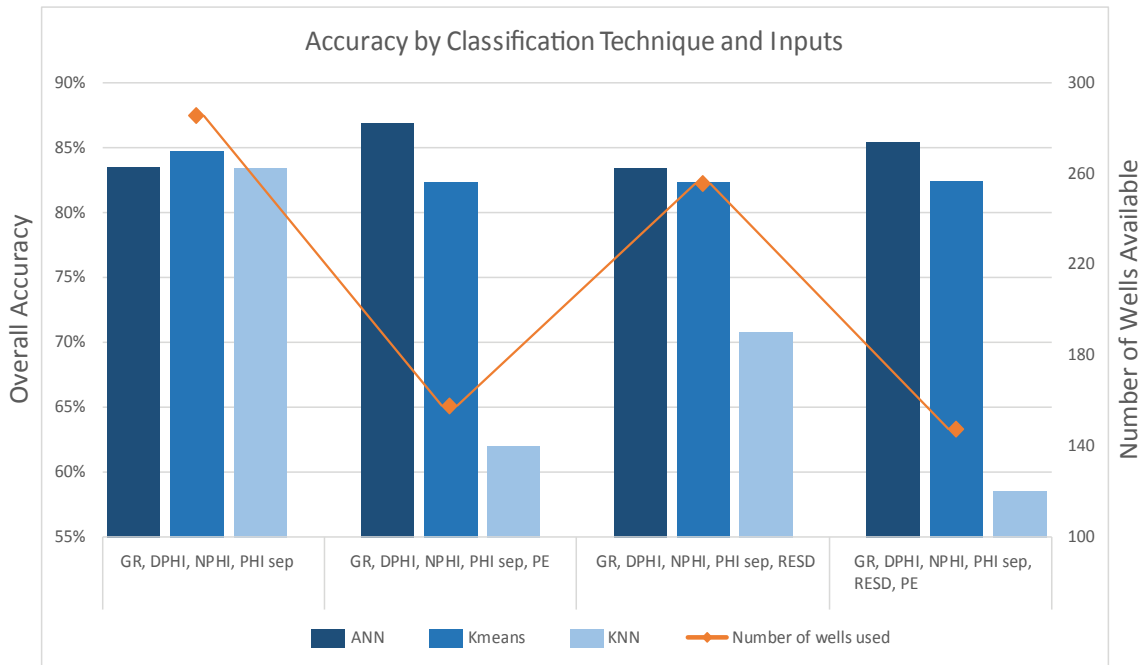
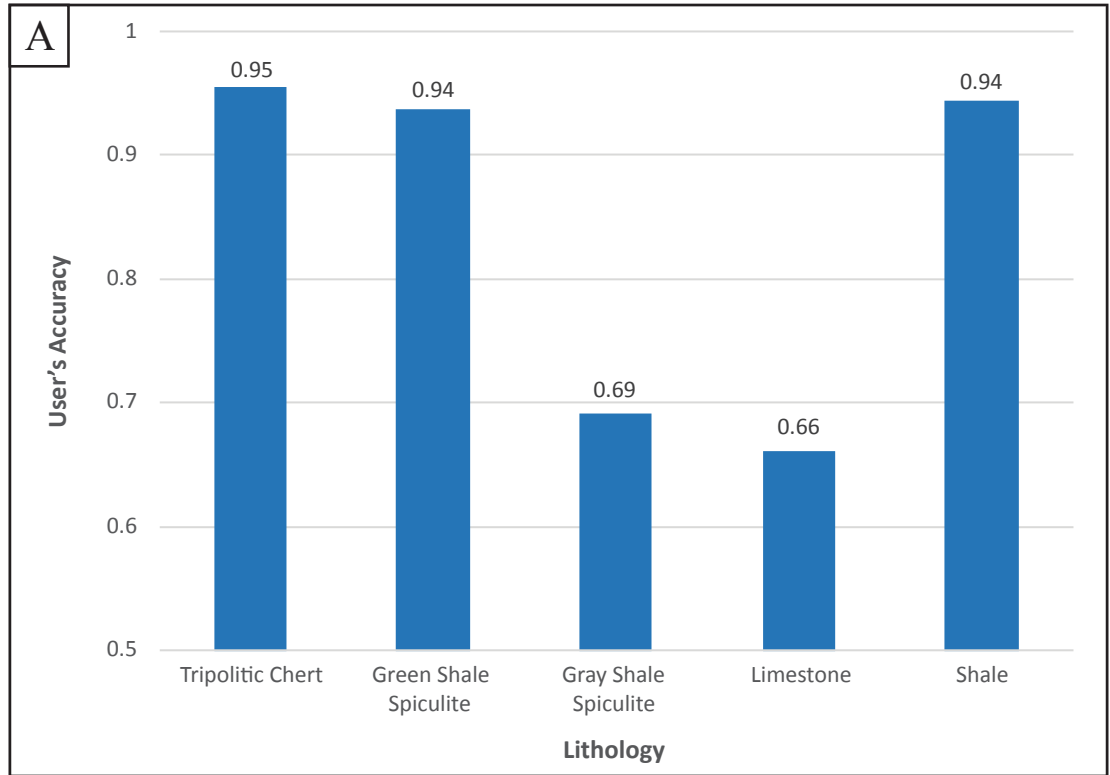


Figure 9. Chart comparing overall accuracies of electrofacies classification techniques for each set of log curves used as inputs (GR: Gamma Ray; DPHI: Density Porosity; NPHI: Neutron Porosity; PHI sep: NPHI DPHI separation; RESD: Deep Resistivity; PE: Photoelectric Effect). Diamonds represent the number of wells that contain each set of inputs. This is used as an estimate to compare how well each set of inputs is able to cover the area of study.

Prediction of lithologies through artificial neural networks (ANN) yielded high overall accuracies, with a best case of 87% when using the GR, DPHI, NPHI, PHI Separation, PE assemblage (Figure 9). User's accuracies for this case were 90.5%, 95.5%, 68.8%, 69.2%, and 94.8% for chert breccia, green shale spiculite, gray shale spiculite, limestone and shale, respectively. A confusion matrix (Figure 10) shows that lower accuracies associated with gray shale spiculite are due to confusion in differentiating green shale and gray shale spiculite. These two lithologies are very similar and tend to grade into one another, so some difficulty distinguishing them in logs is not unexpected. Low user's accuracy for limestone stems from failures to classify the Pierson Limestone, which can be relatively shaly and cherty generating similar log responses to spiculite lithologies. Issues with predicting these specific lithologies persisted regardless of classification technique or input assemblages used. ANN's seemed to produce the most consistent results, remaining relatively unaffected by additional input logs. In fact, the lowest overall accuracy given by ANN was 83%, only 4% worse than its highest.

Kmeans clustering provided an overall accuracy of 85% using the simplest set of inputs (GR, DPHI, NPHI, PHI Separation). In fact, this exceeded the overall accuracy of the ANN using the same inputs (83%). Individual user's accuracies were 95.5%, 93.7%, 69.1%, 66.1%, and 94.4% for chert breccia, green shale spiculite, gray shale spiculite, limestone and shale, respectively. Other combinations of logs produced marginally lower accuracies than those achieved through neural network. The negligible difference of these results is somewhat surprising. Supervised classification techniques are generally assumed to outperform unsupervised methods (Dubois et al., 2007) as they



B

Predicted Lithologies	Actual Lithology				
	Tripolitic Chert	Green Shale Spiculite	Gray Shale Spiculite	Limestone	Shale
Tripolitic Chert	274	1	0	0	6
Green Shale Spiculite	13	598	213	42	1
Gray Shale Spiculite	0	27	484	35	31
Limestone	0	0	0	162	0
Shale	0	12	3	6	635
User's Accuracy	95.47%	93.73%	69.14%	66.12%	94.35%

Figure 10. (A) Histogram showing how well each lithology was predicted using PCA Kmeans clustering. Tripolitic chert, green shale spiculite, and shale were predicted very well, with accuracies over 90%, while gray shale spiculite and limestone were not as easily identified. (B) Shows the confusion matrix with user's accuracies as well as common misclassification errors. Blue highlighted cells represent correctly classified classes, while all other cells indicate incorrect classifications. Gray shale spiculite was often misclassified as green shale spiculite, while limestones were confused with both green shale spiculite and gray shale spiculite lithologies. Similar plots for ANN and KNN techniques can be found in Appendices C 8-11.

are trained with hard data, whereas the unsupervised methods used for this study are trained with soft data (logs). These results confirm that individual lithologies in the Mississippian section have distinct, distinguishable log responses. In other words, there is a very good correlation between grouped lithologies described in core and what can be observed in well logs.

KNN clustering was a capable, but highly inconsistent, method of lithology prediction. For the simplest set of inputs (GR, DPHI, NPHI, PHI Separation), KNN yielded an overall accuracy of 83% with the chert breccia, green shale spiculite, gray shale spiculite, limestone and shale lithologies giving user's accuracies of 95.9%, 90.4%, 70.1%, 61.2%, and 93.8% respectively. In comparison, when using the most complex combination of inputs (GR, DPHI, NPHI, PHI Separation, RESD, PE) a meager overall accuracy of 58% was achieved. Thus, despite using PCA to reduce dimensionality, the introduction of additional inputs for KNN clustering obscures prediction capabilities. It is possible these accuracies could be improved by adjusting the K value, however this was not tested as part of this study due to software limitations.

Three control wells are used to assess correctness; the Woosley A-5 Oakes, the Woosley B-1 Wiley, and the Woosley C-1 Miller. The first two represent full cored wells, from which detailed descriptions were obtained (Mazzullo and Wilhite, 2016, personal communication). The third well, Woosley C-1 Miller, was added to account for inconsistent log suites between the two cored wells. A cuttings log for this well provided fairly detailed descriptions of lithology, which was used to validate predicted classes. Additional validation of predicted lithologies was derived from a neutron-

density cross plot (Appendix C-4). Plotting relative mineralogic concentrations not only highlights the compositional uniqueness of each lithology, but also reinforces some of the mineralogic observations made in core and thin section samples. For example, abundant dolomite rhombs were observed in thin sections of lithofacies within gray shale spiculite (Figure 8E), which is supported by the plotted data's proximity to the theoretical dolomite line.

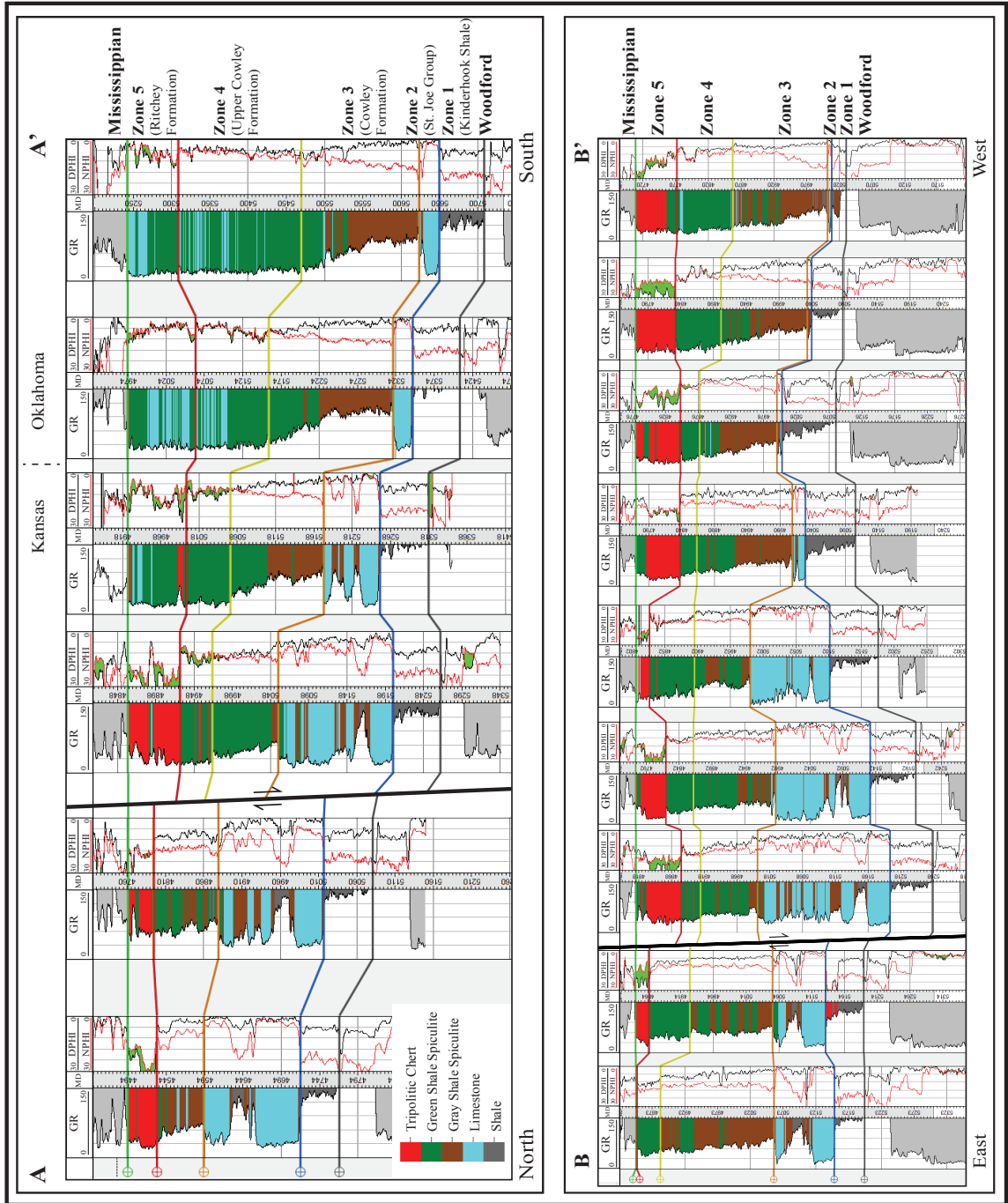
Despite the accuracy attained by electrofacies classification techniques in this study, there are significant limitations that must be addressed (Appendix C-5).

Stratigraphic and Structural Framework

The complex stratigraphic architecture of the Mississippian interval calls for a detailed interpretation of stratigraphic variability in terms of age, formation, and depositional process through detailed well-log correlations guided by core data, revealing log manipulations, and the results of electrofacies classifications (Figure 11).

The Mississippian section was separated into five major stratigraphic zones which are correlated across the study area. These intervals are characterized on wireline logs by distinct GR, RESD, DPHI, NPHI, and PE values. Divisions between interpreted zones generally correspond to formational boundaries, but can also be tied to changes in depositional environment elicited by Milankovitch scale (3rd-order) cyclicality.

The basal zone (zone 1) is recognized by an approximately 75 ft (23 m) thick shale-rich Kinderhookian package. This interval displays generally high gamma ray values (above 125 API) that show a slight cleaning upward trend. High NPHI and DPHI separation along with PE values between 3 and 4 are characteristic of a shale dominated interval. Core data show these deposits are dark silty, spiculitic shales with variable



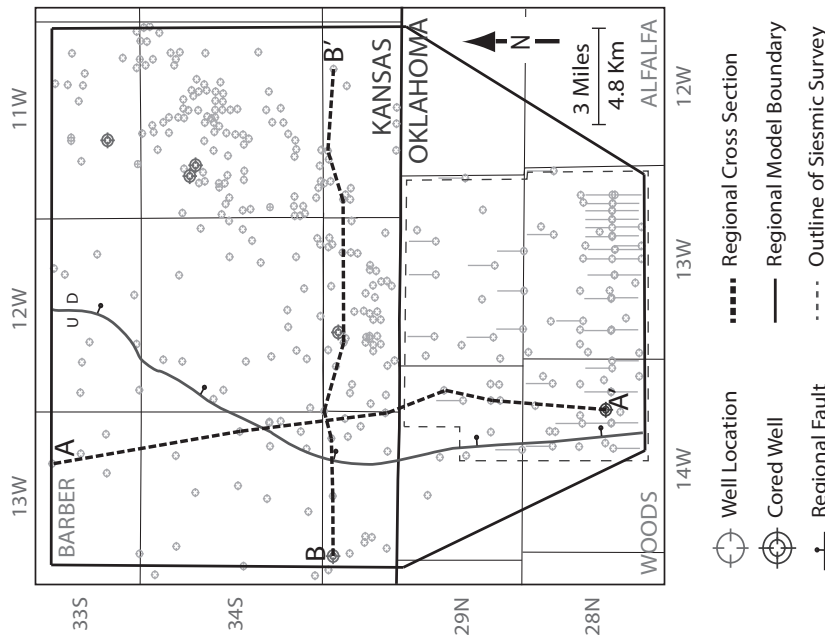


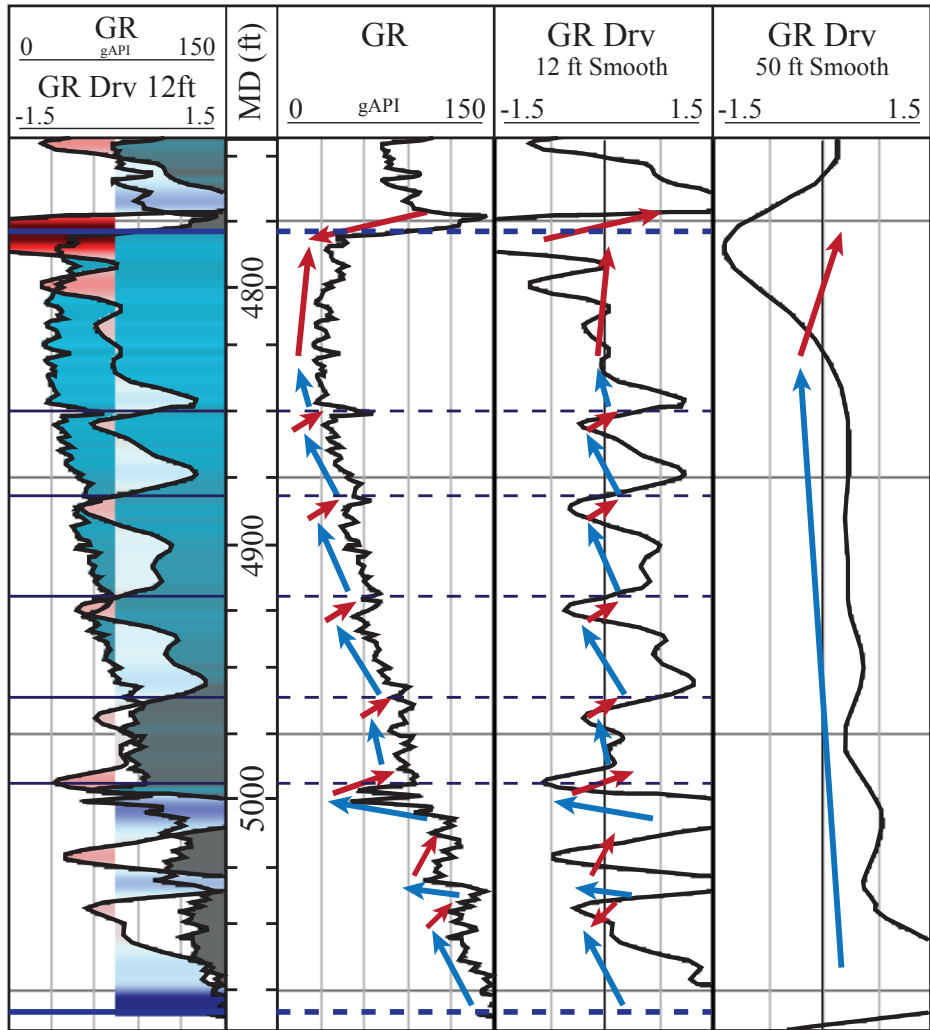
Figure 11. Regional cross sections through the area of study flattened on the top of the Mississippian with major stratigraphic zones correlated. GR track shows results of electrofacies classifications, which were used as a guide to aid in correlation. Inset map on the left for reference (A) North-south oriented cross-section showing increasing thickness to the south as well as changes in log character that represent lithologic and depositional variations. There is an increase in thickness on the downthrown (south) side of the major fault. (B) East-west oriented cross section showing increases in thickness on the downthrown side of the fault, as well as changes in log character suggesting a downdip direction to the west. Zone 2 (equivalent to Compton, Northview, and Pierson deposits of the St. Joe Group) thin out to the west, which is attributed to unconformity related erosion beneath the Cowley as well as a more distal depositional setting.

pyrite content. Moderate to deep water fossils suggest an open shelf, marine depositional environment (Mazzullo et al., 2016), which aligns with late Devonian – early Mississippian deep euxinic seas described by Northcutt et al. (2001). During this time, it is likely that water level was slowly dropping with a progressively decreasing rate of subsidence (Feinstein, 1981). In correspondence with this gradual sea-level drop, zone 1 is characterized by mild regression. Formationally, this interval is interpreted as the Kinderhook Shale (sometimes referred to as the Hannibal Shale in Kansas).

The second zone is characterized by carbonate packages separated by a shale, and has a highly variable thickness ranging from 0 to 210 ft (0-64 m). Thickness of this zone appears to be both structurally and stratigraphically controlled, with thick intervals observed near the downthrown side of a major north-south trending fault, and rapid thinning toward the east and south (Figure 11). Zone 2 is stratigraphically equivalent to the units of the St. Joe Group. In the area of interest, the St. Joe Group includes three components; the Compton Limestone, Northview Formation, and Pierson Limestone. Zone 2 was therefore subdivided accordingly. The basal subdivision (equivalent to the Compton Limestone), is a laterally continuous tight limestone of variable thickness that records characteristic high RESD and PE values (>20 ohm m and ~5 respectively). The Compton is composed mainly of gray bioturbated cherty limestone and core samples show a range of shale content (Mazzullo et al., 2016). The transition to this zone likely represents a rapid drop in sea level from an open-marine environment to an inner-ramp shallow-water setting. The second subdivision of zone 2 includes the Northview Formation. This relatively thin interval, up to 20 ft (6 m) thick, can be locally absent. Log responses are similar to zone 1, distinguished only by slightly lower GR values.

Thin lenses of bioturbated wackestone to packstone occur near the base and middle of the formation. Core samples reveal a dark, shaly lime mudstone with common crinoid and bivalve fragments (Mazzullo et al., 2016). This subzone represents a transgressive event, returning to a deep-water setting. The final subdivision of zone 2 is characterized by low GR and porosity values, along with a moderate to high RESD, similar to the underlying Compton Limestone. This interval is equivalent to the Pierson Limestone, and is highly variable in terms of thickness, reaching up to 150 ft (46 m). In core samples the Pierson is a medium gray to tan limestone that contains fairly common gray and green shale layers (Mazzullo et al., 2016).

The third major stratigraphic zone can be distinguished by a gradually cleaning upward GR signature, as well as an increasing DPHI and static NPHI. This interval is relatively thin toward the north (25 ft, 8 m), and can reach thicknesses of up to 250 ft (76 m) near central and eastern areas. The transition from zone 2 to zone 3 marks a transgressive event and the beginning of a new set of cycles, likely deposited under silica and nutrient-rich water conditions. Three to four internal cleaning upward cycles are recognizable in GR curves within this zone (Figure 12). These cycles are not consistently present across the study area due to erosion, non-deposition, or diagenetic overprinting. Cyclic profiles become increasingly well-defined toward central and eastern locations, where the zone is thickest, and thinning of the underlying St. Joe Group is evident. In general, cycle thickness tends to decrease toward the south, and overlying cycles extend further south than underlying ones forming a prodgradational architecture. This zone thins and moves down section toward the south into Oklahoma, where GR values tend to increase, indicative of a deeper water environment. Core



- Decreasing process energy
- Increasing process energy

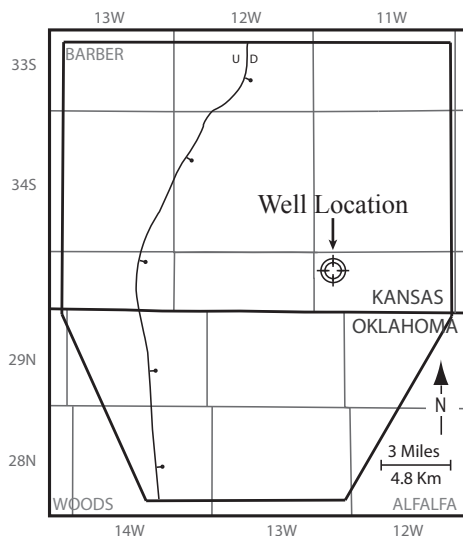


Figure 12. Identification of Mississippian cycles aided by gamma ray derivative curves (GR Drv). The first track shows a GR curve overlain by its derivative curve to highlight possible regressive (coarsening upward) and transgressive (fining upward) intervals. The second and third tracks show the same curves separated and annotated with relative changes in process energy, where blue arrows represent increases in process energy and red arrows indicate decreases. For this study, it was determined that GR Drv with a 12ft smoothing window approximates 3rd order cycles, while using a 50 ft smoothing window represents 2nd order cyclicity (shown in track 4). In this region of the model area, several 3rd order cycles are well defined from gamma ray motifs.

samples show a general decrease in shale content upward, from dark gray shale at the base to pale green shale near the top. Depending on location, the St. Joe Group (zone 2) is unconformably overlain by either the Reeds Spring Limestone or the heterogeneous Cowley Formation. Log signatures of the Reeds Spring and lower Cowley are nearly identical (Mazzullo et al., 2016), so differentiating between them is a difficult task without adequate core coverage. Based on regional interpretations from Mazzullo (2009) and Wilhite and Mazzullo (2013), the Cowley is believed to dominate in the area of study. Stratigraphically, the Reeds Spring should be encountered before the Cowley Formation, however the base of the Cowley represents a major unconformity (Mazzullo et al., 2009; 2016), so the potential for associated underlying erosion favors the presence of Cowley over Reeds Spring. Erosion related with this unconformity is also responsible for the thinning of the St. Joe Group to the east. While the Cowley has been observed to overlay units of various ages from Devonian to Mississippian, the youngest observed underlying deposits are latest Osagean in age (Lee, 1940; Mazzullo et al., 2016). This stratigraphically dates the Cowley as earliest Meramecian.

The fourth zone is recognized by low GR values (<30 API) and very little to no DPHI-NPHI separation. Towards the south, this interval reaches 175 ft (53 m) in thickness, while towards the north, it is completely absent (Figure 11A). This zone contains green shale spiculite, limestone, and tripolitic chert lithologies depending on location, and is interpreted as a shallow-marine environment with relatively static process energy. Occasional porosity spikes within this zone may indicate intermittent periods of subaerial exposure. This zone is interpreted as Meramecian in age, corresponding to the upper portion of the Cowley Formation toward the north and lower

Meramecian limestones toward the south.

The uppermost zone is very high porosity (~30%), low density interval, whose irregular lower and upper boundaries can generate widely varying thicknesses over short distances. At its thickest, zone 5 reaches roughly 75 ft (23 m). This interval lies directly below the sub-Pennsylvanian unconformity, and is also bounded by a basal unconformity. Recent stratigraphic examinations from Mazzullo et al. (2016) describe a similar interval as the Meramecian Ritchey Formation. This zone is highly diagenetically influenced, showing definitive signals of subaerial exposure in both core and logs. Core samples are composed of brecciated chert, which can originate from autobrecciation, karstification, and solution collapse processes (Montgomery et al., 1998; Rogers, 2001; Watney et al., 2001; Ramaker et al., 2014; Birch, 2015). The zone changes character down-dip to the south, where GR becomes cleaner and porosity decreases, reflecting an environment of deposition less prone to subaerial exposure.

As a whole, the Mississippian section thins significantly towards the north in accordance with increased up-dip erosion from the sub-Pennsylvanian unconformity. Thickness variations of each of the five major stratigraphic zones observed from log correlations and isopach maps reveals a uniform, flat lying zone (zone 1) over which successive intervals prograde southeastward (zones 2 through 4). The uppermost zone unconformably overlies these prograding units. This stratigraphic architecture is the product of several key factors including erosion, structural tilting, shifts in depositional setting, and sedimentation dictated by a slowly regressing sea level. Implicit in this architecture, the Cowley Formation is correlated to the south into Oklahoma. This is significant when considering the recent assignment of the formation as Meramecian in

age (Mazzullo et al., 2016). Currently, most subsurface interpretations in northern Woods County suggest the Mississippian interval contains a significant Osagean section with a comparatively minor interval of overlying Meramecian (Nissen et al., 2004; Costello, 2014; Lindzey, 2015; Montalvo, 2015). Correlations from this study, however, imply most of the Mississippian interval observed south of the Kansas-Oklahoma border is actually Meramecian (or younger) in age (Appendix D). A lack of conodonts to biostratigraphically age-date the Cowley Formation means there is a heavy dependence on log correlations, which have an intrinsic level of subjectivity. Despite this uncertainty, reasonable ties can be made from comparing closely spaced logs, which place the base of the early Meramecian Cowley Formation just above the Compton Limestone in northeast Woods County (Figure 11). These correlations suggest that for the area of study, the Mississippian subcrop should be entirely represented by Meramecian units.

The Mississippian interval comprises a single 2nd-order cycle with several higher-order cycles embedded (Figure 12) (Sloss, 1963). Much like the interpreted stratigraphic zones described above, these cycles are believed to form clinoformal geometries, with successively younger cycles progressing southward (LeBlanc, 2014; Jaeckel, 2016). In this study, 3rd-order cycles are interpreted based primarily on lithologic transitions as approximated by log signatures (GR trends in particular). Two major cycles are inferred within the basal two stratigraphic zones (lower Mississippian). The first is represented by the abrupt transition from deep-water shales associated with the Kinderhook zone to shallow-water carbonates of the Compton Limestone. Immediately overlying exists a second, similar cycle in which the Northview Formation

shale grades into the shallow Pierson Limestone. Younger, upper Mississippian cycles are more gradational in character. Within zone 3 (Cowley Formation), up to four stacked cleaning-upward GR signatures are noted, equivalent to the depositional cycles described by Watney et al. (2001) and Jaeckel (2016). These cycles represent gradual facies variations associated with a narrow range in depositional settings, where mid- to outer-ramp shales are overlain by mid- to inner-ramp spiculites. Interruption of cycles by frequent and prolonged episodes of subaerial exposure make identification and correlation of discrete cycles in the uppermost Mississippian difficult. Thus, differing numbers of cycles are observed depending on location.

An examination of sea-level fluctuations (Appendix A-1) and ramp morphology during the Mississippian may help explain the discrepancies between lower and upper Mississippian cycles. The Mississippian period marks a transition from icehouse to greenhouse conditions. Icehouse times (early Mississippian), are characterized by high-amplitude sea-level fluctuations (~ 330 ft or 100 m), whereas greenhouse conditions (latest Mississippian) generally reflect much smaller amplitude oscillations (~33 ft or 10 m) (Moore, 2001). Substantial base-level fluctuations in the early Mississippian align with the shale to limestone transitions observed. Paired with these sea-level changes are common evolutionary growth tendencies of carbonate ramps. During early stages of ramp development, gradients are expected to be very low (0.5° - 2°) as hemipelagites dominate sedimentation. Over time, carbonaceous mud mounds begin to form topographic relief. With continued highstand conditions or gradual sea-level regression, deposition occurs through prodgradational clinofolds that steadily increase in height and volume, creating a progressively steeper platform. Eventually, given the necessary

preexisting topography, biotic components, and time, a low relief homoclinal ramp will transition into a rimmed carbonate platform (Schlager, 1992; Kerans, 2012). In the Mississippian, we do not expect a rimmed platform to develop, in part due to an absence of reef-building biota; however, the transition from a homoclinal ramp during the early Mississippian to a slightly distally steepened ramp by the late Mississippian is likely. This is supported by debris-flow deposits noted in nearby upper Mississippian units (Montgomery et al., 1998; Lindzey, 2015).

Low structural relief and high-amplitude sea-level fluctuation during the early Mississippian provide the potential for vast changes in ramp position caused by base-level rise or fall. An increased slope and attenuated sea-level oscillations by the late Mississippian would narrow the range of ramp settings impacted by an equivalent base-level change. Thus, an increase in ramp slope compounded by a decreasing amplitude of sea-level fluctuations lead to the changing profile of Mississippian cycles. Additionally, it is plausible that the disparity in the nature of upper and lower cycles stems from differences between spiculite and carbonate dominated systems. Though occasional spicules are reported in the lower Mississippian, there is a significant escalation observed in the overlying Meramecian units. In a spicule-deficient carbonate system, shallow-marine limestones can sequentially transition into deeper-marine shales, whereas in a spiculite-dominated system, siliceous bioherms are expected to occupy the intermediate interval between shallow limestones and deep shales (Ehernberg et al., 2001).

Structural Interpretation

Structure-contour maps show structural relief dipping toward the south and

southeast. This supports the regional understanding of an east-west to northeast trending ramp margin giving way to a basin setting toward the south (Figure 1). A major north-south oriented fault cuts through the center of the study area (Figure 3). The fault closely aligns with the western boundary of Hardtner field. This feature was initially identified through seismic in Woods County, where minor offset is detected near the northern edge of the survey. The trend of this offset aligns with high relief areas observed in structure maps to the north. Thus, the fault observed in seismic is continued northward and its position is based on offset in neighboring wells and trends from an isopach map of the Mississippian interval (Figure 13). This isopach shows a clear east to west structurally controlled thickening trend toward the center of the study area. The fault was placed on the western margin of this thickening trend, near maximum gradients of change. Increases in thickness of Osagean limestones on the downthrown block suggest the fault was syndepositional. The fault is assumed to be near vertical based on its profile in seismic, with the western block downthrown by as much as 275 ft (84 m). An orientation parallel to the Pratt anticline may indicate an origin associated with tectonic stresses from the Central Kansas uplift.

A similarly oriented feature has been noted by Watney et al. (2001). They recognized a northeast-southwest-trending structure based on analysis of magnetic and gravity data, which he refers to as “lineament A.” Watney et al. (2001) suggests this lineament could be a basement-involved structure that had multiple periods of reactivation. He argues that the lineament separates an early Mississippian sag basin to the northwest, and a small recessive part of the shelf margin defining the extent of the Cowley Formation to the southeast.

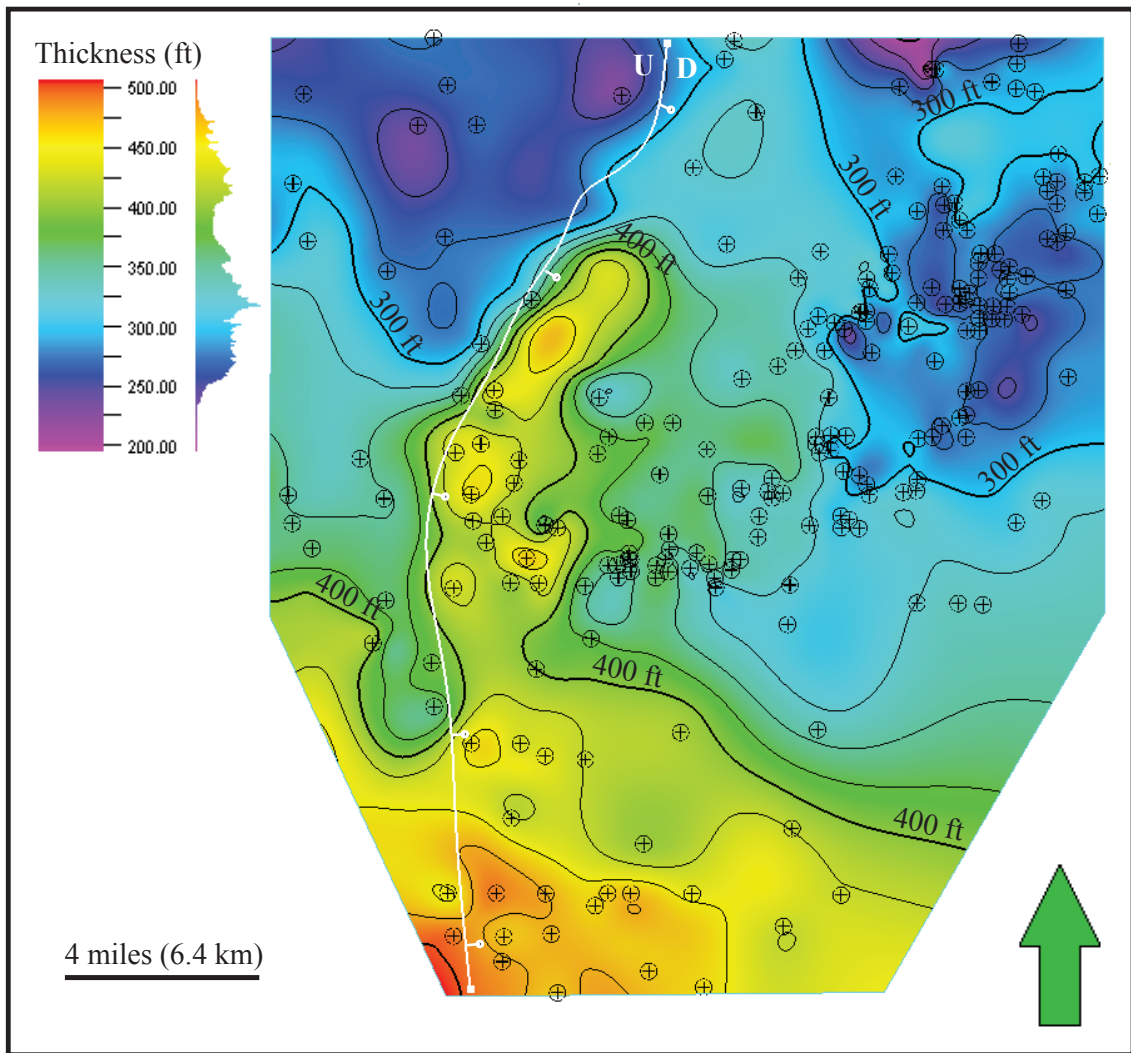


Figure 13. Isopach map of the Mississippian interval showing general thickening toward the south. Increased thickness near the center of the study area was used as a guide when placing the fault trace (shown in white). Thickening across the fault suggests syndepositional timing. Wells used as data points for this map are shown in black.

Spatial Distribution of Lithologies

A 3-D reservoir model using the stratigraphic correlations and structural interpretations described above was populated with electrofacies classification results to reveal spatial tendencies of each lithology (Figures 14F and 15). The Mississippian interval around the mid-continent region overlies the organic-rich Woodford shale. Above the Mississippian are Pennsylvanian shales, conglomerates, and sandstones. In general, the Mississippian section around southern Barber County is characterized by basal shales and limestones overlain by spiculites and cherts. The distribution of lithologies aligns with the progradational architecture observed from the interpreted stratigraphic framework (Figure 15).

The area of interest can be subdivided into 3 representative zones: northwest, northeast, and south (Figure 16). A vertical proportion curve (VPC) for each of these sections was created based on upscaled well logs. A VPC is a chart showing vertical variations in percentages of constituents, and is a useful tool for observing how lithology changes stratigraphically. For the study area as a whole, Figure 16A shows vertical trends in lithology in reference to each major zone.

Following a consistent basal zone composed nearly entirely of shale, zone 2 shows two limestone intervals with an intervening unit of shale and gray shale spiculite. The first limestone unit, the Compton Limestone, is comprised of 79% limestone with minor amounts of gray shale spiculite and shale near the top and base. Above this, the Northview Formation is divided roughly equally between shale and gray shale spiculite (44% and 53% respectively). The second limestone unit, the Pierson Limestone, is 63% limestone with an increased proportion of both green and gray shale spiculite. When the

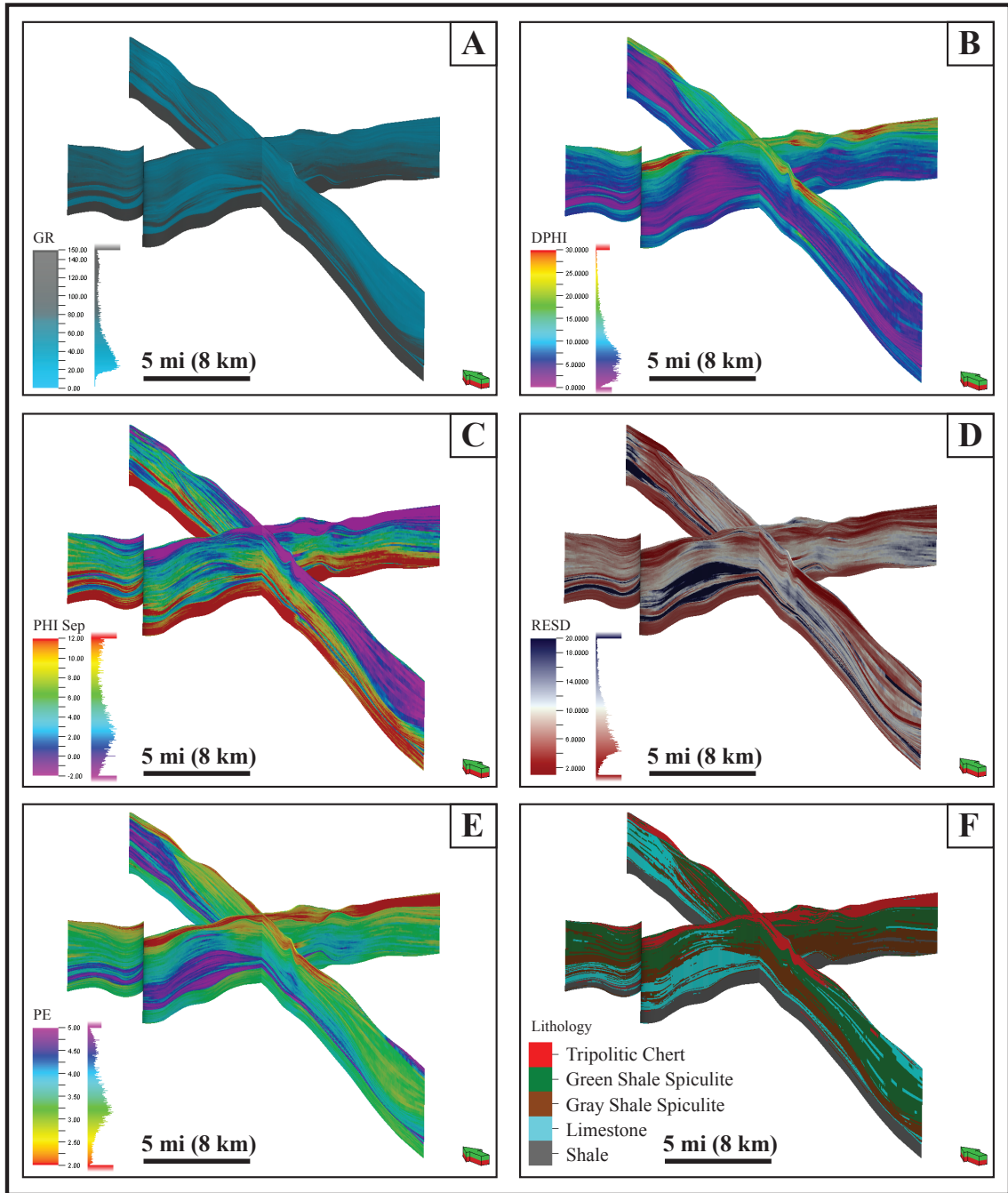


Figure 14. North-south and east-west slices of 3-D model results. (A) GR model (B) DPHI model (C) NPHI-DPHI separation (D) RESD (E) PE model and (F) lithology model using an artificial neural network. Models A through E were used as inputs for electrofacies classification, and when comparing each of these models to the lithology model (F), it is apparent how certain log values control the output lithology classification. For example, areas of low GR, high RESD and high PE on models (A), (D), and (E) closely correspond to limestone in model (F).

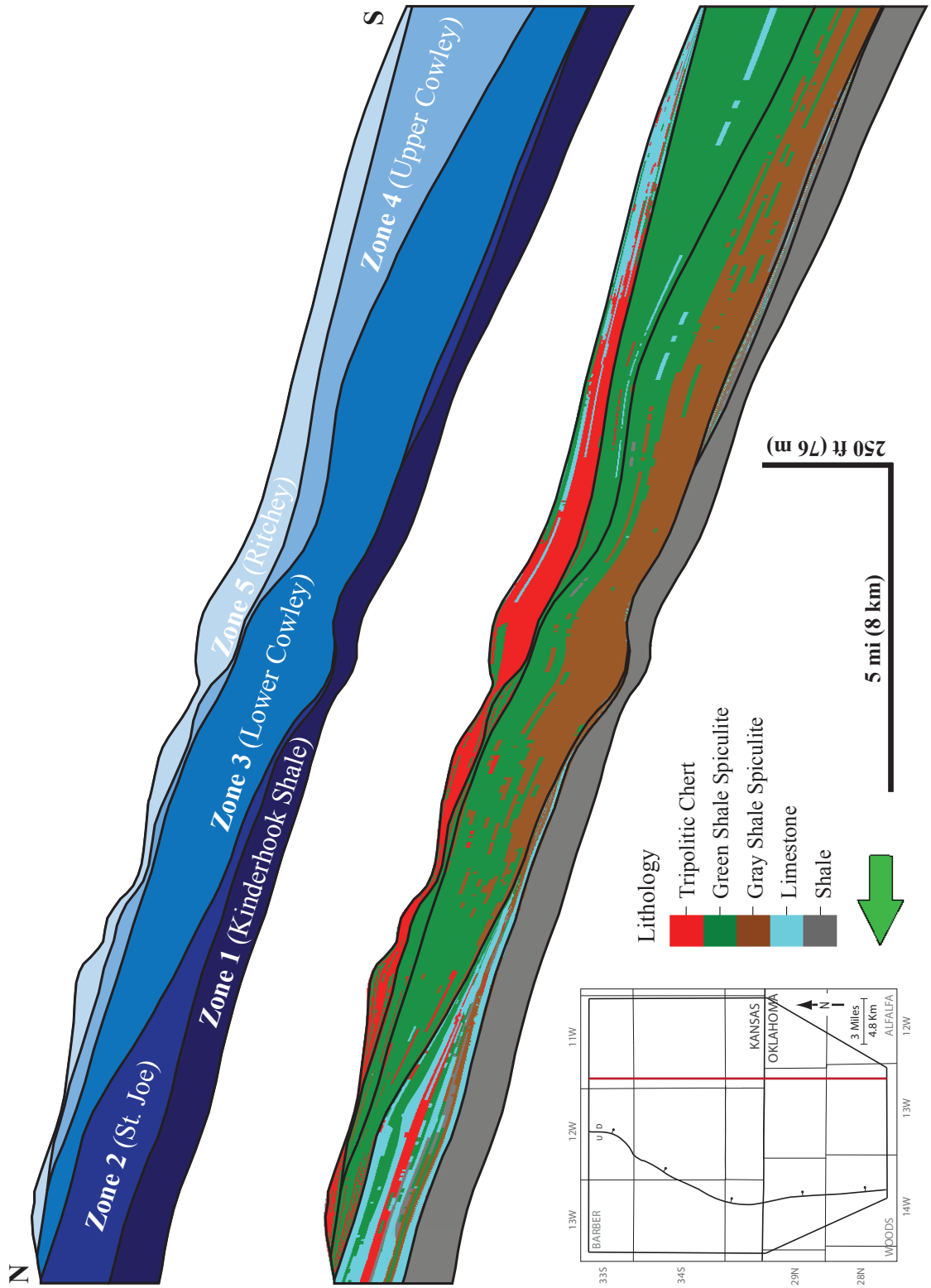
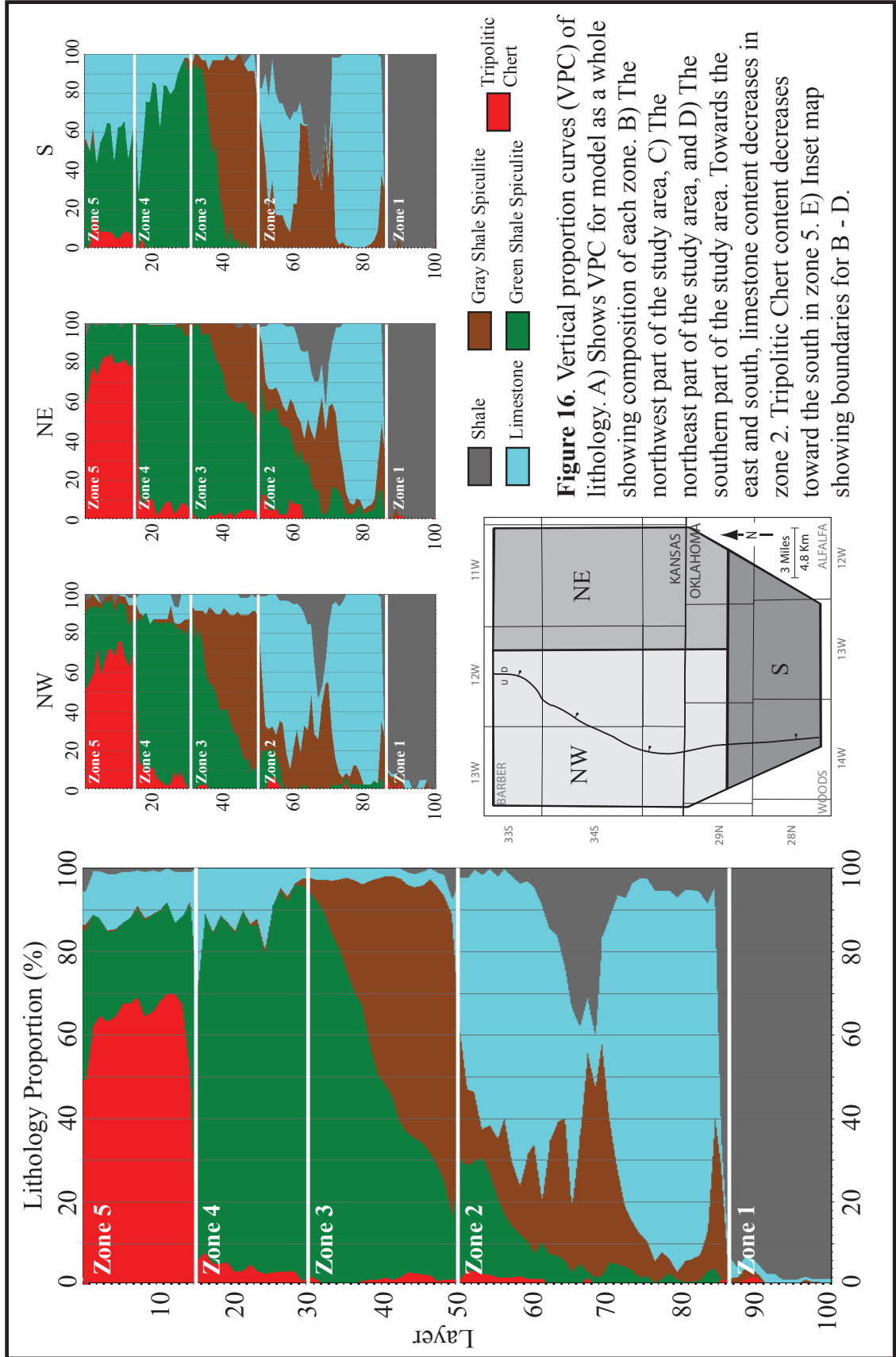


Figure 15. Representative north-south oriented slices of 3-D model results showing stratigraphic architecture. The top slice shows each of the five major stratigraphic zones, with a flat-lying basal zone, progradational geometries of zones 2 through 4, and an overlying zone 5 related to the sub-Pennsylvanian unconformity. The bottom slice shows the lithologic composition of each major zone. Zone 1 is dominated by shale, while zone 2 shows stratigraphically variable lithologies which coincide with the members of the St. Joe Group. Zone 3 is dominantly green shale spiculite towards the north, and transitions into gray shale spiculite southward. Zone 4 is comprised mostly of green shale spiculite, along with minor amounts of limestone toward the south. Zone 5 shows an irregular lower boundary associated with an unconformity, and is composed mainly of tripolitic chert. Towards the south, this tripolitic chert gives way to a limestone rich interval.



study area is partitioned into three zones, certain spatial trends are brought to light. For the northwest area, the overall percentage of limestone in zone 2 is high. This is mostly attributed to a thick, well defined Pierson Limestone that is 75% limestone. In the northeast, the proportion of limestone in the Pierson drops significantly to an average of 36%. In place of this limestone, an increasing quantity of green shale spiculite is observed. This aligns with the erosional pinch out of the Pierson Limestone from a sub-Meramecian unconformity, over which spiculitic Cowley rocks were deposited. Similarly, towards the south the Pierson Limestone is less distinct, while gray shale spiculite and shale become dominant (Figure 15).

Zone 3 is consistent across the study area, transitioning from gray shale spiculite to green shale spiculite. In the northeast, green shale spiculite dominates, while in the south, gray shale spiculite prevails. The northwest displays minor amounts of limestone, which may be attributed to its structurally up-dip topography. This zone marks a shift from dominantly shale and limestone lithologies below, to spiculitic lithologies above. This lithologic transition may suggest a shift in ocean chemistry. Nutrient and silica-rich waters tend to favor spiculite deposition over carbonates (Mazzullo et al., 2009; Ehernberg et. al, 2001; Watney, 2015), so this change may signify increased upwelling of nutrient-rich waters, effectively drowning out the carbonate production. Conversely, zone 3 may represent a deeper water environment, where ocean waters are rich in nutrients. However, based on a regional understanding of 2nd-order shallowing and prodgradational sedimentation, such a shift to deeper settings seems unlikely. The stacked cleaning-upward GR trends that characterize Zone 3 represent oscillating transitions from slightly deeper gray shale spiculites to slightly

shallower green shale spiculites.

The fourth zone is also relatively consistent. The composite VPC (Figure 16A) shows an average of 83% green shale spiculite, with supplementary limestone and tripolitic chert content completing the remainder. The limestone component is derived from the northwest and southern areas. Predominance of green shale in spiculitic rocks within this zone can be an indication of shallower settings in comparison to underlying units.

Zone 5 is characterized by an abundance of tripolitic chert with secondary quantities of green shale spiculite and limestone. This high tripolitic chert content is ascribed to the composition of the northern portions of the study area (especially the northeast). In contrast, there is a very conspicuous decrease in the porous tripolitic chert lithology in towards the south. This is presumably due to a shift in depositional environment to a setting less prone to subaerial exposure. In place of tripolitic chert in the southern area, there is an observable increase in limestone, inferred as unaltered Meramecian carbonates prograding on top of silica-rich spiculite. This change in lithology observed in zone 5 may signify a return to carbonate conducive water conditions.

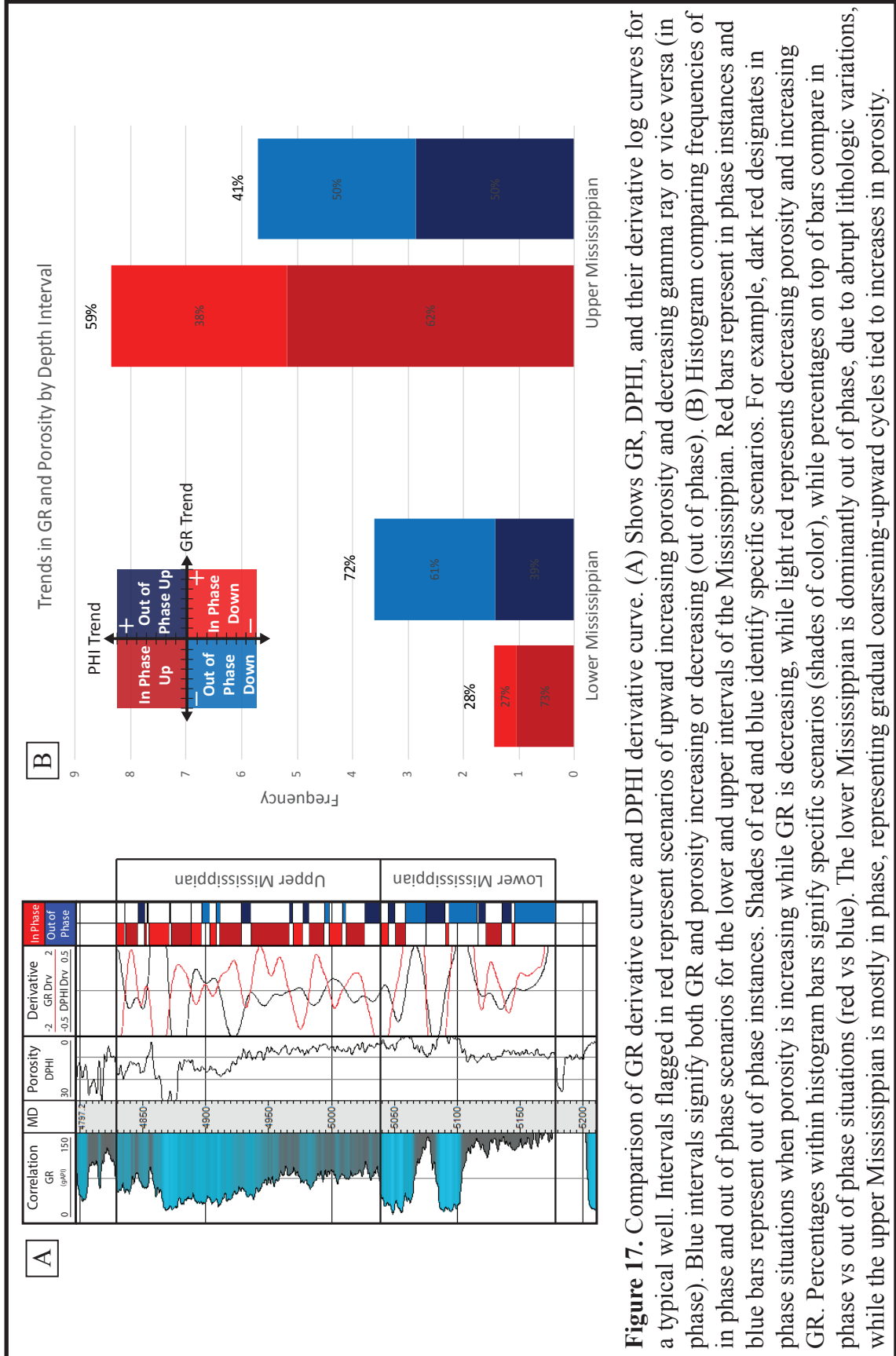
A close visual examination of each petrophysical model (Figures 14 A-E) in comparison to the lithology model (Figure 14 F) reveals how certain combinations of logs were used to predict each lithology. These models effectively characterize the changes in important physical properties observed across the study area, and are instrumental to an improved understanding of the subsurface

Porosity Distribution

Porosity within the Mississippian interval increases upward, grading from low porosity shales and limestones near the base to a highly porous brecciated chert cap. Vertical porosity distribution is examined in detail using derivative trend analysis (DTA) techniques for GR and DPHI curves (Figure 17). Gamma-ray derivatives were compared to DPHI derivatives to uncover the relations between lithology, depositional cycles, and porosity. Both GR and DPHI curves were smoothed in order to isolate the scale of signatures that equate to 3rd-order cycles, removing higher order sequences that are not correlative beyond minor distances (LeBlanc, 2014).

Trends are classified as either “In Phase,” or “Out of Phase” (Figure 17). In phase describes instances where GR and DPHI trends are inversely related. When GR is increasing and DPHI is decreasing, this is referred to as “in phase down,” while decreasing GR and increasing DPHI is labelled “in phase up.” Out of phase represents intervals in which GR and DPHI are directly related. When both trends are increasing, it is categorized as “out of phase up,” and when both are decreasing it is considered “out of phase down.”

The Mississippian is first divided into lower and upper intervals using the base of the Cowley Formation as the partition. Figure 16 shows that the lower Mississippian is out of phase 72% of the time, and the majority of those instances occur when both GR and DPHI are decreasing (out of phase down). In contrast the upper Mississippian is characterized by mostly in phase intervals, which are dominantly in phase up scenarios (that is, cleaner GR signatures corresponding to higher porosities). This difference in porosity is likely a function of the contrasting lower and upper Mississippian cycle



character noted above, with abrupt lithologic interbedding below and gradual facies transitions above. Below the Cowley Formation, the transitions between tight limestone intervals and relatively porous shale intervals results in either increases or decreases in both GR and DPHI, leading to a high proportion of out of phase intervals. The upper Mississippian is comprised of stacked shoaling upward cycles (Watney et al., 2001; Mazzullo et al., 2009; LeBlanc, 2014; Childress and Grammer, 2015) which, in the area of study, can be approximated from decreasing GR motifs (Jaekel, 2016). These shoaling upward trends are generally accompanied by increases in porosity (Figure 17), implying carbonate cycles become gradually more porous upward. This aligns with findings from Watney (2001) and Mazzullo (2009) who have shown that favorable reservoir facies are often found near the tops of cycles, where increasing diagenetically enhanced spiculite is noted. These relationships are further supported by cross plots of GR and DPHI for the upper and lower Mississippian (Appendix C-6). Carbonate cyclicity of this scale is commonly controlled by sea-level oscillations in which regressions deposit progressively shallower water lithologies with lower shale content. The result is a steady decrease in radioactivity (GR curves) that can be roughly tied to regressions. Based on the data in this study, regressive phases of 3rd-order sequences can therefore be connected to vertical increases in porosity in the upper Mississippian. A similar conclusion was ascertained through sequence-stratigraphic investigations of nearby areas (LeBlanc, 2014; Jaekel, 2016).

Lateral porosity trends are observed through 3-D modeling (Figure 18 B). Highest porosity values are found in the northeast portion of the study area, where thick, weathered, and brecciated chert deposits are common. Middle Mississippian (Compton

and Pierson) Limestones are dominant near the downthrown side of the regional fault and grade into slightly more porous spiculitic rocks to the east. This porosity escalation can be linked to the eastern component of the southeast progradational architecture that summarizes regional depositional style. Alternatively, this area may have been susceptible to hydrothermal fluid migration, which can have a porosity enriching effect (Ramaker et al., 2014), however no petrographic evidence was found to confirm this. Towards the south, porosities tend to decrease in correspondence with a reduction in chert breccia facies and prograding limestone-rich Meramecian strata (Figure 18 B).

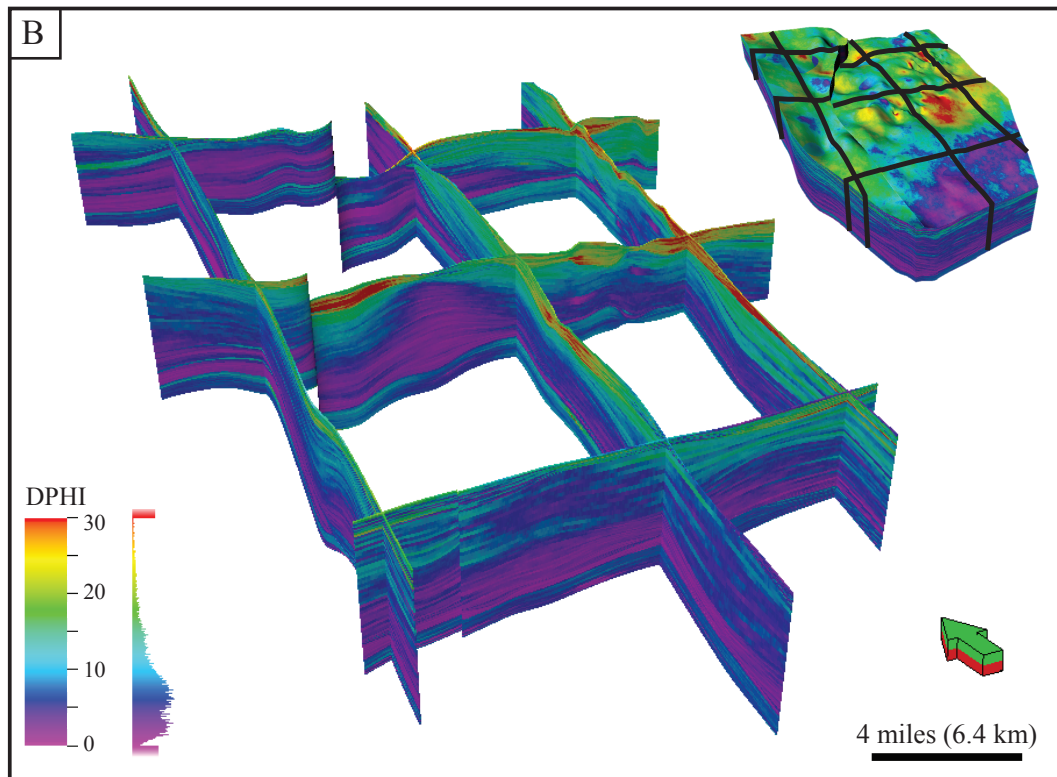
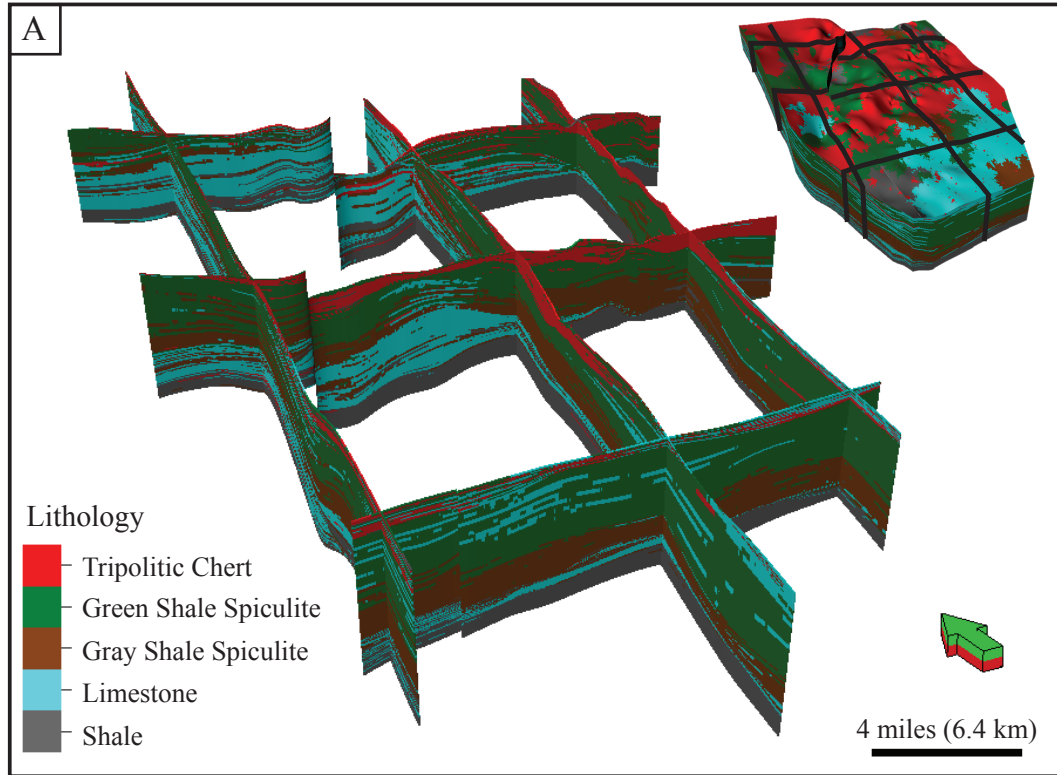


Figure 18. North-south and east-west oriented slices of (A) 3-D lithology model and (B) 3-D porosity model showing lateral and vertical trends. Limestone content decreases toward the southeast, while porosity generally increases upsection and toward the northeast of the survey.

CONCLUSIONS

The Mississippian Limestone is a stratigraphically complex oil and gas play controlled by periods of uplift, subsidence, subaerial exposure, carbonate cyclicity, and diagenesis. The Mississippian section in the area of interest is comprised of 9 dominant lithofacies. These include: 1) chert breccia, 2) bedded spiculite, 3) clast/bedded cherty spiculite, 4) interbedded lenticular spiculitic wackestone, 5) argillaceous dolomitized cherty spiculite, 6) lenticular gray shale spiculite, 7) shaly limestone, 8) gray bioturbated cherty limestone, and 9) dark spiculitic shale. These lithofacies are grouped into 5 distinct lithologies including 1) tripolitic chert, 2) green shale spiculite, 3) gray shale spiculite, 4) limestone, and 5) shale.

This study has shown that Mississippian lithologies can be accurately and consistently predicted using artificial neural networks, producing a maximum accuracy of 87%. Combining PCA and Kmeans clustering is also an effective method of classification (maximum accuracy of 85%), and can be a serviceable technique when core data are missing or inadequate. Despite these similar success rates, unsupervised methods are generally less preferable to supervised. This is evidenced by results attained through combining PCA and KNN clustering. While some accuracies using this method were high (up to 83%), results were considerably inconsistent and unreliable when using complex input assemblages.

3-D stratigraphic models produced from this study reveal a relatively uniform, flat lying basal section that is likely comprised of Kinderhookian strata, overlain by prograding clinofolds of limestone, shales, and spiculites deposited during Osagean and Meramecian times. The sequence is capped by a high-porosity unit likely associated

with subaerially exposed strata (Figure 15). Hardtner Field is located on the downthrown block of a major north-south trending fault, where a relatively thick interval of Osagean limestones is overlain by spiculitic units. Towards the east and south, limestones thin significantly and are replaced by spiculites. The Mississippian section as a whole thins up-dip toward the north, where extended exposure led to significant erosion.

The identification and correlation of depositional cycles from quantitative gamma-ray trends using derivative trend analysis (DTA) can be an effective first step to developing a sequence-stratigraphic framework in the absence of adequate core data. For this study, core samples, wireline logs, and 3-D lithology models show that the Mississippian section is characterized by an overall shallowing 2nd-order sequence, with stacked higher order internal cycles that oscillate from outer ramp to inner ramp lithologies. Cyclic shifts in depositional setting appear more extreme in the lower Mississippian (Kinderhookian to Osagean strata) than in the upper Mississippian (Meramecian units). Base-level changes in the lower Mississippian result in abrupt lithologic transitions, while the upper Mississippian shows somewhat more gradual facies variations. This changing cycle profile may be the result of an increase in ramp slope compounded by a decreasing amplitude of sea-level fluctuations.

Optimal Mississippian reservoirs are affiliated with regressive phases of 3rd-order cycles. In particular, Meramecian Cowley reservoirs have been quantitatively shown to display increasing porosity values during cleaning-upward gamma-ray cycles. Typically, favorable reservoir lithofacies are found in a constrained depth range where sea levels were deep enough to encourage siliceous sponge bioherm growth, but

shallow enough to become subaerially exposed during times of sea-level drop. These intervals are highly spiculitic, where diagenetically enhanced moldic and intercrystalline porosity has created prolific hydrocarbon reservoirs.

REFERENCES

- Allen, D. B., and M. J. Pranter, 2016, Geologically constrained electrofacies classification of fluvial deposits: an example from the Cretaceous Mesaverde group, Uinta and Piceance basins: AAPG Bulletin, V. 100, no. 12, p. 1775-1801.
- Birch, C. B., 2015, Reservoir-scale stratigraphy, sedimentology, and porosity characteristics of Mississippian reservoirs, northeastern Anadarko shelf, Oklahoma, master's thesis, University of Oklahoma, Norman, Oklahoma, 81 p.
- Childress, M., and G.M. Grammer, 2015, High resolution sequence stratigraphic architecture of a mid-continent Mississippian outcrop in southwest Missouri: The Shale Shake, v. 66, no. 4, p. 206-234.
- Comer, J. B., 1991, Stratigraphic analysis of the upper Devonian Woodford formation, Permian basin, west Texas and southeastern New Mexico: Bureau of Economic Geology Report of Investigations, no. 201, p. 20-35.
- Costello, D., M. Dubois, and R. Dayton, 2014, Core to Characterization and Modeling of the Mississippian, North Alva Area: 2014 Mid-continent Section AAPG Core Workshop, p. 165-174.
- Doveton, J. H., 1973, Numerical analysis relating location of hydrocarbon traps to structure and stratigraphy of the Mississippian 'B' of Stafford County, Kansas: Kansas Oil Exploration Decision System Technical Report, Kansas Geological Survey, p. 56.
- Dubois, M. K., G. C. Bohling, and S. Chakrabarti, 2007, Comparison of four approaches to a rock facies classification problem: Computers & Geosciences, v. 33, p. 599-617.
- Duren, J. D. 1960, Some petrophysical aspects of the Mississippian "chat," Glick field, Kiowa County, Kansas: Shale Shaker, v. 11, p. 2-8.
- Ehrenberg, S. N., N. A. H. Pickard, L. B. Henriksen, T. A. Svana, P. Gutteridge, and D. Macdonald, 2001, A depositional and sequence stratigraphic model for cold-water, spiculitic strata based on the Kapp Starostin Formation (Permian) of Spitsbergen and equivalent deposits from the Barents Sea: AAPG Bulletin, v. 85, p. 2061-2087.
- Elebiju, O. O., S. Matson, G. R., Keller, and K. J. Marfurt, 2011, Integrated geophysical studies of the basement structures, the Mississippian chert, and the Arbuckle Group of Osage County region, Oklahoma: AAPG Bulletin, v. 95, p. 371- 393.

- Feinstein, S., 1981, Subsidence and thermal history of Southern Oklahoma aulocogen – implications for petroleum exploration: AAPG Bulletin, v. 65, p. 2531-2533
- Franseen, E. K., 2006, Mississippian (Osagean) shallow-water, mid-latitude siliceous sponge spicule and heterozoan carbonate facies: An example from Kansas with implications for regional controls and distribution of potential reservoir facies: Current Research in Earth Sciences Bulletin, v. 252, part 1, p. 1–23: <http://www.kgs.ku.edu/Current/2006/franseen/index.html>
- Gutschick, R. C., C.A. Sandberg, 1983, Mississippian continental margins of the conterminous United States: SEPM Special Publication 33, p 79-96.
- Handford, C. R., 1986, Facies and bedding sequences in shelf-storm-deposited carbonates Fayetteville shale and Pitkin Limestone Mississippian, Arkansas: Journal of Sedimentary Petrology, v. 56, p. 123-137
- Hartigan, J. A., 1975, Clustering algorithms: New York, John Wiley & Sons, p. 84-107.
- Haq, B. U., and S. R. Schutter, 2008, A chronology of Paleozoic sea-level changes: Science, v. 322, p. 64-68.
- Jaekel, L., 2016, High-resolution sequence stratigraphy and reservoir characterization of mid-continent Mississippian carbonates in north-central Oklahoma and south-central Kansas, master's thesis, Oklahoma State University, Stillwater, Oklahoma, 356 p.
- Janssen, L.F., F.M. van der Wel, 1994, Accuracy assessment of satellite derived land-cover data: a review: Photogrammetric Engineering and Remote Sensing, vol. 60, 419 – 426.
- Kerans, C., 2012, Ramp-to-rim transition in the Guads – role of “mixed system” and inherited topography, AAPG Search and Discovery Article #50667
- Kumar, B., and M. Kishore, 2006, Electrofacies classification – a critical approach: 6th International conference and exposition on petroleum geophysics, Kolkata, India, p. 822-825.
- Lane, H. R., and T. L. De Keyser, 1980, Paleogeography of the late Early Mississippian (Tournaisian 3) in the central and south-western United States, Paleozoic Paleogeography of the west-central United States: Rocky Mountain Section SEPM, p. 149-158.
- LeBlanc, S. L., 2014, High resolution sequence stratigraphy and reservoir characterization of the “Mississippian limestone” in north-central Oklahoma,

- master's thesis, Oklahoma State University, Stillwater, Oklahoma, 443 p.
- Lee, W., 1940, Subsurface Mississippian rocks of Kansas: State Geological Survey of Kansas Bulletin, v. 33, 112 p.
- Lindzey, K., 2015, Geologically constrained seismic characterization and 3-D reservoir modeling of Mississippian reservoirs, north-central Anadarko shelf, Oklahoma, master's thesis, University of Oklahoma, Norman, Oklahoma, 97 p.
- Mazzullo, S. J., H. Cao, and B. W. Wilhite, 2008, Chert reservoirs in the Cowley formation (Mississippian) south-central Kansas: paragenesis, oxygen and silicon isotope geochemistry, and timing of silicification and porosity formation: Kansas Geological Society Bulletin, v. 83, no. 2, p. 14-20.
- Mazzullo, S. J., B. W. Wilhite, and I.W. Woosley, 2009, Petroleum reservoirs within a spiculite- dominated depositional sequence: Cowley Formation (Mississippian: Lower Carboniferous), south-central Kansas: AAPG Bulletin, v. 93, no. 12, p. 1649-1689.
- Mazzullo, S. J., B. W. Wilhite, D. R. Boardman, B. T. Morris, and C. J. Godwin, 2016, Stratigraphic architecture and petroleum reservoirs in lower to middle Mississippian strata (Kinderhookian to basal Meramecian in subsurface central to southern Kansas and northern Oklahoma: Shale Shaker, v. 67, p. 20-49.
- Montalvo Lliteras, L. G., 2015, Petrography and paragenesis of diagenetic mineral phases in cherty and dolomitic spiculite strata, Mississippian, south-central Kansas, master's thesis, University of Kansas, Lawrence, Kansas, 173 p.
- Montgomery, S.L., J. C. Mullarkey, M. W. Longman, W. M. Colleary, and J. P. Rogers, 1998, Mississippian chat reservoirs, south Kansas: Low-resistivity pay in a complex chert reservoir: AAPG Bulletin, v. 82, no. 2 p. 187-205.
- Moore, C. H., 2001, Carbonate reservoirs: porosity evolution and diagenesis in a sequence stratigraphic framework: Amsterdam, Elsevier.
- Nissen, S. E., K. J. Marfurt, and T. R. Carr, 2004, Identifying subtle fracture trends in the Mississippian saline aquifer unit using new 3-D seismic attributes, KGS Open File Report, no. 56.
- Northcutt, R.A., K. S. Johnson, and G. C. Hinshaw, 2001, Geology and petroleum reservoirs in Silurian, Devonian, and Mississippian rocks in Oklahoma: Oklahoma Geological Survey Circular 105, p. 1-15.
- Parham, K. D., and R. A. Northcutt, 1993, Mississippian chert and carbonate and basal Pennsylvanian sandstone – central Kansas uplift and northern

- Oklahoma, D. Bebout, W. White, and T. Hentz, eds.: Atlas of major Midcontinent gas reservoirs, Austin, Bureau of Economic Geology, p. 57-59.
- Peeler, J. A., 1985, Reservoir characterization of the Mississippian “chat,” Hardtner field, southern Barber County, Kansas: Master’s thesis, Wichita State University, Wichita, Kansas, p. 120.
- Price, B., 2014, Identification of high-frequency cyclicity in the Mississippian (Osagean) Bentonville Formation, northwestern Arkansas, master’s thesis, Oklahoma State University, Stillwater, Oklahoma, 226 p.
- Ramaker, E. M., R. H. Goldstein, E. K. Franseen, and W. L. Watney, 2014, What controls porosity in cherty fine-grained carbonate reservoir rocks? Impact of stratigraphy, unconformities, structural setting and hydrothermal fluid flow: Mississippian, SE Kansas, *in* S. M. Agar, and S. Geiger, eds., *Fundamental controls on fluid flow in carbonates*: Geological Society, London, Special Publications 2014, v. 406, p. 179-208.
- Rogers, J. P., M. W. Longman, and R. M. Lloyd, 1995, Spiculitic chert reservoir in Glick Field, south-central Kansas: *The Mountain Geologist*, v. 32, p. 1-22.
- Rogers, S. M., 2001, Deposition and diagenesis of Mississippian chat reservoirs, north-central Oklahoma: *AAPG Bulletin*, v. 85, no.1, p 115-129.
- Serra, O., and H. T. Abbott, 1982, The contribution of logging data to sedimentary sedimentology and stratigraphy: *Society of Petroleum Engineers Journal*, v. 22, p. 117–131.
- Schlager, W., 1992. Sedimentology and sequence stratigraphy of reefs and carbonate platforms: *AAPG Course Notes n.34*, p.1-71.
- Shapiro, L. G., and G. C. Stockman, 2000, *Computer vision*: Upper Saddle River, NJ, Prentice Hall, p. 170.
- Sloss, L. L., 1963, Sequences in the cratonic interior of North America: *Geological Society of America Bulletin* 74, p. 93-114.
- Smith, L. I., 2002, A Tutorial on Principal Component Analysis: University of Otago:http://www.cs.otago.ac.nz/cosc453/student_tutorials/principal_components.pdf
- Ting, K. M., 2011, Confusion matrix, *in* C. Sammut and G. I. Webb, eds., *Encyclopedia of machine learning*, 1st ed.: New York, Springer, 209 p.
- Turnini, A.M., 2015, Stratigraphic and structural controls on Mississippian

limestone and tripolitic chert reservoir distribution using seismic-constrained reservoir characterization and modeling, northern Oklahoma, master's thesis, University of Oklahoma, Norman, Oklahoma, 83 p.

Watney, W. L., W. J. Guy, and A. P. Byrnes, 2001, Characterization of the Mississippian chat in south-central Kansas: AAPG Bulletin, v. 85, no. 1, p. 85-113.

Watney, W. L., 2015 A maturing Mississippian lime play in the midcontinent – a perspective on what we know and need to know: AAPG Search and Discovery Article #80445

Wilhite, B. W., and S. J. Mazzullo, 2013, Regional aspects of stratal architecture of the subsurface Mississippian in Kansas based on wireline log cross-sections and seismic: AAPG Search and Discovery Article #30307

Young, R. T., 1968, C. Hardtner Field, Barber County, Kansas, Natural Gases of North America, Volume Two, p. 1566-1569.

Appendix A. Geologic Setting

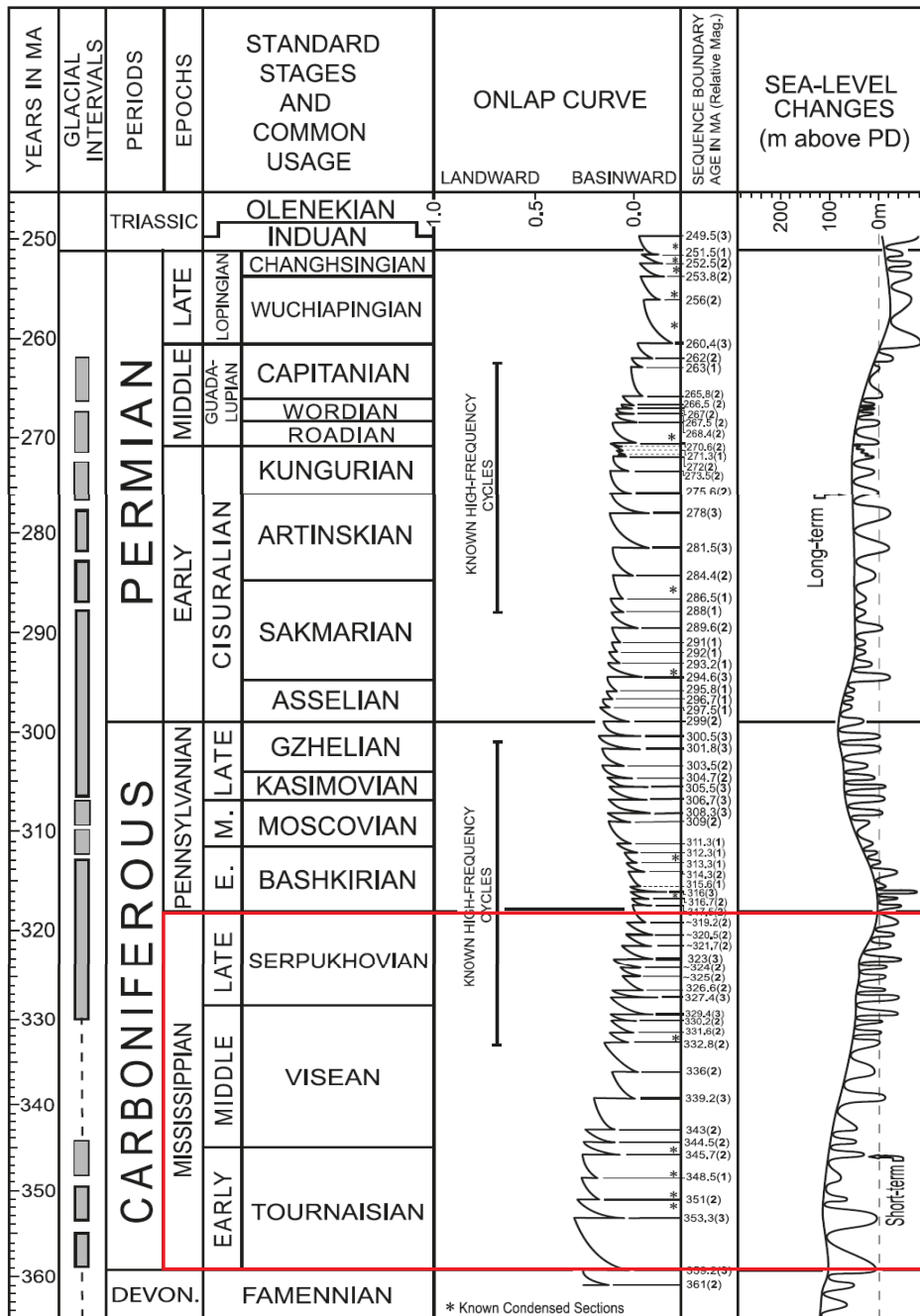


Figure A-1. Sea Level Curve for Carboniferous-Permian with Mississippian Epoch outlined in red. Modified from Haq and Schutter, 2008.

Appendix A-2. Geologic Setting

Mississippian Stages

The Mississippian is divided into four stages. These include; Kinderhookian, Osagean, Meramecian, and Chesterian. Erosion from subaerial exposure can exclude younger stages from the stratigraphic record, particularly in northern areas where erosion was most significant. In addition, the progradational nature of deposition causes each stage to vary in sediment thickness by location, with early stages expected to be thicker toward the north, and later stages thicker toward the south.

The Kinderhookian Stage in the mid-continent marked the transition from relatively deep, oxygen-poor waters that produced late Devonian marine shales (e.g. Woodford Shale) to an inundation of warm, shallow, well oxygenated waters (Northcutt et al., 2001). This resulted in the deposition of a series of shales and limestones. Key formations within the Kinderhookian include the dark gray/black basal Kinderhook or Hannibal Shale, Compton Limestone and the locally glauconitic and shaly lime mudstone of the overlying Northview Formation (Watney et al., 2001). Mazzullo et al. (2016) have identified a strike oriented paleotopographic high known as the Kanoka Ridge that formed during the Kinderhookian as a forebulge associated with pulses of Ouachita compression.

During the Osagean Stage, the same warm, shallow, oxygenated sea was regionally dominant while scarce tectonic activity led to laterally continuous deposition of shallow water limestones (Northcutt et al., 2001; Parham and Northcutt, 1993). Significant Osagean formations include the Pierson limestone, Reeds-Spring

limestone, the Burlington Keokuk Limestone, and the lower part of the Cowley formation. In the area of study, spiculitic chert is first observed in the youngest Osagean deposits (Mazzullo et al., 2009).

Fairly continuous sedimentation in generally marine conditions during the Meramecian produced the spiculitic upper Cowley formation, the Ritchey (Warsaw) Limestone, Salem Limestone, St. Louis Limestone, and St. Genevieve Limestone (Mazzullo et al., 2016; Northcutt et al., 2001). These formations show somewhat significant lateral thickness variations caused by sedimentation into sporadic basins created by uplift and subsidence of the ramp (Parham and Northcutt, 1993).

The Chesterian Stage saw an increase in tectonic activity related to the Proto-Ouachita Orogeny, which made the Ouachita Foreland Trough an important influence on basin-ward deposits (Northcutt et al., 2001). Chesterian uplift along with a drop in sea level led to deposits of shallow marine limestones up-dip, and shales with discontinuous sandstones downdip, though Chesterian strata is sparsely present in the study area (Mazzullo et al., 2009).

Tectonic framework

The paleogeography of North America during the Mississippian was shaped as the result of three major tectonic events. The first was the Acadian Orogeny in the Middle Devonian to Early Mississippian, where portions of the Avalonian and Laurasian continents collided in modern northeastern America (Gutschick and Sandberg, 1983). Compression created the Eastern Interior trough, which served as a basin for deposition large alluvial clastic wedges. The Eastern Interior trough would

eventually outline the eastern border of an expansive carbonate shelf (Figure 4). Around the same time, the Antler Orogeny was shaping Western North America through oceanic/continental convergence, creating the Antler highlands along the plate boundary and the Antler Foreland Trough inland to the East (Figure 4) (Gutschick and Sandberg, 1983). The third orogenic event was the Proto-Ouachita Orogeny (which continued into the late Pennsylvanian) in which the South American plate began to converge northward. This created the Ouachita Foreland Trough, which formed the southern boundary of the Mississippian carbonate shelf (Figure 4) (Gutschick and Sandberg, 1983; Northcutt et al., 2001). Combined motion of these events formed the Transcontinental Arch, which separated the Madison Carbonate Shelf to the WNW, and the Burlington Shelf to the ESE. By the early Mississippian, the summation of this tectonic activity had produced a shallow marine shelf spanning most of North America. A warm epeiric sea blanketed the Burlington Shelf, and gave way to slope and basin environments down dip to the south.

Diagenesis

Diagenetic events played a central role in shaping the Mississippian interval. Montalvo (2015) found 26 distinct diagenetic events within the Cowley Formation in south central Kansas. These events are categorized into three main settings of diagenesis, including marine (syndepositional), meteoric, and burial. The sequence of diagenetic events in this system is generally marked by initial silica replacement and dolomitization, followed by dissolution and brecciation associated with exposure, cementation, then fracturing, compaction, and dissolution

from burial.

Diagenetic events had a major impact on porosity development in Mississippian reservoirs of south central Kansas (Montalvo, 2015; Ramaker et al, 2014). While porosity development is closely tied to major instances of subaerial exposure, there is also evidence of late stage porosity enhancement. Porosity rims around chert nodules are cross cut by compactional fractures, meaning they likely developed during subaerial exposure and prior to burial and lithification (Ramaker et al, 2014). While an influx of hydrothermal fluids (as is evidenced by precipitation of megaquartz and baroque dolomite) advocates for late stage porosity enhancement. These hydrothermal fluids likely flowed preferentially through fracture networks and highly porous intervals (Ramaker et al, 2014).

Evidence of diagenesis is readily apparent in Mississippian deposits, perhaps none more compelling than the pervasive abundance of chert. Chert is common polymorph of microcrystalline quartz that is associated with a biogenic or chemically precipitated origin. Three forms of chert are found throughout the Mississippian, representing three generations of silicification (Mazzullo et al., 2009). Initially, syndepositional chert replacement of unstable siliceous biogenic spicules occurred from super saturated marine pore fluids (Mazzullo et al., 2009). Second-generation silicification is thought to have occurred post-depositionally as continued growth from nucleation on first generation chert. Third-generation chert was formed by replacement of clay matrix in shallow breccias as well as some of the previously formed second generation chert (Mazzullo et al., 2009). Second and third-generation chert occurrence is associated with unconformities, suggesting

they formed during periods of subaerial exposure where silica-saturated meteoric water influx was prevalent (Mazzullo et al., 2009). Exposure of this chert led to significant weathering and physical abrasion producing highly porous intervals of tripolitic chert breccia (Parham and Northcutt, 1993). The cumulative result of these stages of in-situ residual chert replacement is the foundation of the productive Mississippian “chat” interval, which is found at the Mississippian-Pennsylvanian unconformity. (Rogers, 2001; Parham and Northcutt, 1993; Mazzullo et al., 2009).

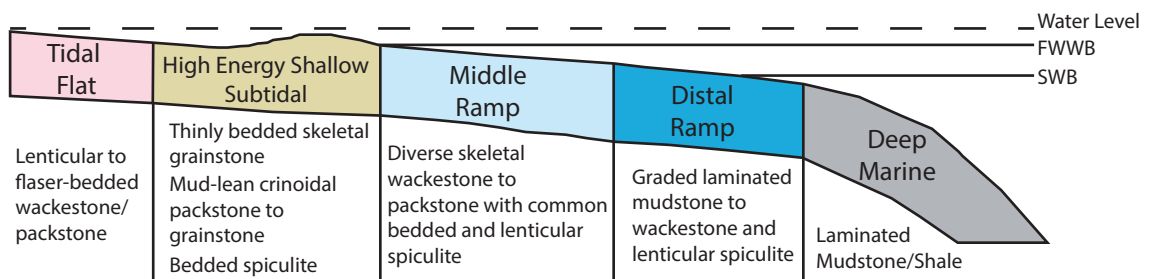
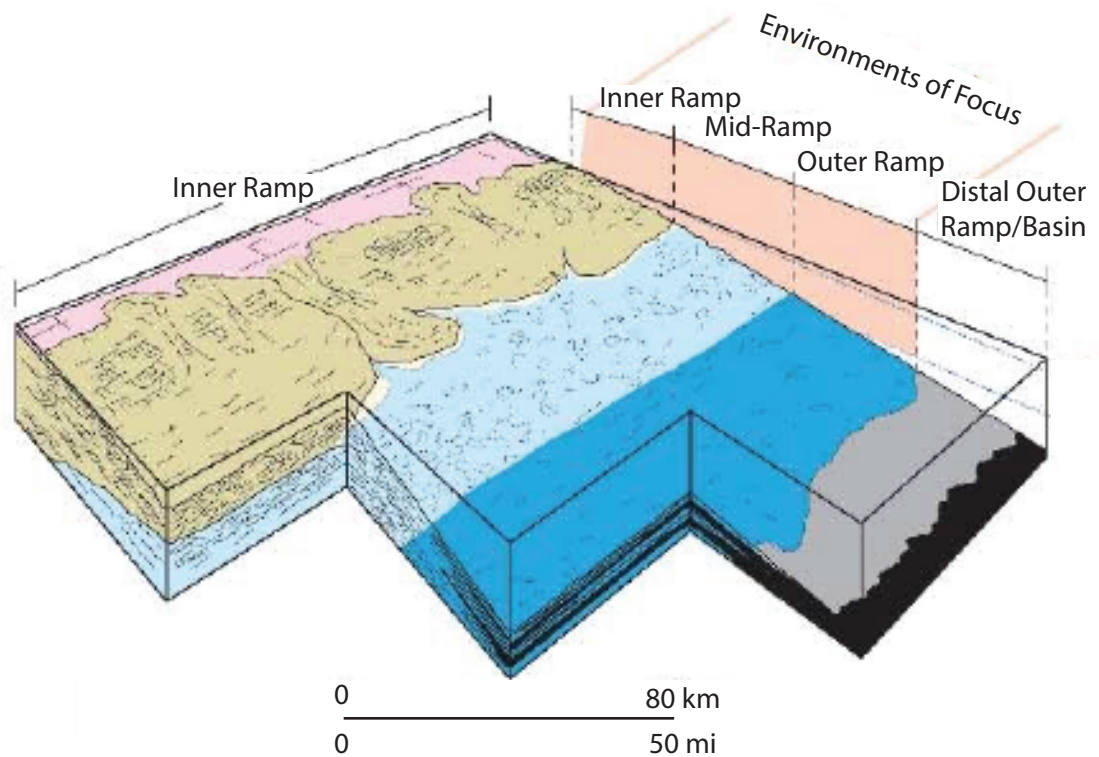


Figure A-3. Model of depositional environments represented within the area of study ranging from inner ramp, tidal flat deposits to basinal deep marine mudstones and shales. (Modified from Handford, 1968 and Jaekel, 2016)

Appendix A-4. Lithofacies Descriptions and Interpretations

Chert Breccia

Angular grain-supported chert clasts in a shale matrix (Figure 7A, Figure 8A). Clasts are variable in size (microscopic to centimeter scale) and chaotically oriented. Chert clasts are typically white in color and show dark organic rich alteration rinds around their perimeter. Clasts are composed nearly entirely of silicified and amalgamated spicules, while the matrix is a microcrystalline quartz groundmass with scattered microscopic porous altered spiculite clasts. Up to three generations of chert development are apparent in core samples of this facies (Mazzullo et al., 2008). The initial silicification manifests as dark brown chert that acted to consolidate spicules. Further exposure to replacement encouraging conditions resulted in second generation chert, which shows up as opaque light grey to blue nodules or beds within first generation chert. Third generation chert is tan to light yellow and results from silica replacement of the pale green shale matrix. In-situ autobrecciation is interpreted where fractures are filled with internally sourced brecciated material. Oil stained vugs are noted in core samples, especially around the rims of diagenetically altered chert clasts. Logs signatures show very high porosities (up to 40%) and characteristic low density and photoelectric responses. Core plug MCIP and NMR porosities for this facies ranged from 6% to 15% (Appendix A-4), significantly less than most log measured porosity, indicating the potential for variable porosity. FTIR and XRD mineralogic analysis shows extensive silica replacement with trace amounts of chlorite, muscovite and ankerite. Chert breccia is the primary facies that comprises the well-studied upper Mississippian “chat” intervals.

This is a common facies that occurs near the top of the Mississippian section and is often associated with both major and minor unconformities. It forms from exposure and vadose migration of fluids in conjunction with late Mississippian erosion. The origin of chert breccias is inherently tied with subaerial exposure processes including autobrecciation, karstification, and solution collapse (Birch, 2015; Ramaker et al., 2014; Montgomery et al., 1998; Rogers, 2001; Watney et al., 2001).

Clast/bedded chert Spiculite

This highly altered facies is recognized by irregular chert clasts that sometimes form continuous beds within dark brown spiculite and clay rich layers almost entirely replaced by microcrystalline quartz (Figure 7B) (Montalvo, 2015). Chert clasts are typically light gray with a hint of blue and often display a mottled fabric. Occasional parallel and cross stratified laminations are apparent within chert clasts. Abundant vuggy and intergranular porosity is observed within the brown microcrystalline quartz matrix and near the edges of chert clasts, where dark alteration “rinds” can be identified in thin section (Figure 8B). As with the lenticular spiculitic wackestones, variable degrees of chert development are observed, with nodules ranging from microscopic to centimeter scale. This facies is found near the top of the Mississippian, and can be observed grading into brecciated chert intervals. Porosity from NMR and MCIP core plug measurements were both roughly 14% (Appendix A-4). FTIR and XRD mineralogic analysis shows this facies is composed mostly of silica with minor amounts of carbonate and clay minerals. This indicates pervasive silica replacement. Well log readings for this facies are characterized by fairly high porosities (generally greater than

10%), moderate to low (less than 50 API) log gamma rays, and low resistivities (less than 20 ohm m).

Montalvo (2015) described a similar facies in which he associated extensive alteration under subaerial processes. Chert clasts are irregularly shaped, often sharing diffuse boundaries with the matrix. This supports significant diagenetic impact. This facies likely represents a similar depositional environment to bedded spiculites, however its stratigraphic position and level of alteration may suggest a slightly shallower setting.

Bedded Spiculite Packstone

Brown to tan generally structureless grain supported spiculite with little shale content (Figure 7C). Variable quartz cementation is evident in both core sample and thin sections resulting in a range of porosity values, however typically porosity exceeds 15%. Macroscopic vugs are abundant as well as moldic porosity from dissolved sponge spicules. Occasional faint inclined laminations are visible in some samples. Bedded spiculites are usually found overlying interbedded lenticular spiculites. Log signatures show this facies is fairly porous with very little radioactivity and low resistivity. Thin section along with XRD and FTIR mineralogic analysis shows a high silica content associated with abundant siliceous spicules (Figure 8C). This facies showed high porosity values in core samples, with NMR and MCIP measurements ranging from 23% to 30% (Appendix A-4). Trace amounts of pyrite and dolomite are observed in thin sections. While not apparent in core samples observed for this study, Mazzullo and others (2009) have noted numerous internal unconformities within bedded spiculites,

which they tie to subaerial exposure surfaces.

This facies has been described by Mazzullo and others (2009) as the most important reservoir facies within the Cowley Formation. This is supported by significant oil staining observed in core samples. Cross-laminations are indicative of a moderate to high energy, inner ramp, shallow setting. Thin sections show occasional *Thalassinoides* burrows, which are regarded as a shallow water ichnofossil (Mazzullo et al., 2009). Chaotic fabric of spicules may also suggest agitation from wave and current movement in a shallow environment, possibly associated with late Mississippian falling sea levels.

Interbedded lenticular spiculite

Continuous and discontinuous wavy laminations of green shale heterolithically interbedded with lenses of spiculite rich wackestone (Figure 7D). This facies is very common in the Cowley Formation, particularly towards the top. Wackestone lenses are comprised almost entirely of sponge spicules, however rare crinoid and bryozoan skeletal fragments can also be observed. These lenses are pervasively replaced with fabric retentive microcrystalline quartz, with rare remnant calcite grains occasionally noted (Figure 8D). Instances of dolomitization are evident by scattered euhedral rhombs within spiculite and shale layers. Abundant white and blue chert nodules can be present in both shale and spiculite layers forming a poikilotopic fabric (generally white nodules are associated with shales, while blue nodules are found within spiculite lenses). Spiculite lenses exist in a range of colors from white/tan to brown/purple. This is likely dependent on the degree of alteration, including physical and mechanical weathering,

brecciation, and hydrothermal dissolution (Montalvo, 2015; Ramaker et al., 2014). Scanning Electron Microscopy (SEM) reveals multiple generations of silica replacement within dark brown spiculite lenses (Appendix A-4). Variable degrees of chert development are observed, and in general chertification decreases down-dip and down section. Thin sections reveal moldic, intercrystalline and vuggy porosity. Large silicified evaporate nodules can be observed within this facies. This facies displays a variable log response in accordance with its abundance and type of shale. In general, this facies is characterized by low resistivities driven by an exceptionally high silica content. Moderate to low GR responses are usually observed with increasing porosity values up section.

This facies is interpreted to represent a moderate to shallow water depositional environment. Sponge spicule content is generally indicative of nutrient and silica rich moderately deep water, while abundance of green shale suggests suboxic, fairly shallow water conditions during deposition (Mazzullo et al., 2009). Thus, nutrient rich silica saturated waters are inferred to have upwelled. Lenticular bedding may be the result of pelagic shale sedimentation periodically interrupted by current reworking of spiculite intervals. Bioturbation and early compactional dewatering may also explain the irregular interbedding of these intervals (Mazzullo et al. 2009; Ehrenberg et al. 2001; Franseen, 2006).

Dolomitized lenticular cherty spiculite

Deformed layers of light grey chert replaced spiculite within dark grey argillaceous dolomitic matrix (Figure 7E). Spiculite lenses are matrix supported,

commonly porous and contain rare crinoids. Significant compactional and syndepositional deformation is evident by irregular wavy bedding. Common elongated and elliptical burrows are found within wackestone to packestone clasts and can crosscut deformational sedimentary structures. Pervasive dolomitization within the matrix is evident by abundant euhedral dolomite rhombs (Figure 8E). Remnant calcite grains are present in some samples. Small pyrite inclusions are observed in thin section. Petrography also reveals a characteristic blue color that is not associated with epoxy, but rather appears linked to microcrystalline quartz (Figure 8E). This facies is observed below interbedded lenticular spiculite, near the middle of the Cowley section. Relatively high GR, low porosity, and moderate resistivities are characteristic for this facies.

This facies is interpreted as a mid to outer ramp deposit. Abundant bioturbation suggests with slightly deeper, calmer water depths than inferred by interbedded lenticular spiculite. Periodic wave and current influence may explain the interbedding of argillaceous material with bioclastic spiculite and crinoid intervals.

Lenticular Gray Shale Spiculite

Dark gray shaly lime mudstone interbedded with lenses of fine grained spiculite. Spiculite lenses are generally light gray in color, and can be compactionally deformed. Lenticular to flaser bedding is observed up section, with lenses of dark gray shaly lime mudstone dominant down section. Variable glauconite content is described in shale rich intervals, particularly down section. Local evidence of bioturbation includes common *Planolites* and rare to common *Chondrites* burrows. This facies is partially calcitic and

contains rare opaque white chert nodules. Silicified bryozoan and bivalve fragments are noted. Typically, this facies is described stratigraphically below interbedded lenticular spiculite and dolomitized lenticular cherty spiculite. In wireline logs, lenticular gray shale spiculite is recognized by high neutron porosity compared to density porosity, moderate to high gamma ray values, and relatively low resistivities.

A high shale content and evidence of bioturbation suggests this is a moderately deep water facies. However, flaser to lenticular bedding imply occasional involvement of current or wave action. Therefore, this facies is interpreted as a mid-ramp environment, likely just above storm wave base.

Gray Cherty Bioturbated Limestone

Medium to light gray wackestone to packstone with variably sized horizontal and subvertical burrows. Burrow fills are typically filled with coarse grained material, and scattered bivalve, crinoid, and brachiopod fragments are common. Small opaque gray chert nodules are common, however are not observed in all instances. Occasional vertical and horizontal fracturing along with clay-filled vugs is described. This facies is generally observed in lower Mississippian intervals, often directly underlying lenticular gray shale spiculite facies and overlying shaly limestone. This facies emits low radioactivity as is evidenced by clean GR curves, and has a characteristically high resistivity.

This facies is interpreted as a shallow deposit with rare instances of exposure evident from fracturing and incipient in situ brecciation. Limestones are scattered with skeletal fragments that suggest shallow marine deposition (Mazzullo et al., 2016).

Shaly Limestone

Green to gray shaly lime mudstone to wackestone. Shale type can range from pale green to gray and are slightly pyritic. Bedding is characterized by thin, parallel to slightly wavy laminations. Occasional spicules are identified along with accessory bivalve and partly silicified crinoid fragments. Horizontal burrows are commonly observed within shaly limestones, and in some instances can be glauconized. These deposits are observed in the lower Mississippian, often below and within gray cherty bioturbated limestone units. This facies is relatively non porous and shows high resistivity values along with moderate GR measurements.

This facies is likely a subtidal somewhat shallow deposit. While green shale can indicate suboxic conditions, burrowing points to fairly quiescent conditions during deposition. Glauconite and pyrite content may suggest reducing, anaerobic conditions with slow sedimentation rates (Montalvo, 2015).

Dark Spiculitic Shale

Medium to dark gray silty shale with occasional faint laminations. A slight green color is common. Samples are variably pyritic. *Planolites* and *Orbiculoides* are noted throughout. Silt content is believed to represent spicules. Occasional fining upward packages are described. This facies is found near the base of the Mississippian interval. This facies is identified in wireline logs by high GR values and high neutron porosity in comparison to density porosity.

A very high shale content advocates this facies as a deep marine, outer ramp

deposit dominated by pelagic sedimentation. Common deep water burrows (*Planolites*) support this interpretation. Variations in spiculite content may be cyclically influenced, meaning while this is certainly a deep water facies, it is locally shallow enough to be influenced by base level fluctuations. Marginal spiculite content may be transported from up-dip. This facies correlates with high sea levels associated with the beginning of a 2nd order shallowing upward sequence that summarizes the Mississippian interval (Watney et al., 2001; Jaeckel, 2016)

Appendix B. Quantitative Mineralogy and Petrophysical Measurements

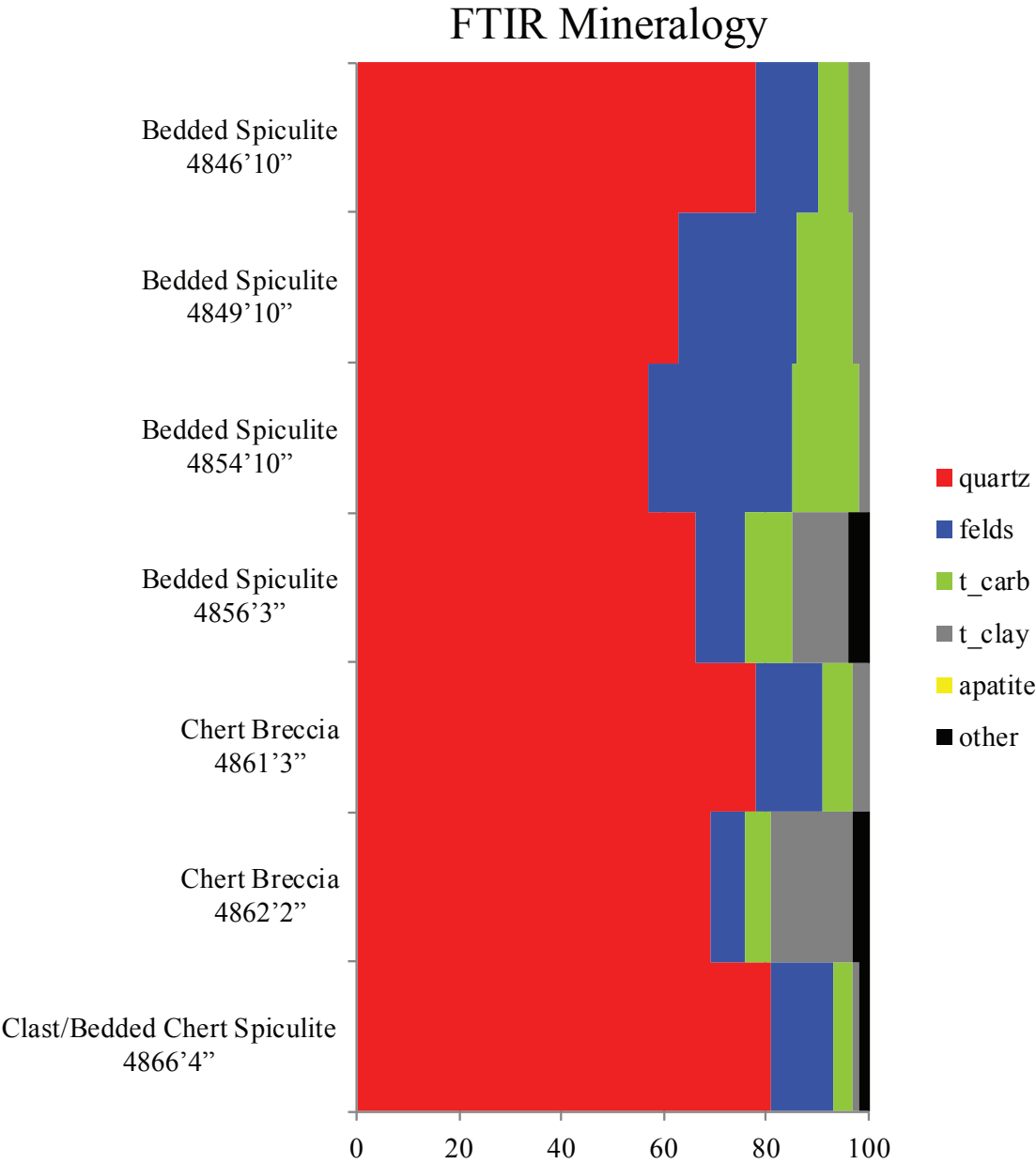
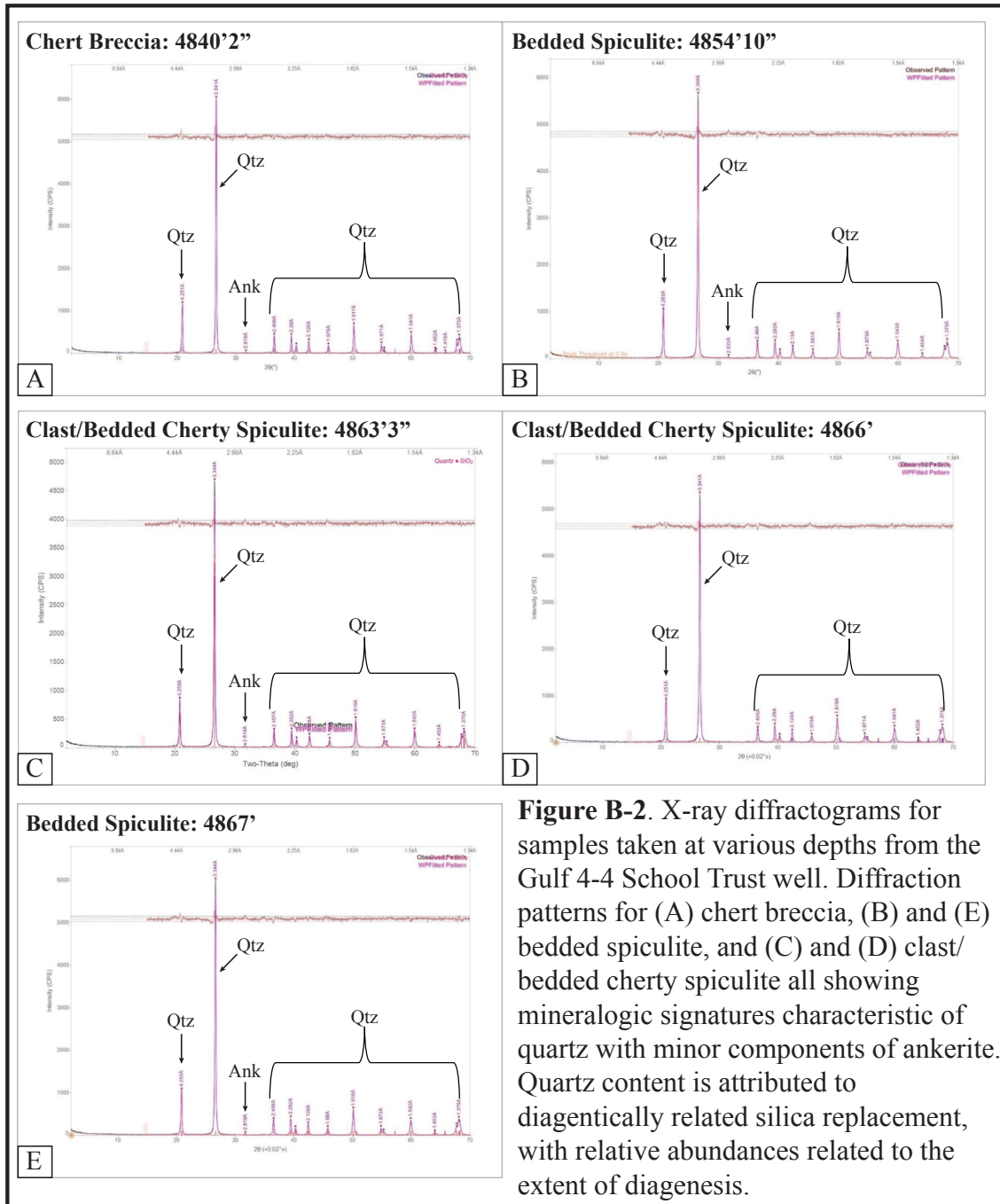


Figure B-1. Fourier transform infrared spectroscopy (FTIR) results showing relative mineral abundances for core plug samples from Gulf 4-4 School Trust.



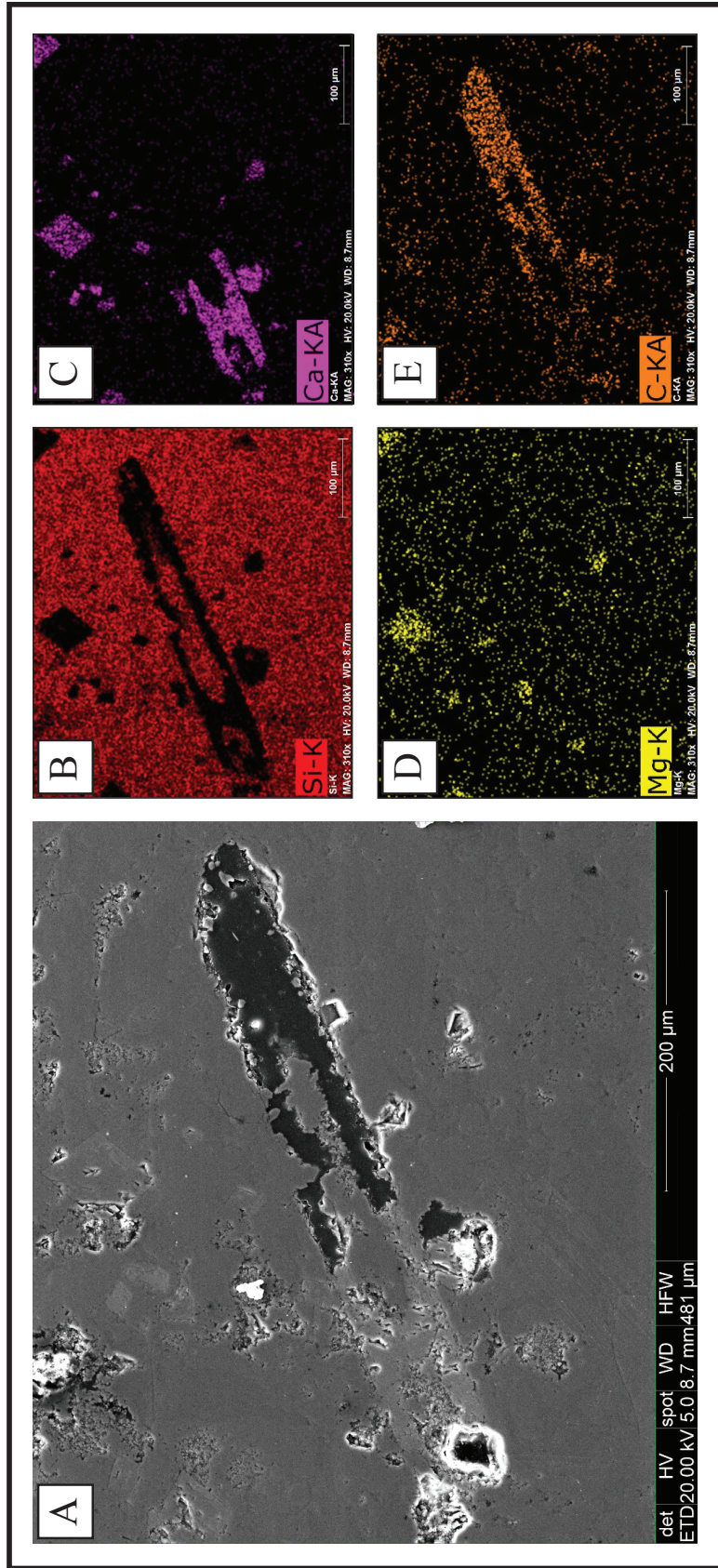


Figure B-3. SEM images of a sponge spicule pore within a chert clast. (A) ETD image showing textural features. (B) Mineralogy map of silica concentrations showing extent of silica replacement. (C) Mineralogy map of calcium concentrations showing areas not replaced by silica. (D) Mineralogy map of magnesium concentrations with clusters showing general positions of dolomite. (E) Mineralogy map of carbon concentrations showing epoxy (pore space).

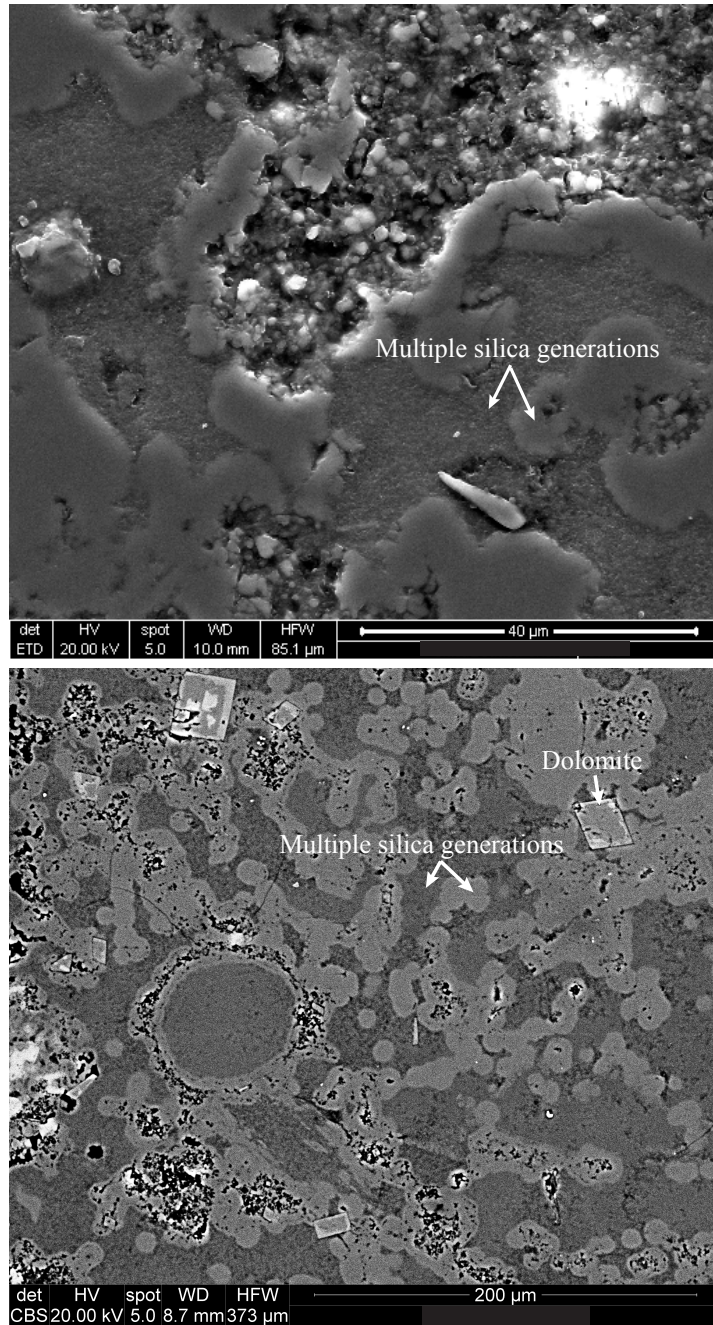


Figure B-4. SEM images showing multiple generations of silica development within samples of (A) clast/bedded chert spiculite and (B) interbedded lenticular spiculite.

Sample	Lithology	P conf	MCIP Porosity	NMR Porosity	K air	K klink	Slip	Alpha	Beta	V bulk	V pore	Length	Diam	Weight
4846.83	Bedded	826.1	23.777		5.629	5.108	5.322	3.29E+02	1.99E+10	29.003	6.896	6.142	2.452	58.422
4846.83	Spiculite	999.9	23.775	23.294	5.437	4.927	5.4	3.42E+02	2.15E+10	29.003	6.896	6.142	2.452	58.422
4846.83		2112.4	23.463		4.412	3.967	5.851	3.78E+02	2.95E+10	29.003	6.805	6.142	2.452	58.422
4849.17	Bedded	792.4	23.682		22.778	21.618	2.795	1.94E+02	2.78E+09	25.908	6.135	5.42	2.467	48.895
4849.17	Spiculite	1023.6	23.721	28.581	22.966	21.802	2.783	1.98E+02	2.80E+09	25.908	6.146	5.42	2.467	48.895
4849.17		2025.4	23.643		22.664	21.514	2.79	2.01E+02	2.88E+09	25.908	6.125	5.42	2.467	48.895
4854.83	Bedded	819.3	30.006		8.92	8.23	4.347	3.45E+02	1.30E+10	29.339	8.803	6.113	2.472	52.974
4854.83	Spiculite	994.2	30.229	30.330	8.99	8.301	4.314	3.48E+02	1.29E+10	29.339	8.869	6.113	2.472	52.974
4854.83		2010.6	30.203		8.849	8.166	4.349	3.51E+02	1.33E+10	29.339	8.861	6.113	2.472	52.974
4856.25	Bedded	811.2	23.702		7.211	6.611	4.729	2.75E+02	1.29E+10	27.303	6.471	5.698	2.47	51.286
4856.25	Spiculite	995.4	23.837	28.70272	7.208	6.609	4.724	2.79E+02	1.30E+10	27.303	6.508	5.698	2.47	51.286
4856.25		2106.3	23.613		6.863	6.281	4.831	2.88E+02	1.42E+10	27.303	6.447	5.698	2.47	51.286
4861.25	Brecciated	825.3	6.506		1.031	0.839	12.019	6.72E+02	2.47E+11	26.503	1.724	5.54	2.468	64.091
4861.25	Chert	1005.1	6.046	6.996	0.964	0.78	12.38	7.33E+02	2.91E+11	26.503	1.602	5.54	2.468	64.091
4861.25		2084.7	5.869		0.647	0.505	14.661	7.03E+02	4.30E+11	26.503	1.555	5.54	2.468	64.091
4862.13	Brecciated	835.3	11.37		114.858	103.836	5.556	2.24E+02	6.65E+08	27.965	3.18	5.78	2.482	62.575
4862.13	Chert	999.7	11.221	14.890	96.62	86.777	5.939	2.27E+02	8.08E+08	27.965	3.138	5.78	2.482	62.575
4862.13		2072.4	10.727		39.949	38.345	2.191	3.56E+02	2.87E+09	27.965	3	5.78	2.482	62.575
4866.33	Clast/Bedded	784.6	13.616		0.855	0.675	13.927	1.50E+03	6.87E+11	27.847	3.792	5.902	2.451	63.007
4866.33	Chert	1007.4	13.585	13.958	0.828	0.652	14.105	1.59E+03	7.54E+11	27.847	3.783	5.902	2.451	63.007
4866.33	Spiculite	1970.7	13.513		0.67	0.517	15.451	1.81E+03	1.08E+12	27.847	3.763	5.902	2.451	63.007

Table B-5. Summary of core plug measurements from Gulf 4-4 School Trust, including MCIP porosity for different confining pressures and average NMR porosity.

NMR for Gulf 4-4 School Trust

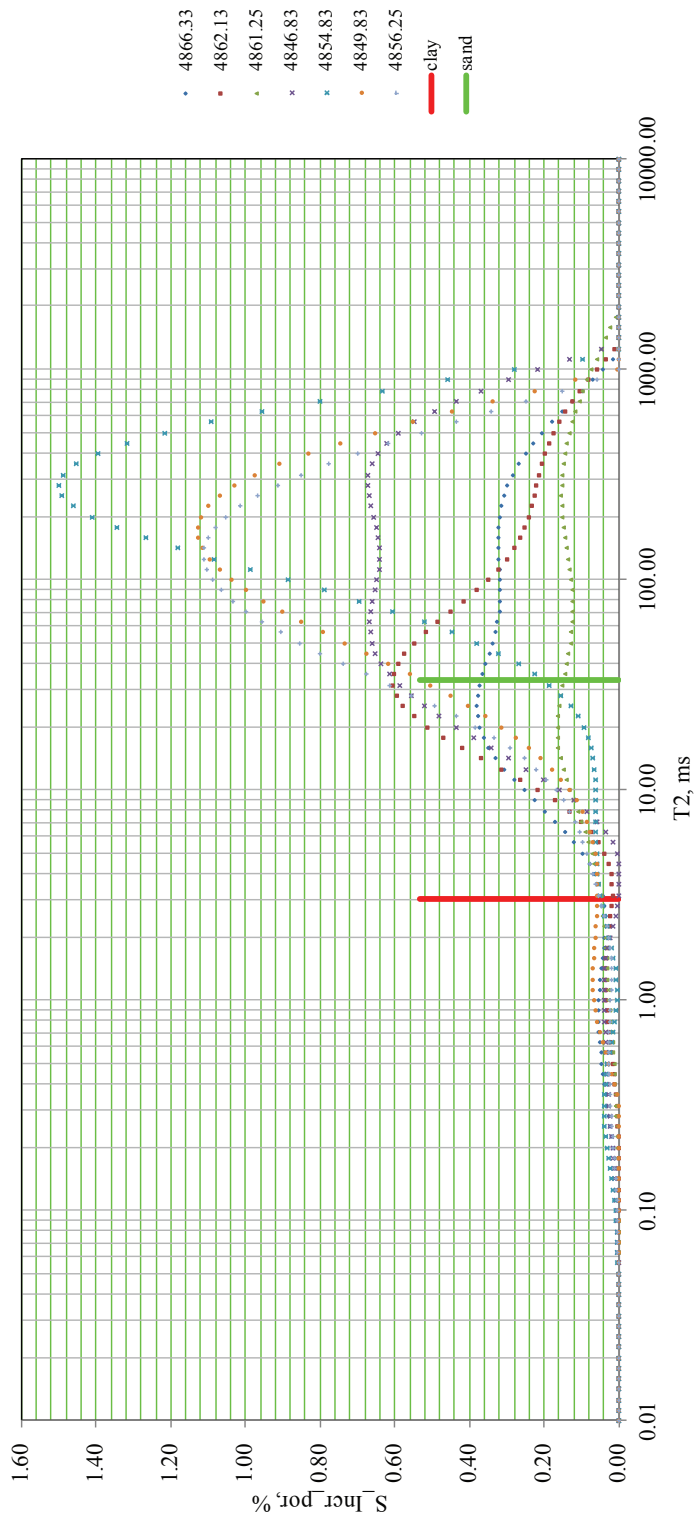


Figure B-6. Nuclear Magnetic Resonance (NMR) data from 7 core plugs taken from Gulf 4-4 School Trust.

Appendix C. Lithology and Electrofacies

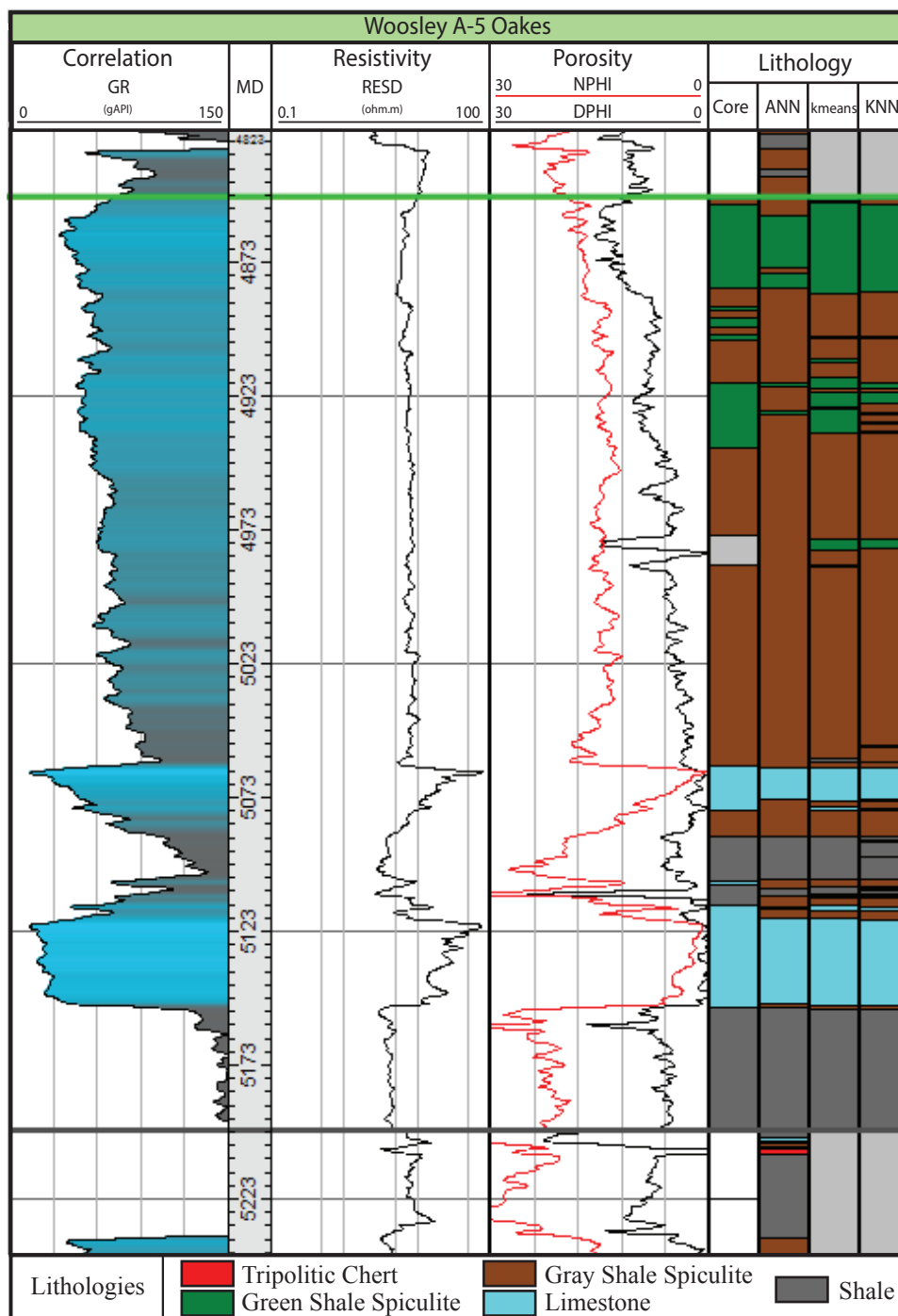


Figure C-1. Well log signatures through the Mississippian for the Woesley A-5 Oakes showing gamma ray, deep resistivity, and porosity. The tracks on the right represent core defined lithology, lithology estimated from ANN, lithology estimated from kmeans, and lithology estimated from KNN.

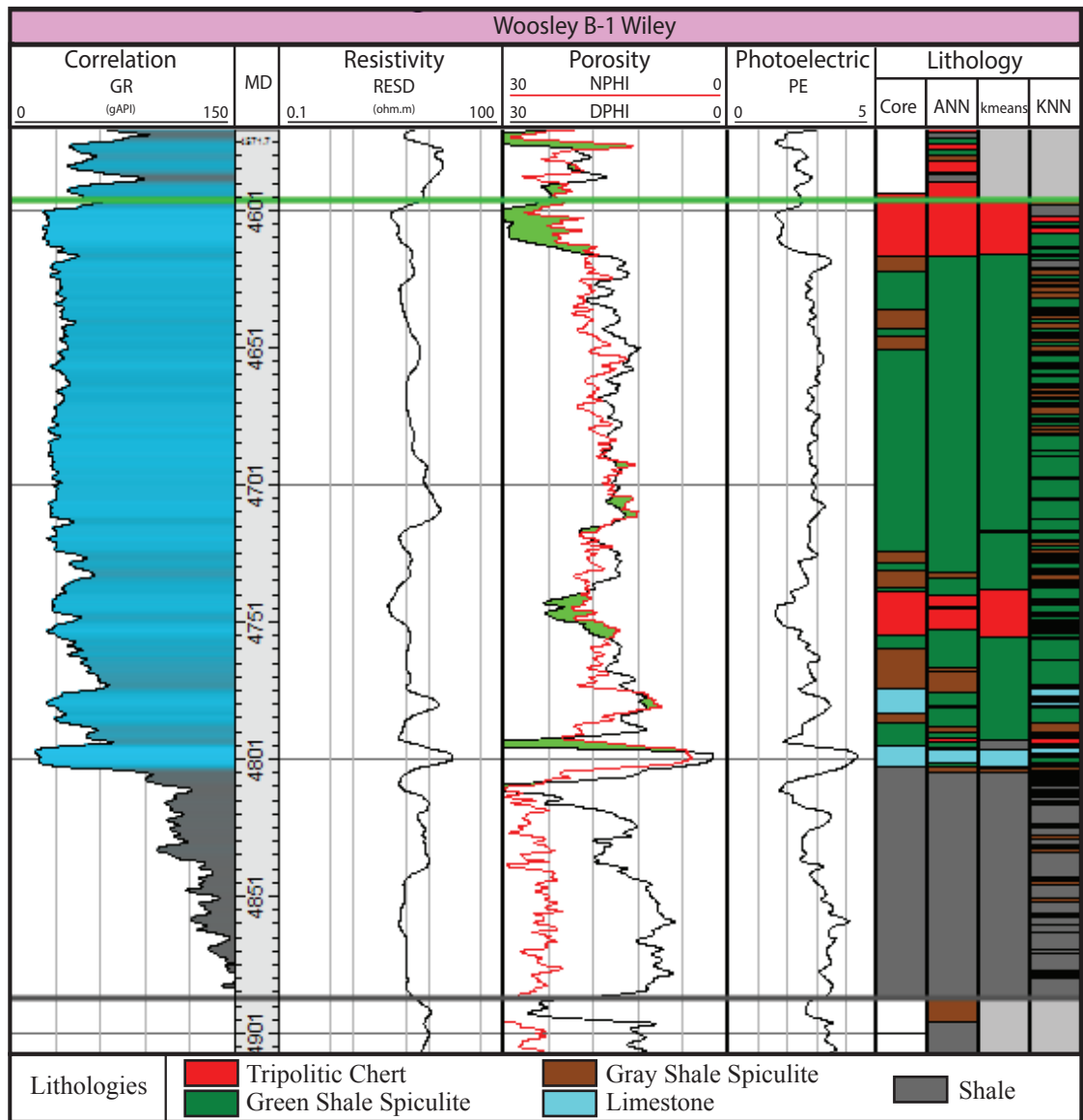


Figure C-2. Well log signatures through the Mississippian for the Woosley B-1 Wiley showing gamma ray, deep resistivity, porosity, and PE. The tracks on the right represent core defined lithology, lithology estimated from ANN, lithology estimated from kmeans, and lithology estimated from KNN.

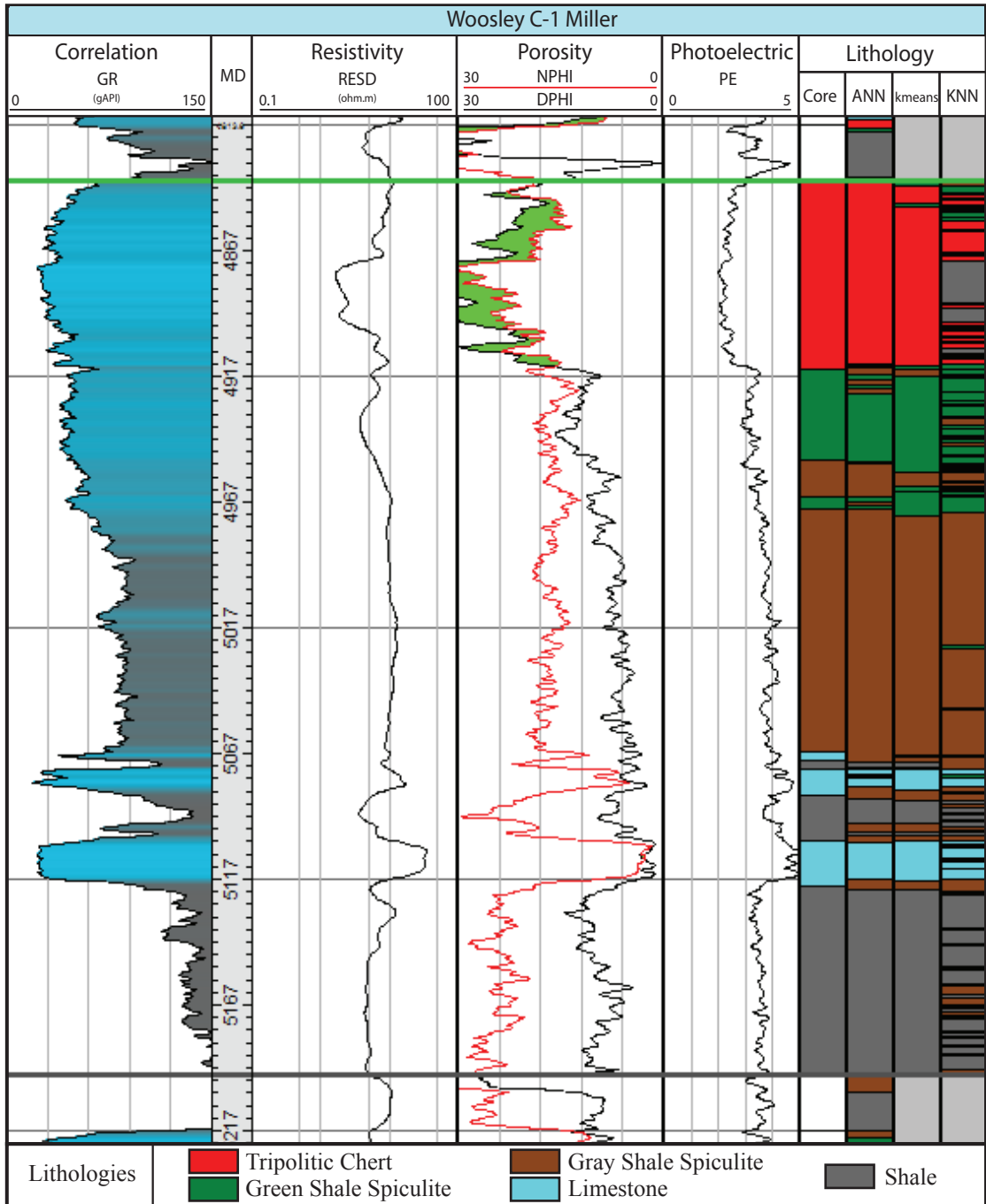


Figure C-3. Well log signatures through the Mississippian for the Wosley C-1 Miller showing gamma ray, deep resistivity, porosity, and PE. The tracks on the right represent core defined lithology, lithology estimated from ANN, lithology estimated from kmeans, and lithology estimated from KNN.

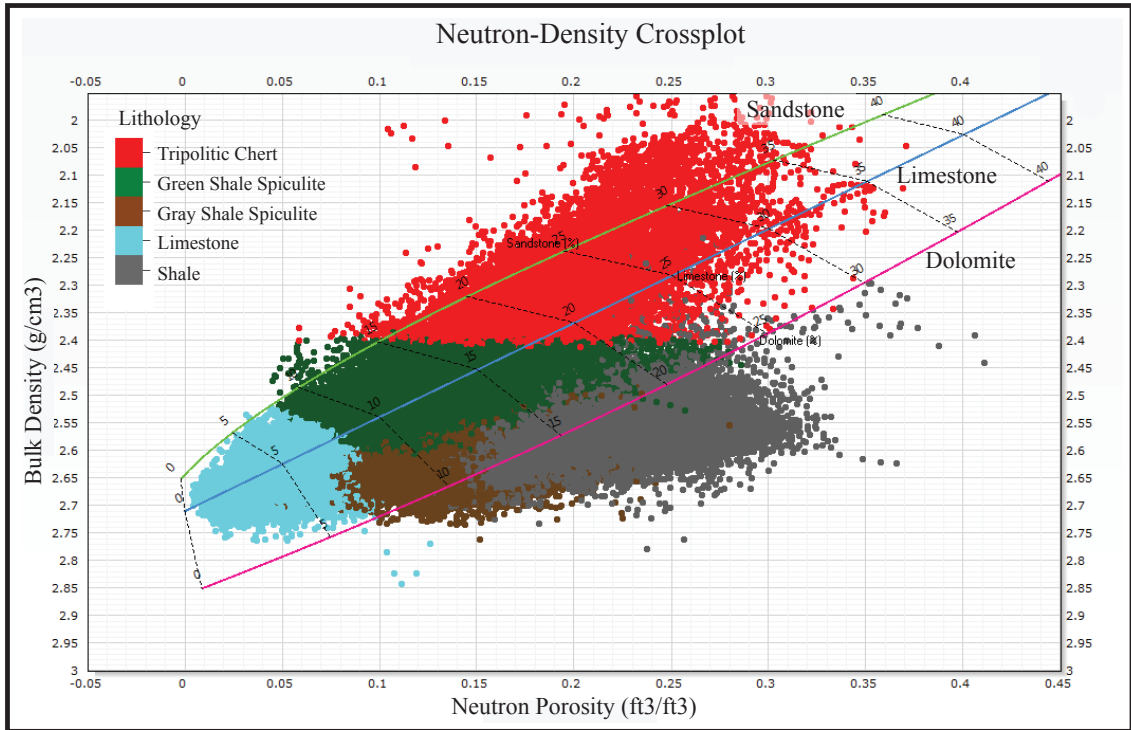


Figure C-4. Neutron-Density multi-well crossplot using all available wells within the study area. Data points are color coded by predicted lithology. Overlaying the data is a mineralogy chart showing sandstone, limestone, and dolomite divisions. Data points plotting between lines indicate a mix of component minerals. Predicted limestones tend to plot near the limestone line. Dolomite is detected in shale and spiculitic lithologies, which is supported by thin section analysis. The tripolitic chert lithology shows a fairly wide range of values, but is generally low density and high porosity. This could be caused by the presence of gas and high silica content.

Appendix C-5. Limitations of Electrofacies Classifications

As with any machine learning approach, there are some limitations and drawbacks associated with the electrofacies classification techniques used for this study. The most fundamental issue that applies to all methods is risk of misclassification. The ultimate goal is to minimize misclassification to within certain “acceptable” threshold. The accuracy of an electrofacies technique is the primary limiting factor. If a satisfactory accuracy is not achieved, the technique will not be able to serve its purpose.

For artificial neural networks (ANN’s) in particular, one of the potential issues that can impact classification competence is core coverage. Without representative core coverage to reveal the full spectrum of lithofacies present in the interval of interest, successfully validating any results is very difficult. For this study, many available core samples only covered the uppermost interval of the Mississippian. This obstacle was averted by incorporating core descriptions of full Mississippian cores used from prior studies (Sal Mazzullo, 2016, personal communication). Another limitation of ANN’s are their dependency on a consistent suite of logs. For many new wells this is less of an issue, however for some older wells limited logging technology meant only certain measurements were recorded. In order to use a well as part of an ANN, it must contain all of the inputs (log curves) specified. Thus, there is an important balance that must be reached between incorporating data points to ensure sufficient coverage and using inputs that may improve the accuracy of the ANN but are not available in all wells.

The same issue pertains to clustering. While core data is not necessary for

this unsupervised classification technique, choosing the optimal log curves to use as inputs is vital. In addition, for any electrofacies classification method, one is limited by the resolution of well logs. In most cases, log resolution is not high enough to differentiate every lithofacies, especially in a carbonate environment where lithofacies exist on a continuum. Therefore, grouping and upscaling lithofacies are important steps to ensure effective classification.

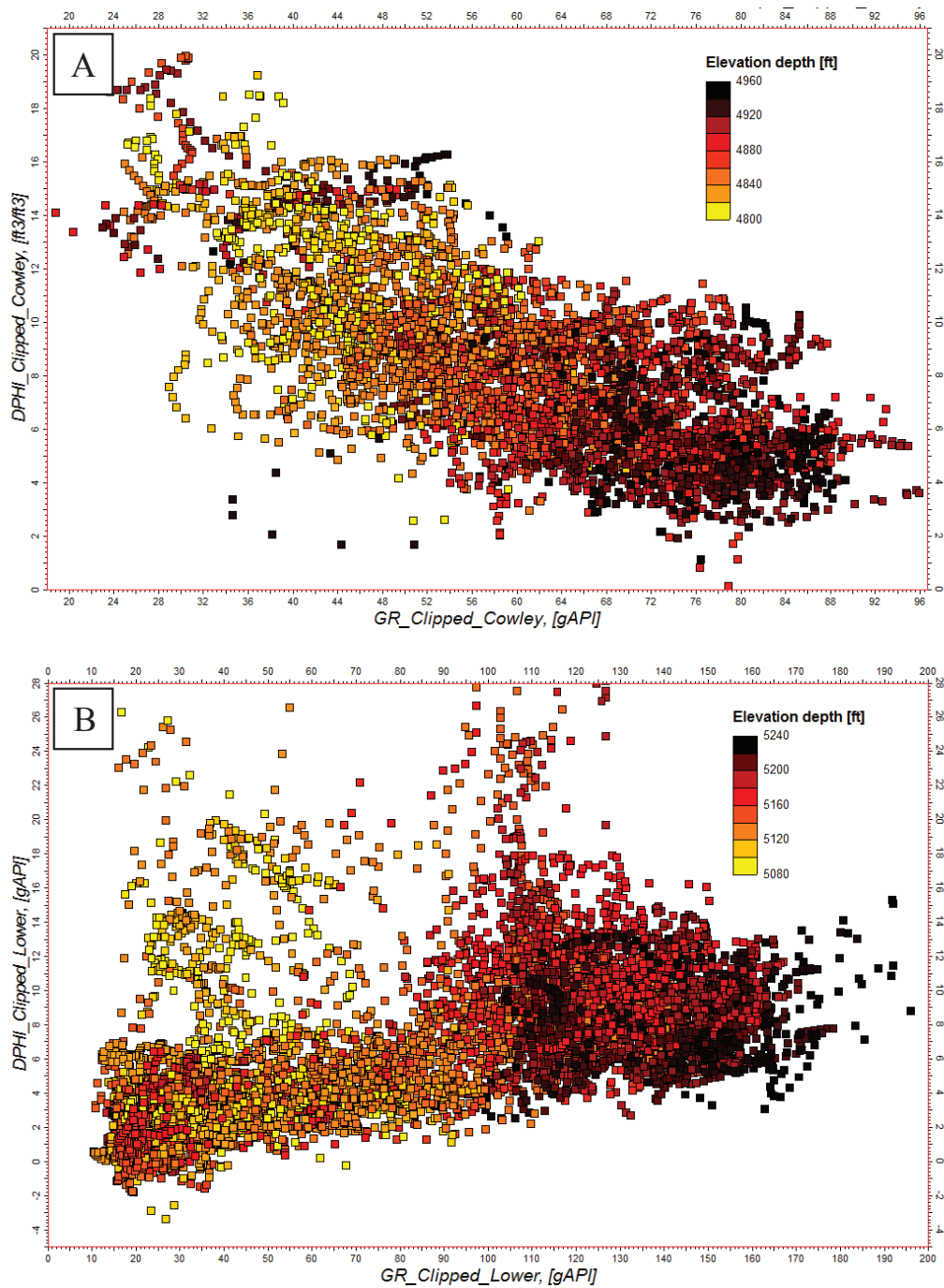


Figure C-6. Cross plots of GR and DPHI for (A) the upper Mississippian interval (Cowley and above) and (B) the lower Mississippian interval (below Cowley). In the upper Miss, gamma ray and density porosity appear inversely proportional, whereas in the lower Miss they show a direct relationship.

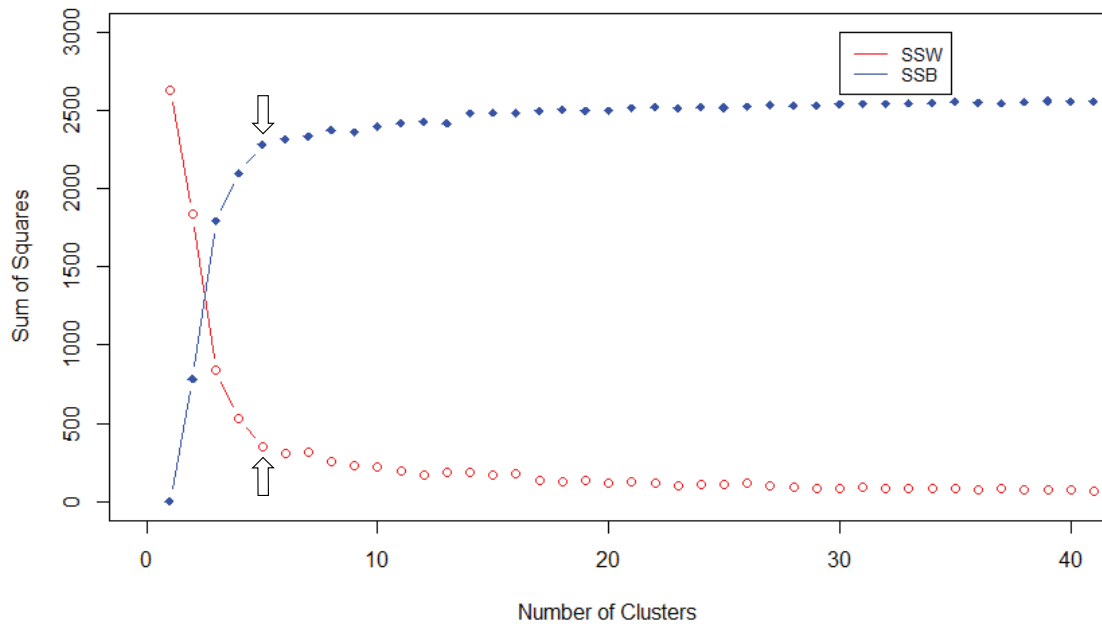


Figure C-7. Plots of Sum-of-Squares Between (SSB) and Sum-of-Squares Within (SSW). A SSW plot compares the cumulative distance of each point to its centroid with increasing K values. As more classes are added (increasing K), the distance between centroids and data points inherently decreases. A SSB plot compares the cumulative distance of each centroid to the global centroid with increasing K values. The optimal K value is chosen at the inflection point where the slope of the SSW and SSB plots decrease, known as the elbow point (arrows). In this study, the elbow point occurs at a K value of 5.

Formation/Zone	Lithology	Major Horizontal Range (ft)	Minor Horizontal Range (ft)	Vertical Range (ft)	Direction of Anisotropy	Lithology (%)
Zone 5	Chert Breccia	30000	15000	45	70	64.0
	Green Shale Spiculite	15000	15000	20		24.9
	Gray Shale Spiculite	15000	15000	20		1.1
	Limestone	15000	15000	20		9.2
	Shale	15000	15000	20		0.8
Zone 4	Chert Breccia	30000	15000	35	70	5.0
	Green Shale Spiculite	45000	40000	50	70	59.5
	Gray Shale Spiculite	15000	15000	35		1.9
	Limestone	10000	10000	40		31.9
	Shale	10000	10000	10		1.7
Zone 3	Chert Breccia	30000	15000	25	70	1.1
	Green Shale Spiculite	45000	40000	50	70	45.0
	Gray Shale Spiculite	40000	40000	50		46.9
	Limestone	10000	10000	20		5.6
	Shale	10000	10000	20		1.4
Zone 2	Chert Breccia	30000	15000	10	70	1.3
	Green Shale Spiculite	15000	15000	25		11.1
	Gray Shale Spiculite	15000	15000	30		26.6
	Limestone	40000	40000	20		47.9
	Shale	30000	30000	25		13.1
Zone 1	Chert Breccia	10000	10000	15		0.6
	Green Shale Spiculite	10000	10000	10		0.0
	Gray Shale Spiculite	10000	10000	20		3.1
	Limestone	10000	10000	20		1.7
	Shale	40000	40000	40		94.6

Figure C-8. Horizontal and vertical variogram ranges by zone for lithology modeling. Values were attained based on seismically constrained estimations (Lindzey, 2015) and experimental variogram fitting. Both horizontal and vertical ranges were decreased for petrophysical modeling to account for internal variability within lithologies.

ANN Predicted Lithologies 83.5% overall accuracy	Actual Lithology				
	Chert Breccia	Green Shale Silicified	Gray Shale Spiculite	Limestone	Shale
Chert Breccia	263	6	0	1	0
Green Shale Silicified	39	537	157	36	0
Gray Shale Spiculite	3	95	542	48	37
Limestone	0	0	0	160	0
Shale	0	0	1	0	636
User's Accuracy	86.23%	84.17%	77.43%	65.31%	94.50%

Kmeans Predicted Lithologies 84.7% overall accuracy	Actual Lithology				
	Chert Breccia	Green Shale Spiculite	Gray Shale Spiculite	Limestone	Shale
Chert Breccia	274	1	0	0	6
Green Shale Spiculite	13	598	213	42	1
Gray Shale Spiculite	0	27	484	35	31
Limestone	0	0	0	162	0
Shale	0	12	3	6	635
User's Accuracy	95.47%	93.73%	69.14%	66.12%	94.35%

KNN Predicted Lithologies 83.4% overall accuracy	Actual Lithology				
	Chert Breccia	Green Shale Silicified	Gray Shale Spiculite	Limestone	Shale
Chert Breccia	254	1	0	0	6
Green Shale Silicified	11	572	198	43	1
Gray Shale Spiculite	0	48	487	47	35
Limestone	0	0	0	150	0
Shale	0	12	10	5	631
User's Accuracy	95.85%	90.36%	70.07%	61.22%	93.76%

Appendix C-9. Confusion matrices for each electrofacies classification method using the GR, DPHI, NPHI, PHI separation input assemblage.

ANN Predicted Lithologies 86.9% overall accuracy	Actual Lithology				
	Chert Breccia	Green Shale Spiculite	Gray Shale Spiculite	Limestone	Shale
Chert Breccia	276	10	0	0	0
Green Shale Spiculite	20	489	126	16	1
Gray Shale Spiculite	8	13	278	25	26
Limestone	0	0	0	92	0
Shale	1	0	0	0	491
User's Accuracy	90.49%	95.51%	68.81%	69.17%	94.79%

Kmeans Predicted Lithologies 82.3% overall accuracy	Actual Lithology				
	Chert Breccia	Green Shale Spiculite	Gray Shale Spiculite	Limestone	Shale
Chert Breccia	282	10	0	0	0
Green Shale Spiculite	14	488	203	40	1
Gray Shale Spiculite	0	5	201	14	27
Limestone	0	0	0	74	0
Shale	0	9	0	5	490
User's Accuracy	95.27%	95.31%	49.75%	55.64%	94.59%

KNN Predicted Lithologies 62% overall accuracy	Actual Lithology				
	Chert Breccia	Green Shale Spiculite	Gray Shale Spiculite	Limestone	Shale
Chert Breccia	97	13	0	4	10
Green Shale Spiculite	108	342	132	45	15
Gray Shale Spiculite	3	147	259	16	114
Limestone	4	2	0	62	1
Shale	63	8	13	6	388
User's Accuracy	35.27%	66.80%	64.11%	46.62%	73.48%

Appendix C-10. Confusion matrices for each electrofacies classification method using the GR, DPFI, NPFI, PHI separation, and PE input assemblage.

ANN Predicted Lithologies 83.4% overall accuracy	Actual Lithology				
		Green Shale Spiculite	Gray Shale Spiculite	Limestone	Shale
Chert Breccia	250	4	0	0	0
Green Shale Spiculite	52	558	175	32	1
Gray Shale Spiculite	3	75	524	43	38
Limestone	0	1	0	169	0
Shale	0	0	1	1	634
User's Accuracy	81.97%	87.46%	74.86%	68.98%	94.21%

Kmeans Predicted Lithologies 82.3% overall accuracy	Actual Lithology				
		Green Shale Spiculite	Gray Shale Spiculite	Limestone	Shale
Chert Breccia	276	36	5	0	6
Green Shale Spiculite	11	571	210	53	5
Gray Shale Spiculite	0	19	482	54	28
Limestone	0	0	0	131	0
Shale	0	12	3	7	634
User's Accuracy	96.17%	89.50%	68.86%	53.47%	94.21%

KNN Predicted Lithologies 70.9% overall accuracy	Actual Lithology				
		Green Shale Spiculite	Gray Shale Spiculite	Limestone	Shale
Chert Breccia	146	17	3	1	7
Green Shale Spiculite	77	486	165	56	7
Gray Shale Spiculite	13	83	460	85	68
Limestone	0	0	1	96	0
Shale	29	47	66	7	591
User's Accuracy	55.09%	76.78%	66.19%	39.18%	87.82%

Appendix C-11. Confusion matrices for each electrofacies classification method using the GR, DPHI, NPHI, PHI separation, and RESD input assemblage.

ANN Predicted Lithologies 85.5% overall accuracy	Actual Lithology				
		Green Shale	Gray Shale		
	Chert Breccia	Spiculite	Spiculite	Limestone	Shale
Chert Breccia	266	6	0	2	0
Green Shale Spiculite	35	497	156	17	0
Gray Shale Spiculite	4	9	248	22	20
Limestone	0	0	0	91	0
Shale	0	0	0	1	498
User's Accuracy	87.21%	97.07%	61.39%	68.42%	96.14%

Kmeans Predicted Lithologies 82.5% overall accuracy	Actual Lithology				
		Green Shale	Gray Shale		
	Chert Breccia	Spiculite	Spiculite	Limestone	Shale
Chert Breccia	279	1	0	0	4
Green Shale Spiculite	17	494	198	40	0
Gray Shale Spiculite	0	5	206	22	22
Limestone	0	0	0	65	0
Shale	0	12	0	6	492
User's Accuracy	94.26%	96.48%	50.99%	48.87%	94.98%

KNN Predicted Lithologies 58.5% overall accuracy	Actual Lithology				
		Green Shale	Gray Shale		
	Chert Breccia	Spiculite	Spiculite	Limestone	Shale
Chert Breccia	144	4	13	7	15
Green Shale Spiculite	25	432	217	51	30
Gray Shale Spiculite	42	42	106	36	101
Limestone	6	0	2	23	3
Shale	58	34	66	16	379
User's Accuracy	52.36%	84.38%	26.24%	17.29%	71.78%

Appendix C-12. Confusion matrices for each electrofacies classification method using the GR, DPHI, NPHI, PHI separation, PE, and RESD input assemblage.

ANN Predicted Lithologies 42.1% overall accuracy	Actual Lithofacies				
	Chert Breccia	Clast/bedded Chert Spiculite	Bedded Spiculite	Lenticular Spiculite	Argillaceous Dolomitized Spiculite
Chert Breccia	60	72	6	19	5
Clast/Bedded Chert Spiculite	49	33	5	37	3
Bedded Spiculite	18	8	31	12	0
Lenticular Spiculite	0	0	0	10	21
Argillaceous Dolomitized Spiculite	0	0	16	28	83
User's Accuracy	47.24%	29.20%	53.45%	9.43%	74.11%

Figure C-13. Confusion matrix for artificial neural network classifications of core defined lithofacies. A low total overall accuracy of 42.1% was achieved. Lithofacies can be highly variable and are often defined based on small scale features that do not manifest in log signatures. In addition, only the first 5 lithofacies could be tested from firsthand core described samples. Thus, lithologies were classified instead of lithofacies for this study.

Appendix D. Stratigraphic Framework

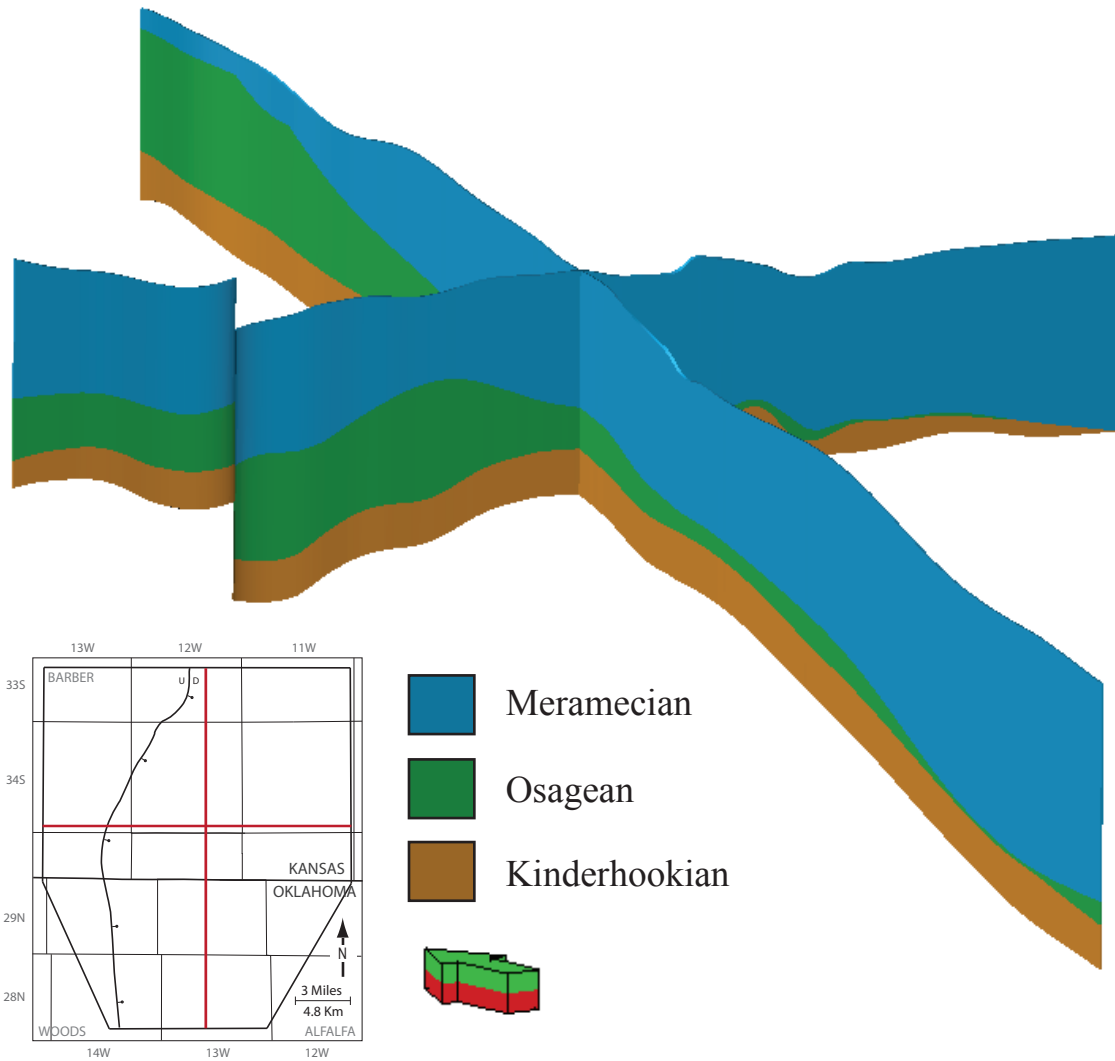


Figure D-1. Interpreted stratigraphic framework showing relative distribution of Kinderhookian, Osagean, and Meramecian aged strata. Osagean deposits thin out toward the south and east, and are replaced by Meramecian units while Kinderhookian deposits remain relatively consistent in thickness. The implication of this proposed framework is a thinner Osagean interval than previously interpreted, particularly in Woods county. Inclusion of the Cowley formation as Meramecian in age is based on recent studies of Mazzullo et al. (2016). Note: Zone classified as Meramecian includes all younger units as well, although no Chersterian deposits are interpreted in this study area.

